2010

EOCENE CALCAREOUS NANNOFOSSIL BIOSTRATIGRAPHY, PALEOECOLOGY AND BIOCHRONOLOGY OF ODP LEG 122 HOLE 762C, EASTERN INDIAN OCEAN (EXMOUTH PLATEAU)

Jamie L. Shamrock
University of Nebraska-Lincoln, jamie.l.shamrock@exxonmobil.com

EOCENE CALCAREOUS NANNOFOSSIL BIOSTRATIGRAPHY, PALEOECOLOGY AND BIOCHRONOLOGY OF ODP LEG 122 HOLE 762C, EASTERN INDIAN OCEAN (EXMOUTH PLATEAU)

by

Jamie L. Shamrock

A DISSERTATION

Presented to the Faculty of

The Graduate College at the University of Nebraska

In Partial Fulfillment of Requirements

For the Degree of Doctor of Philosophy

Major: Earth and Atmospheric Sciences (Geology)

Under the supervision of David K. Watkins

Lincoln, Nebraska

November, 2010

EOCENE CALCAREOUS NANNOFOSSIL BIOSTRATIGRAPHY, PALEOECOLOGY AND BIOCHRONOLOGY OF ODP LEG 122 HOLE 762C, EASTERN INDIAN OCEAN (EXMOUTH PLATEAU)

Jamie L. Shamrock, Ph.D.

University of Nebraska, 2010

Adviser: David K. Watkins

A relatively complete section of Eocene (~33.9-55.8 Ma) pelagic chalk from offshore northwestern Australia was used to analyze range and abundance data of ~250 Eocene species to test the efficacy of the existing CP (Okada and Bukry 1980) and NP (Martini 1971) biostratigraphic zonation schemes. Changes in nannofossil diversity, abundance, and community structure were monitored through several Eocene paleoenvironmental events, as identified by changes in $\delta^{13}C$ and $\delta^{18}O$ data, to examine variations in surface water conditions. Major changes in nannofossil assemblages, as indicated by dominance crossovers, correspond to paleoenvironmental shifts such as the Paleocene-Eocene Thermal Maximum and the Early Eocene Climatic Optimum. This research also provides systematic paleontology and range data for nine new species and one new genus, and addresses several taxonomic issues in other Eocene species.

Examination of the calcareous nannofossil biostratigraphy (Section I) showed several potential hiatuses within the stratigraphic section at Hole 762C. The presence of these hiatuses was supported by cross-correlation of planktonic foraminiferal P-zones, magnetostratigraphic reversals and $\delta^{13}C$ and $\delta^{18}O$ isotopic excursions. A portion of the dissertation was conducted to

fulfill the need for a new, integrated age model for Hole 762C, utilizing biostratigraphic, magnetostratigraphic, and stable isotopic data published in the Leg 122 *Initial Reports* (Haq et al. 1990) and *Scientific Results* (von Rad et al. 1992) with the calcareous nannofossil data generated in Section I. This new age model allowed revision of sedimentation rates at Site 762, and these revised rates were used to estimate the ages of calcareous nannofossil bioevents, which are compared to several additional, globally distributed localities.

ACKNOWLEDGEMENTS

This research used samples and data provided by the Deep Sea Drilling Program (DSDP) and Ocean Drilling Program (ODP). The DSDP and ODP are sponsored by the National Science Foundation (NSF) and participating countries under the management of Joint Oceanographic Institutions (JOI) Inc. The author would like to thank David K. Watkins, Mary Anne Holmes, Tracy Frank (University of Nebraska-Lincoln, Earth & Atmospheric Sciences) and Paul Hanson (UN-L, School of Natural Resources) and Kurt Johnston (ExxonMobil) for their role as doctoral committee members and for their collaboration and revisions on this dissertation. The author would also like to thank Jackie Lees and Tom Dunkley-Jones (Imperial College London) for their revisions on the manuscript published in the Journal of Nannoplankton Research (Section II).

TABLE OF CONTENTS

LIST OF MULTIMEDIA OBJECTS

Figures:

Tables:

Specimen Photo Plates:

Appendices:

DISSERTATION INTRODUCTION

The following dissertation was presented to the faculty of the Graduate College at the University of Nebraska as partial fulfillment of requirements for the Degree of Doctor of Philosophy, majoring in the Department of Earth & Atmospheric Sciences. This research is a micropaleontological study of calcareous nannoplankton from the Eocene epoch (~33.9-55.8 Ma), examining the biostratigraphy, paleoecology, and geochronology from Ocean Drilling Program (ODP) Leg 122 Hole 762C in the eastern Indian Ocean (northwest Australian continental shelf; Figure 1).

The dissertation is divided into three sections. As partial fulfillment of PhD requirements in the Department of Earth & Atmospheric Sciences, research projects should be of sufficient scope and complexity to produce a minimum of three research papers suitable for publication in scientific journals. Each of the following sections represents one such prospective publication.

Section I

This section of the dissertation was conducted to fulfill a need for a continuous Eocene calcareous nannofossil reference section, using samples from Leg 122 Hole 762C. A primary goal was to collect and analyze range and abundance data for a vast number of Eocene species, relative to the preexisting CP (Okada and Bukry 1980) and NP (Martini 1971) biostratigraphic zonation schemes. This data is used to examine the changes in nannofossil diversity, abundance, and community structure through several Eocene paleoenvironmetnal events, as identified by changes in $\delta^{13}C$ and $\delta^{18}O$ data. This research also provides systematic paleontology and range data for eight new species and one new genus, and addresses several taxonomic issues in other Eocene species (Appendix A).

Section II

This section is a taxonomic study describing a new species, *Sphenolithus perpendicularis* **n.sp**, from the middle Eocene (Lutetian). The distinct morphology and short stratigraphic range of this species,

and sister species in this *Sphenolithus* lineage, indicate good potential for biostratigraphic utility. This may be particularly true in this biostratigraphic interval (CP13 of Okada and Bukry 1980), where primary biomarkers may be rare. This portion of the dissertation has been published in 2010 in the Journal of Nannoplankton Research (volume 31, no. 1).

Section III

The final section of this dissertation was conducted in response to data and results generated in Section I. Ideally, that research would utilize a relatively complete and expanded succession of strata with good nannofossil abundance and preservation that could function as a reference section. Arguably the best existing section for such a purpose was cored by Ocean Drilling Program Leg 122 off of northwest Australia in 1990, as indicated by data from that expedition (Golovchenko et al. 1992; Haq et al. 1992; Siesser & Bralower 1992). Reexamination of the calcareous nannofossil biostratigraphy (Section I) showed several potential hiatuses within the stratigraphic section at Hole 762C. The presence of these hiatuses was supported by cross-correlation of planktonic foraminiferal P-zones, magnetostratigraphic reversals and $\delta^{13}C$ and $\delta^{18}O$ isotopic excursions. This section of the dissertation was conducted to fulfill the need for a new, integrated age model for Hole 762C, utilizing biostratigraphic, magnetostratigraphic, and isotopic data published in the Leg 122 *Initial Reports* (Haq et al. 1990) and *Scientific Results* (von Rad et al. 1992) with the calcareous nannofossil data generated in Section I. This new age model allowed revision of sedimentation rates at Site 762, and these revised rates were used to estimate the ages of calcareous nannofossil bioevents, which are compared to several additional, globally distributed localities.

Section I - Eocene calcareous nannofossil biostratigraphy and community structure from Exmouth Plateau, Eastern Indian Ocean

Chapter 1 - INTRODUCTION

The Eocene Epoch is a critical transition period from the global greenhouse conditions of the Late Cretaceous and early Paleogene to the icehouse of the later Cenozoic. The lower boundary is marked by a distinct pulse of global warmth, the PETM (Paleocene-Eocene thermal maximum), and the upper boundary by cooling associated with the onset of Antarctic glaciation, with a significant proportion of research focused on the conditions governing its lower and upper boundaries with the Paleocene and Oligocene, respectively.

The recent advances in our knowledge of calcareous nannofossils (Bown and Pearson 2009; Dunkley-Jones et al. 2008; Agnini et al. 2006; Bown 2005; Raffi, Backman and Pälike 2005; Tremolada and Bralower 2004, others) provide an opportunity to reevaluate the Eocene biostratigraphic succession and the nannofossil assemblage through significant paleoenvironmetnal changes. This research was conducted to fulfill a need for a continuous Eocene calcareous nannofossil reference section, containing range and abundance data for a vast number of Eocene species, relative to the preexisting CP and NP biostratigraphic zonation schemes. In addition we examine the changes in nannofossil diversity, abundance, and community structure through several Eocene paleoenvironmetnal events. Ideally, this study would utilize a relatively complete succession of strata that could function as a reference section. Arguably the best existing section for such a purpose was cored by Ocean Drilling Program Leg 122 at Hole 762C off of northwest Australia in 1990. The thorough biostratigraphic characterization of Siesser & Bralower (1992) demonstrated a relatively complete and expanded Eocene succession with good nannofossil abundance and preservation. In addition, there are well-documented paleomagnetic (Galbrun 1992) and stable isotopic (Thomas Shackleton and Hall 1992) data for this site.

Several recent studies have been conducted on Eocene calcareous nannofossil biostratigraphy and/or paleoenvironmetnal assemblage trends, producing a wealth of new nannofossil data; however, many of these studies focus on high resolution analysis of a discrete event, such as the PETM (Paleocene-Eocene thermal maximum) (Bown and Pearson 2009; Raffi, Backman and Pälike 2005; Tremolada and Bralower 2004), MECO (middle Eocene climatic optimum) (Jovane et al 2007), and Oi-1 events (Dunkley-Jones et al. 2008), or such research is restricted to only a portion of the epoch (Villa et al. 2008; Agnini et al. 2006). There are few studies where the nannofossil assemblage and range data has been quantitatively examined throughout the entire Eocene, particularly from one locality.

Recent research from the Southern Ocean (Persico and Villa 2008) and Tanzania (Bown Dunkley-Jones and Young 2007; Bown and Dunkley-Jones 2006; Bown 2005) has named a significant number of new calcareous nannofossil species. This research confirms the presence of 41 of these species within the eastern Indian Ocean at Site 762, and expands the ranges of several of these taxa. In addition, we provide systematic paleontology and range data for eight additional new species and one new genus, and address taxonomic issues with several additional forms.

In addition to developments in nannofossil biostratigraphy, the construction of high-resolution $\delta^{13}C$ and $\delta^{18}O$ records (Galeotti et al. 2010; Bohaty et al. 2009; Nicolo et al. 2007; Lourens et al. 2005; Bohaty and Zachos 2003; Zachos et al. 2001; others) has allowed paleoenvironmental events such as the PETM, ETM2 (Eocene thermal maximum 2), ETM3, EECO (early Eocene climatic optimum), MECO and Oi-1 to be identified at Site 762. Lower resolution $\delta^{13}C$ and $\delta^{18}O$ reocords for Site 762 of Thomas Shackleton and Hall (1992) allows identification of many key excursions throughout the Eocene, which allows us to examine the dynamics of the nannofossil community with respect to such paleoenvironmental events. We identify significant assemblage turnovers in the middle Eocene and discuss the possible relationships of these data to both short term environmental perturbations and the long term climate transition from global greenhouse to icehouse.

Chapter 2 - MATERIALS AND METHODS

ODP (Ocean Drilling Program) Leg 122 Hole 762C was selected for this study because of a thick, expanded Eocene succession (~240 m) as well as data from Leg 122 *Initial Reports* (Haq et al. 1990) and *Scientific Results* (von Rad et al. 1992) that indicate relatively continuous sedimentation. Site 762 (19°53.23S, 112°15.24E) is located on the central Exmouth Plateau (northern Carnavon Basin) (Figure 1) and is separated from the Australian Northwest Shelf by the Kangaroo Syncline (von Rad et al. 1992). Though stretched and rifted in its early history, the plateau has been relatively quiescent since the mid-Cretaceous, with fairly uniform thermal subsidence. Hole 762C was drilled in 1360m of water, with decompacted burial curves indicating little change in water depth since the time of original deposition (Haq et al. 1992).

Approximately 240 m of Eocene sediments were penetrated in Cores 3-29 from ~184-422 msbf (meters below sea floor). Core recovery varies throughout this interval, ranging from 12.1 to ≥ 100%, with an average recovery of ~67% (Figure 2). Sedimentation rate estimates are ~1-3 cm/ky in the early Eocene and ~0.5-2 cm/ky in the mid- and late Eocene (Shipboard Scientific Party 1990; Haq et al. 1992). Eocene pelagic sediments from this locality consist of white to green-grey, calcareous oozes, chalks, and marls, indicating an open-ocean setting (von Rad et al. 1992). Clay content and bioturbation increased downward toward the lower Eocene. This interval is divided into three lithologic subunits as described in Haq et al. (1992) and is summarized in Table 1. Calcareous nannofossil data from Siesser & Bralower (1992) show a diverse and robust nannofossil assemblage, and biostratigraphy based on the NP zonation (Martini 1971) suggests a relatively complete Eocene succession. Calcareous nannofossils are extremely abundant and moderately to well preserved, with deposition well above the CCD (carbonate compensation depth).

A total of 187 samples were selected from the recovered core at approximately 0.75 m intervals, as core availability would allow. Of these samples, 102 were used to collect detailed assemblage data,

with the remaining samples used to increase precision of key biostratigraphic markers. Sample intervals and depths are provided in Table 2. All samples span a 1 cm interval (downward), excluding 14-3-125 (2 cm) and 13-2-71, 15-2-52, and 21-5-50.5 (1.5 cm). Though some samples occur on half-centimeter intervals, depths have been rounded to two significant digits. Due to significant expansion of Core 26 (182% recovery), samples from this core required calibration of true depths (in mbsf) by taking the cored interval by the total thickness (4.5 m/7.8 m recovered thickness) to get a ratio (0.616 m true depth/ 1 m recovered thickness). This ratio was applied to samples from Core 26 to generate depths (Table 2). Sample midpoints in Table 3 represent the midpoint of the error between the observed event depth and the sample below (for LOs; lowest occurrence) or the sample above (for HOs; highest occurrence).

Core samples and smear slides, including holotype and paratype materials and photographs, are housed within the collections of the ODP Micropaleontological Reference Center at the University of Nebraska State Museum (UNSM). Smear slide preparation for Hole 762C followed standard techniques as described by Bown and Young (1998) and were mounted using Castolite AP Crystal Clear Polyester Resin. Smear slides were examined at 1000-1250x magnification with an Olympus BX51 and a Zeiss AxioImager A.2 under plane parallel light (PL), cross-polarized light (XPL), and with a one-quarter λ mica interference plate.

Assemblage data was collected by first identifying 500 specimens to species level, except members of Pontosphaeraceae and Syracosphaeraceae, which were rare and sporadic through the section (See appendix A). Additionally, two long traverses were examined to identify rare specimens, which were given a value of 1 and added to the total. These data were used to convert all species and genera to percent abundance for further analysis.

Counts of 300 specimens are considered statistically significant (Revets 2004; Dennison and Hay 1967; Phleger 1960) for identifying species that account for ~ 0.01% of the nannofossil assemblage with $p = 0.05$ (95% confidence interval); however, by generating counts > 456 specimens for percent abundance data, at the 95% confidence interval, the maximum second standard deviation will be ≤ 5% of

the actual proportion (Chang 1967). Diversity and univariate statistical analysis was conducted on the data using PAST (Paleontological Statistics) software (Hammer *et al.,* 2001).

Chapter 3 - RESULTS

Approximately 260 taxa were identified through this Eocene section, including 41 recently named and 8 new species, with nearly all CP and NP zones and subzones identified at Site 762. Calcareous nannofossils were abundant, with >10 – 100 specimens per FOV (field of view). Nannofossil specimens were moderately to well-preserved, with little or some etching, recrystallization, and alteration of primary morphology . Reworked Cretaceous and Paleogene specimens were very rare. Ranges are provided for all species as well as notable abundance trends and taxonomic issues (See appendix).

Several families are believed to inhabit neritic/shelf environments due to their general paucity in open-ocean settings, such as Syracosphaeraceae (Seisser 1998; Roth and Berger 1975), Rhabdosphaeraceae (Perch-Nielsen 1985; Roth and Thierstein 1972), Pontosphaeraceae (Perch-Nielsen 1985), Braarudosphaeraceae (Bybell and Gartner 1972; Sullivan 1965), and most holococcoliths (Gartner, 1969). The nannofossil assemblage at Hole 762C is consistent with an open ocean setting, as all such taxa were rare, sporadic, and/or absent from this locality. Despite the relative absence of some families, the nannofossil assemblage shows high species richness (S) throughout the Eocene ($\mu = 53.4$, Max. = 66, Min. = 41). Additional data and results are incorporated into the biostratigraphy and paleoenvironmental discussions, below.

3.1 - Calcareous Nannofossil Biostratigraphy

Two well known and widely employed biozonation schemes are generally applied in Paleogene calcareous nannofossil biostratigraphy: the low-latitude Okada-Bukry (1980) CP Zonation and the cosmopolitan to high-latitude Martini (1971) NP Zonation. Calcareous nannofossil biostratigraphy for

ODP Leg 122 Site 762C was originally examined by Siesser and Bralower (1992) using a modified version of the NP zonation, that incorporated CP markers, and other alternative markers, where the range and abundance of NP markers were in question. This locality has been reexamined using both the standard CP and NP zonations, with select NP subzones of Aubry (1991), to compare the consistency of these two zonation schemes, as well as to examine the secondary and alternative markers frequently employed. Strict application of some zones was not possible, due to the rarity or absence of some marker taxa at Hole 762C (*R. gladius, D. bifax, N. alata*). Subzones in the NP zonation scheme were not originally applied in Siesser and Bralower (1992) but have been identified based on data from that study. Sample intervals and depths of key marker taxa are provided in Table 3. Figure 2 illustrates the CP and NP nannofossil biostratigraphy at Hole 762C from the current study, as well as from Siesser and Bralower (1992). Placement of boundaries between the Eocene stages is tentative, as no nannofossil bioevents directly mark these horizons (Ogg Ogg and Gradstein 2008). Stage boundaries were approximated using nannofossil events in conjunction with dated isotopic excursions, identified from original ODP Leg 122 $\delta^{13}C$ and $\delta^{18}O$ data of Thomas, Shackleton and Hall (1992) (See "Nannofossil Abundance Trends", below).

The original interpretation of Siesser and Bralower (1992) identified all NP zones with no apparent hiatuses; however, this study identifies zones and subzones that are absent from both the NP and CP zonation schemes. The NP zonal boundaries are essentially congruent between Siesser and Bralower (1992) and this study for NP9, NP11, NP12, NP13, NP15, NP19/20, and NP21. Minor differences are due to core recovery issues, sample spacing between studies, or perhaps time with each sample: Many key taxa were very rare at Site 762, and significant time was spent searching for rare marker taxa, subsequently shifting the zonal boundaries. Significant differences do exist at the NP10, NP14, NP16, NP17, and NP18 boundaries, related to either use of CP and/or alternative markers or from a stratigraphic hiatus, and are discussed in greater detail below. Nannofossil zones are discussed with respect to the basal biomarker, with the top defined by the base of the following zone.

The variations in the NP and CP interpretations, both within our data and in comparison to earlier work, show some issues that can arise with rare, diachronous, and/or secondary taxa. When possible it may be best practice to employ both zonation schemes, as comparison of the two interpretations may shed light on hiatuses and/or marker taxa that occur too high or too low in the section. An increase in latitudinal temperature gradients, as seen in the late Eocene, tends to increase both the degree of taxonomic provinciality and the severity of diachronism for many paleontological proxies. This decreases the resolution of the biostratigraphic record during dynamic transitions when it is most needed, and gives further support to the application of a robust and diverse set of biomarkers whose stratigraphic relationships to one another are well understood.

Zones CP8a/NP9

The basal sample in this study (29-1-50 cm, 422.00 msbf) contains *Discoaster multiradiatus*, the marker taxa for the base of CP8/NP9. Siesser and Bralower sampled significantly deeper through the section and their midpoint for the LO of *D. multiradiatus* also occurs at 422.00 msbf, so our section begins near the base of this zone.

Subzone CP8b is absent from Hole 762C. Both the primary marker (LO *Campylosphaera eodela*) and the secondary marker (LO *Rhomboaster* spp.) are concurrent with the LO of *D. diastypus*, which marks the base of subzone CP9a (28-1-59 cm, 412.59 mbsf). This convergence is most noticeable using CP subzonal markers, and may not be identified with the NP scheme (Figure 2). This hiatus occurs in association with the PETM (412.65 msbf), and corresponds to a notable change in the nannofossil assemblage, treated more thoroughly in the PETM discussion below.

Zones CP9a/NP10

The base of CP9a (LO *Discoaster diastypus*) may be slightly younger than the base of NP10 (LO *Tribrachiatus (Rhomboaster) bramlettei*) (Ogg Ogg and Gradstein 2008); however, these bioevents were

observed in the same sample (28-1-59 cm, 412.59 mbsf). The LO of *D. diastypus* may serve as a proxy for the NP marker in sections where members of Rhomboasteraceae are rare. The secondary marker of Perch-Nielsen (1985), the HO of *Fasciculithus* spp., was also observed in this sample. Though these three bioevents are in good agreement at Hole 762C, this convergence may be due to the underlying hiatus and truncation of the true event depths.

The base of NP10 in Siesser and Bralower (1992) was marked by the LO of *T. contortus* (27-3-99 cm, 406.49 mbsf), as it was observed before the primary marker (LO *T. bramlettei*) (27-1-99 cm, 403.49 mbsf) in that study. We observed the LO of *T. bramlettei* significantly below this depth (28-1-59, 412.59 mbsf). This discrepancy is likely a reflection of the general rarity of these forms at Site 762 and that relationship to probability of identification (see above). Raffi, Backman and Pälike (2005) also note that rarity and identification issues with intermediate forms may hinder use of the *Tribrachiatus* lineage. Agnini et al. (2007a) also questions the reliability of *T. bramlettei* as a primary marker taxa, suggesting that observed diachroniety may be a true environmental signal, or may be a preservational issue, related to dissolution of basal Eocene deposits in conjunction with the PETM.

Zones CP9b/NP11

The bases of both CP9b and NP11 are marked by HO of *Tribrachiatus contortus* (26-1-49 cm, 398.30 mbsf). The secondary marker of Perch-Nielsen (1985), the LO of *T. orthostylus*, is not concurrent in Hole 762C, but occurs immediately above (25-5-43 cm, 394.93 mbsf). This secondary marker taxa may be more readily applied, as *T. orthostylus* is often more abundant that *T. contortus*.

Agnini et al. (2007a) have proposed the LO of *Sphenolithus radians* as an alternate biomarker for the base of NP11/CP9b. The LO of *S. radians* was observed in the same sample as the LO of *T. orthostylus* at Site 762 (Indian Ocean), and agrees with data from the southeast Atlantic (Agnini et al. 2007a), equatorial Pacific (Raffi, Backman and Pälike 2005) and western Tethys (Agnini et al. 2006).

Zones CP10/NP12

The LO of *Discoaster lodoensis* (23-3-51 cm, 373.01 mbsf) marks the base of both CP10 and NP12. One of the secondary bioevents for CP10, the LO *D. kuepperi* (Perch-Nielsen 1985), was concurrent with *D. lodoensis* and significantly more abundant at the base of its range that the primary marker, suggesting high potential as a proxy event. The second alternate marker of Perch-Nielsen (1985) (LO *Rhabdosphaera truncata*) was observed below *D. lodoensis* (24-1-54 cm, 379.54 mbsf) and was relatively rare and sporadic through its range.

Zones CP11/NP13

These zones mark the first real taxonomic divergence of the two biozonation schemes, resulting in quite different interpretations of Hole 762C depending upon which scheme is employed. The base of CP11 is marked by the LO of *Coccolithus crassus* (20-1-50 cm, 341.50 mbsf). NP13 is marked by the HO of *Tribrachiatus orthostylus* (also the 2° marker for CP11 (Perch-Nielsen, 1985))*;* however, there is no apparent separation between this event and the base of NP14a (LO *D. sublodoensis*) at Hole 762C. In fact, extrapolation upward and downward for the HO and LO, respectively, creates a depth crossover as shown in Table 3

Co-occurence of *T. orthostylus* and *D. sublodoensis* (19-2-52 cm, 333.52 mbsf) indicates NP13 is absent from Site 762. The presence of CP11 without NP13 is possible in several ways: The HO of *T. orthostylus* may occur too high in the section (the HO of *T. orthostylus* is noted as unreliable by Wei and Wise (1989b), occurring between 51-54.8 Ma in the south Atlantic and Pacific Oceans). *Discoaster sublodoensis* may show an early first occurrence, reducing the thickness of CP11 and compressing or eliminating NP13 (See below). Additionally, there may be a hiatus that removed NP13 and the upper portion of CP11, leaving only the basal portion of CP11 in the biostratigraphic record. This issue may not have been recognized if only the CP zonation scheme was applied, but is quite obvious in the NP scheme, or when the two are used together.

Zones CP12a/NP14(a)

Both CP and NP zones are marked by the LO of *Discoaster sublodoensis*. As mentioned above, *D. sublodoensis* may occur too low in the section, and we observe the LO of *D. sublodoensis* even deeper (from CP10, 20-3-52, 344.52 msbf) than the LCO (19-1-125, 332.75 m) used here to mark the base of these zones. A similar distribution is also observed by Agnini et al. (2006), Mita (2001), Wei and Wise (1990a), and Monechi and Thierstein (1985) in CP10 and CP11, prior to the LCO and base of CP12a. Only specimens with five straight, pointed rays were identified as *D. sublodoensis,* so it is unlikely that these early forms are misidentified specimens of *D. lodoensis*. Siesser and Bralower (1992) identified this bioevent slightly higher in the section (330.50 msbf) resulting in a modest NP13 in the original interpretation. It is possible that *D. sublodoensis* shows an early LO at Exmouth Plateau, reducing the thickness of both CP11 and NP13.

Zones CP12b/NP14(b)

The LO of *Rhabdosphaera inflata* (17-5-148 cm, 319.98 mbsf) marks the base of both CP12b and NP14b. Though relatively rare, this species is consistently present through its range.

Zones CP13(a-b)/NP15(a-c?)

The base of CP13(a) and NP15 is marked by the LO *Nannotetrina fulgens* (16-4-45 cm, 307.95 mbsf). The secondary marker of Perch-Nielsen (1985) for the base of CP13a, the HO of *Rhabdosphaera inflata* (17-1-51 cm, 313.01 mbsf) occurs in the sample immediately below the LO of *N. fulgens*, and extrapolation of midpoints makes these events nearly isochronous. CP13 is subdivided into CP13b and CP13c by the LO and HO of *Chiasmolithus gigas*, respectively, and these subzonal markers are often similarly applied to NP15. The HO of *Ch. gigas* and the LO of *Reticulofenestra umbilica* were observed in the same sample (292.00 msbf), suggesting a hiatus through this subzone. A very thin interval can be attributed to NP15c (Table 3), as the NP and CP schemes use different taxa for the boundaries above; however, this thin (~0.75 m) interval may be an artifact of sample spacing or rarity of marker taxa.

Zones CP14a/NP16

The base of CP14a is marked by the LO of *R. umbilica*, while the base of NP16 is marked by the HO(s) of *Blackites gladius* and/or *Nannotetrina fulgens*. The 1° zonal marker, *Blackites gladius*, was not observed in this section, so this zone has been identified by the HO *N. fulgens*, though the genus as a whole is notably rare at this locality. The LO of *R. umbilica* (14-6-50; 292.00 mbsf), the HO of *N. fulgens* (14-5-115 cm, 291.15 mbsf) and the HO of *Ch. gigas* (14-6-50 cm, 292.00 mbsf) show very little stratigraphic separation in Hole 762C, indicating a hiatus comprising all of CP13c and at least a significant portion of NP15c.

There appears to be a significant difference in the location of the NP16 boundary between this study and Siesser and Bralower (1992) (Table 3), who use the HO of *Nannotetrina* spp. to identify the base of NP16; however, the HO of *N. fulgens* and the HO of *Nannotetrina* spp. are nearly congruent between studies (2.35 and 0.95 m separation, respectively), and strict application of the NP zonation scheme resolves this apparent offset. The HO of *Nannotetrina* spp. may be observed higher in the section than the HO of *N. fulgens*, which highlights the biostratigraphic issues that occur with rare taxa, where nannofossil workers are often required to use alternative markers that may or may not be well correlated.

Zones CP14b/NP17

The HO *Chiasmolithus solitus* (12-3-125 cm, 269.25 mbsf) marks the base of both CP14b and NP17. This species was rare at Site 762 and was often not identified until > 3 traverses. Siesser and Bralower (1992) identify the HO of *Ch. solitus* significantly lower in the section (13CC, 284.00 mbsf), and do not use the HO of this species to mark the NP17 boundary, due to its rarity. Differences in the apparent range are likely related to the number of FOVs (field of view) and probability of finding rare taxa. This results in low confidence when picking the CP14b/NP17 boundary, particularly at mid- to low-latitude sites where *Chiasmolithus* spp. may be rare (Villa et al. 2008, Tremolada and Bralower 2004). Siesser and Bralower (1992) instead use two events as a proxy for the NP17 boundary: the LOs of

Cribrocentrum (Reticulofenestra) reticulatum and *Helicosphaera compacta*, which they identify at 12-6-100 cm (273.50 mbsf) and 12-5-100 cm (272.00 mbsf), respectively. The authors' events are reasonably near our observed HO of *Ch. solitus* (269.25 msbf); however, these bioevents are placed in CP14a in this study.

Tremolada and Bralower (2004) suggest that the HO of *Ch. solitus* is time transgressive over varying paleolatitudes: common at high latitudes until extinction, but rare and sporadic at lower latitudes prior to the HO, so that the event becomes older as latitude decreases. The predominantly mid- to low-latitude assemblage identified at Site 762 suggests that such rarity and/or diachroniety may affect the HO of this biostratigraphic marker.

These issues highlight the need for a reliable alternative bioevent. The HO of *Discoaster bifax* has also been used to mark the base of CP14b, but, similar to *Ch. solitus*, *D. bifax* can be extremely rare, and few specimens were identified in Hole 762C. In addition, Wei and Wise (1989a) suggest that the morphological transition between *D. praebifax* and *D. bifax* may hinder its use. Alternatively, the FCO of *R. hillae* and the LO of *Dictyococcites (Reticulofenestra) bisectus* (< 10 μm) were both observed in sample 12-4-50 cm (270.0 mbsf), and closely approximate the HO of *Ch. solitus* (12-3-125, 269.25m). Bown (2005) and Marino and Flores (2002) also identify the LO of *D. bisectus* just above the HO of *Ch. solitus*, suggesting potential for this species as an alternate marker for CP14b/NP17.

Zones CP15a/NP18

The base of CP15a is marked by the HO *Chiasmolithus grandis* (10-1-50 cm, 246.5 mbsf), while the base of NP18 is marked by the LO *Ch. oamaruensis* (8-5-50 cm, 233.5 mbsf). These events are shown as nearly contemporaneous in the 2008 Time Scale (Ogg Ogg and Gradstein 2008). The stratigraphic separation between these bioevents in Hole 762C may be artificially expanded by poor recovery of Core 9x (Figure 2). In addition, *Ch. grandis* and *Ch. oamaruensis* are quite rare near their HO and LO, respectively, and were often only identified after >3 traverses across a slide. Use of sample mid-points

greatly reduces this separation, but still results in stratigraphic offset and uncertainty in placement of zonal boundaries (Figure 2). Though some specimens of *Ch. oamaruensis* are readily identified, the narrow angle between cross-bars that defines this species can be difficult to distinguish from similar taxa such as *Ch. altus* and *Ch. eoaltus*, which have a larger angle between cross-bars. This uncertainty, combined with rarity, can create difficulties when applying this marker.

Zones CP15b/NP19/20

The LO of *Isthmolithus recurvus* marks the base of both CP15b and NP19/20. The FCO is used to mark the base of the (sub)zone at Site 762 (7-1-50 cm, 218.0 mbsf), as two isolated specimens were observed deeper in the section (236.96 and 223.46 msbf). Villa, et al. (2008) identify rare occurrences of *I. recurvus* in CP15a, and also use the FCO to mark the base of the subzone.

The secondary CP marker of Perch-Nielsen (1985), the HO of *Cribrocentrum (Reticulofenestra) reticulatum* (4-1-123.5 cm, 190.24 mbsf), was observed significantly above the FCO of *I. recurvus*. This stratigraphic relationship is also shown by Cascella and Dinarés-Turell (2009), Villa et al. (2008), Marino and Flores (2002a, b), Berggren et al. (1995), and Wei and Wise (1989b). Calibration of the HO of *Cr. reticulatum* by Berggren et al (1995) dates the HO of this species approximately 1 My earlier at high latitudes than at low latitudes.

Zones CP16a/NP21

The CP16a and NP21 boundaries are marked by the HO of *D. saipanensis* (and/or the HO *D. barbadiensis*). The HO of *D. saipanensis* (and *D. barbadiensis*) has been problematic at Site 762. Very rare and sporadic specimens of both species were observed quite high in the section, through the highest sample in this study (3-1-49 cm; 184.49 mbsf) and through sample 2-2-100 cm (172.5 mbsf) in the original interpretation. This difficulty in boundary placement due to rarity has also been noted by Dunkley-Jones and others (2008) and Siesser and Bralower (1992). Rare but consistent specimens of *D. saipanensis* and *D. barbadiensis* were observed through 4-3-100 cm (193.0 mbsf), marking the HCO of

both species, and the base of CP16a in this study. The upper two samples in this study are located within CP16a, as both contain *Reticulofenestra oamaruensis* and show a considerable increase in *Clausicoccus* spp., marking the base of this acme event.

Synthesis

Application of both the Okada and Bukry (1980) CP zonation and the Martini (1971) NP zonation facilitated the identification of three stratigraphic hiatuses. Hiatus A was identified with the CP zonation, by the concurrent LOs of *Campylosphaera eodela, Rhomboaster* spp., and *Discoaster diastypus* (412. 59 msbf) and indicates the absence of subzone CP8b. Hiatus B was identified with the NP zonation, by the convergence of the HO of *Tribrachiatus orthostylus* and the LO of D. *sublodoensis* (333.52 msbf), and indicates the absence of NP13. Hiatus C was identified in both the CP and NP zonation, as both the LO of *Reticulofenestra umbilica* and *Nannotetrina fulgens* converge with the HO of *Chiasmolithus gigas*, with the absence of subzone CP13c/NP15c. While hiatus C can be identified with either zonation scheme, both the NP and CP zonation are insufficient to readily identify all three hiatuses. These schemes become more robust when used in conjunction, due to the greater number of nannofossil markers. This allows both greater biostratigraphic resolution when events are offset (LO *R. umbilica*/CP14a and *N. fulgens*/NP16), and greater confidence when two bioevents are nearly isochronous (HO *Ch. gigas*/CP15a and LO *Ch. oamaruensis*/NP18).

The standard CP and NP nannofossil zonation schemes provided a series of bioevents that are extremely useful in biostratigraphy, most of which are consistent, reliable, and well-calibrated; however, some of these taxa are shown to be inconsistent in this research and in several other studies, such as *Discoaster sublodoensis*, *Chiasmolithus oamaruensis*, *Ch. solitus*, and *Tribrachiatus bramlettei.* This is well illustrated when comparing the Site 762 nannofossil biostratigraphy of Siesser and Bralower (1992) to this reexamination, as all significant divergences in interpretations are linked to these problem taxa.

The placement of some zonal boundaries is compromised simply by the rarity of the biomarker that defines it. Such rarity is often linked to paleoecological preference, such as temperature (Villa et al. 2008, Tremolada and Bralower 2004; Perch-Nielsen 1985). The CP and NP biozonation schemes each utilize three species of *Chiasmolithus* (*Ch gigas*, *Ch. grandis*, *Ch. oamaruensis*, and/or *Ch. solitus*. While most morphological characteristics are extremely diagnostic, the cool-water preference of this genus makes these taxa quite rare at mid- to low-latitude sites, particularly during the warm Eocene where latitudinal climate zones were expanded poleward. We compensated for the rarity of such taxa by increasing the number of traverses across a slide; however, additional time is not always available for analysis, and more readily identifiable proxy events will greatly improve biostratigraphic confidence. Paleoecological restriction is also seen in this open-ocean site with respect to the shelf/neritic preference of Rhabdosphaeraceae. While marker taxa such as *Blackites gladius* and *Rhabdosphaera truncata* may be quite useful in some sections (such as Tanzania [Bown and Dunkley-Jones 2006; Bown 2005]), both were extremely rare and sporadic at Site 762. While rarity can be mitigated with increased FOVs, the sporadic nature of these taxa greatly reduced the confidence of these bioevents, and neither could be used in the biostratigraphic scheme at Site 762. Some markers appear rare despite their ecological preference: The warm-water, oligotrophic, open-ocean setting of this site suggests *Discoaster bifax* should be relatively common; however, this species was essentially absent from Hole 762C and rarity prohibited use of this bioevent in the CP zonation scheme.

In addition to rarity, diachroniety may affect other markers in the standard zonations. The relative stratigraphic relationships of the *Tribrachiatus* lineage may be consistent; however, the potential diachroniety of *T. bramlettei* (Agnini et al. 2007a), and the rarity of this group in many sections, warrants calibration of alternate bioevents. Tremolada and Bralower (2004) also identify potential diachroniety in *Ch. solitus*, with HO in low latitudes prior to high-latitude sites. Though issues with diachroniety (Berggren et al. 1995) prohibits use of the HO of *Cr. reticulatum* as a proxy for the LO of *I. recurvus*, the

relative overlap in range may have potential for use as a qualitative paleotemperature proxy, with the greatest overlap at lower latitudes.

Well-calibrated secondary markers are needed to act as substitutes for rare and or/diachronous bioevents. This would allow robust age comparison in different paleoceanographic environments and when marker taxa are rare near their LO or HO. Both the LO of *T. orthostylus* and the LO of *S. radians* appear to be good alternate bioevents for the HO of *T. contortus,* as both closely approximate this event and are frequently more abundant and consistent than *T. contortus*. *Discoaster lodoensis* can be rare near it's LO, and the potentially more abundant secondary event, the LO of *D. kuepperi*, can help identify this zonal boundary. Both the LO of *Cr. reticulatum* and the LO of *D. bisectus* have potential to approximate the HO *Ch. solitus* when that primary marker is rare, but each will need to be assessed from several sites to ensure consistency and to calibrate the age offset from *Ch. solitus*, particularly at varying latitudes.

Discoaster sublodoensis appears to be the most inconsistent bioevent in both zonation schemes and should be applied tentatively: this species marks the base of CP12a/NP14a, but has been identified as low as CP10/NP12 at Site 762 and in several sections globally, at both high- and low-latitudes, even with a strict taxonomic definition. Potential proxies from Site 762 include the HO of *C. crassus* and the LO of *S. spiniger*, but both events require additional calibration.

Most bioevents in the standard NP and CP zonation schemes have proven reliable and consistent in the 30+ years since developed; however, with the growing body of nannofossil data, it is becoming clear that several of these biomarkers are compromised by rarity and/or diachroniety. Several alternative bioevents have been suggested, in this work and in others, to act as proxies for these primary marker taxa. Additional bioevents are provided in Table 4, showing the biostratigraphic potential of the Eocene succession. Secondary bioevents need not be synchronous with the primary event, so long as the relative offset is well calibrated. This calibration must be across varying paleolatitudes and paleodepths, to fully understand the spatial and temporal distribution of such proxies.

Additional potential proxies may be present in well known species, but a large body of recently named Eocene taxa (>70 species) (Shamrock and Watkins 2010; Persico and Villa 2008; Bown Dunkley-Jones and Young 2007; Bown and Dunkley-Jones 2006; Bown 2005, and this work) may also contain potential alternative bioevents. Currently, the CP and NP schemes each give a stratigraphic resolution of > 1 My through the Eocene (15-16 events in >20 My). In addition to identifying taxa that may serve as proxies for existing biomarkers, we should also strive to calibrate and integrate additional events in hopes of increasing current the biostratigraphic resolution to < 0.5 My. The best hope for such improvement may be in the development of the high-resolution, high-precision orbitally-tuned biochronology (Galeotti et al. 2010; Pälike et al. 2006; Raffi et al. 2006), which will greatly increase our understanding of the placement of bioevents in the biostratigraphic record.

3.2 - Nannofossil Abundance Trends and Paleoenvironmental Events

The Eocene Epoch is a critical transition period from the global greenhouse conditions of the Late Cretaceous and early Paleogene to the icehouse of the later Cenozoic. The lower boundary is marked by a distinct pulse of global warmth, the PETM, and the upper boundary by a cooling associated with the onset of Antarctic glaciation. As concern with anthropogenic CO_2 emissions rises, interest in Eocene climate has increased as the most recent greenhouse analogue; however, a large proportion of research focused on the conditions governing its lower and upper boundaries with the Paleocene and Oligocene, respectively.

Between these extremes, the Eocene had been viewed as a time of relatively uniform decline in global temperatures and CO_2, setting the stage for the icehouse transition. It is now understood that the Eocene was not a monotonous climatic decline, but contains several distinct periods of warming and cooling (Galeotti et al. 2010; Bohaty et al. 2009; Nicolo et al. 2007; Lourens et al. 2005; Bohaty and Zachos 2003; Zachos et al. 2001; and others). Calcareous nannofossil assemblages also show several fluctuations in diversity and dominance through the Eocene (Bown and Pearson 2009; Jiang and Wise 2009; Agnini et al. 2006; Tremolada and Bralower 2004; and others). Many fluctuations observed in Hole

762C correlate closely with known isotopic excursions (discussed below), and are likely in response to environmental variability. These events include the PETM, the ETM2 (H1) and ETM3 ("X") hyperthermal events, Early Eocene climatic optimum (EECO), Middle Eocene climatic optimum (MECO), and a period of warming within an overall cooling trend within the Priabonian. The depths of these events as identified in Hole 762C, as well as the event data and primary references, are given in Table 5. Changes in nannofossil diversity through the Eocene broadly mirror changes in temperature, as reflected in $\delta^{18}O$ values, with diversity increasing during warming events and decreasing during cool periods, particularly within the Lutetian (Figure 3). Isotopic data ($\delta^{18}O$ and $\delta^{13}C$) are taken from the original Scientific Results of Site 762 (Thomas, Shackleton and Hall 1992). Many planktic taxa show assemblage trends that fluctuate across latitudinal climate zones, and have been seen to contract and expand with changes in climate (Kahn and Aubry 2004; Lees 2002; Aubry 1992; Wei and Wise 1990b; Haq and Lohmann 1976); however, the direct relationship between diversity, temperature, and nutrient levels may be difficult to distinguish (Villa et al. 2008). These intervals and the calcareous nannofossil response will be discussed in greater detail below.

Paleocene-Eocene thermal maximum (PETM)

Interest in the PETM and the associated CIE (carbon isotope excursion) that mark the Paleocene-Eocene boundary has generated several recent studies on the nannofossil assemblage changes through this event. Raffi, Backman and Pälike (2005) synthesized these assemblage changes from several studies across 18 sites in the northern Indian, Atlantic, Pacific, and Mediterranean. Additional research has confirmed these shifts, adding further evidence to several distinct, seemingly global, assemblage changes across the PETM (Bown and Pearson 2009; Jiang and Wise 2009; Agnini et al. 2007a, 2007b; Agnini et al. 2006; Gibbs et al. 2006a, 2006b; Raffi, Backman and Pälike 2005; Tremolada and Bralower 2004). To date, the eastern Indian Ocean has been excluded from such studies, allowing Site 762 to add to the understanding of the global nature of the nannofossil response across the PETM, discussed below.

Many PETM specific studies were conducted at centimeter-scale sample spacing to capture the rapid sequence of bioevents across this isotopic excursion, resulting in a robust set of nannofossil events, including short ranging 'excursion' taxa and assemblage turnovers. Poor recovery of Cores 28 and 29 (22.1% and 48.4%, respectively) (Figure 2) makes Exmouth Plateau less than ideal for studying the PETM interval, and sample spacing for biostratigraphy and isotope data is much greater than PETM-specific studies; however, nannofossil studies covering longer time intervals are often conducted at lower resolution, and it is important to understand which bioevents can be identified across the PETM at a greater sample spacing. Despite poor core recovery, a notable $\delta^{13}C$ excursion (-1.3 ‰, 412.65 msbf) is accompanied by an $\delta^{18}O$ shift of -0.39‰ (Thomas, Shackleton and Hall 1992), indicating that this event may be partially captured at this locality (Figure 3). The overall magnitude of the CIE at Site 762 is low relative to several other sites (Ex: Site 690 = ~2.4‰, Site 1263 = ~2.5‰), and may be truncated by Hiatus A, identified through the PETM between 413.25-412.59 msbf (Figure 2, Table 3). This hiatus includes all of CP8b, but may also include a portion of CP8a and/or CP9a (See biostratigraphy section).

Several authors noted a barren interval associated with the CIE at other localities (Jiang and Wise 2009; Monechi and Angori 2006; Kahn and Aubry 2004), as well as the selective dissolution of more fragile taxa across and above the PETM boundary (Agnini et al. 2007b, Agnini et al. 2006; Tremolada and Bralower 2004). This includes low species richness and dominance of dissolution resistant taxa such as *Fasciculithus, Sphenolithus,* and *Discoaster* spp. (Bown and Pearson 2009; Jiang and Wise 2009; Monechi and Angori 2006; Kahn and Aubry 2004). Raffi and De Bernardi (2008, fig 5) attribute these observations to truncation of the basal PETM sequence from acidification and dissolution, and this is likely responsible for at least a portion of Hiatus A.

A notably reduced and poorly preserved nannofossil assemblage is also observed in Hole 762C just below and at the CIE, with the lowest species richness (25 and 29) and Shannon H diversity (2.33 and 2.41) of the entire Eocene section (Table 6, Figure 3). In general, the assemblage is quite similar to data from Site 1263 (Raffi and De Bernardi 2008), composed primarily of etched *Discoaster*, *Coccolithus*, and

Toweius spp., with anomalously high abundance of *Fasciculithus* spp. (Table 6). At Site 762, *Fasciculithus* spp., *T. eminens*, *D. multiradiatus*, and *P. bisulcus* account for 53.0% and 48.5% of the assemblage immediately below and during the CIE, respectively. The notable enrichment in *Fasciculithus* spp. (Table 6) is also noted by Tremolada and Bralower (2004) and Bralower (2002). *Toweius* spp. are also notably abundant, particularly large specimens (8-14 μm) of *T. eminens* (Table 6). Both species richness and diversity increase immediately above the PETM interval (46 and 2.90, respectively).

One of the most consistently noted changes in the nannofossil assemblage at various sites is the 'crossover' between *Fasciculithus* spp. and *Zygrhablithus bijugatus* across the PETM. Many authors note the HO of *Fasciculithus* spp. near the top of the CIE, and a sharp increase in *Z. bijugatus* in the upper portion of, or immediately above, the CIE (Bown and Pearson 2009; Jiang and Wise 2009; Raffi and De Bernardi 2008; Agnini et al. 2007a, b; Agnini et al. 2006; Monechi and Angori 2006; Raffi, Backman and Pälike 2005; Tremolada and Bralower 2004; Bralower 2002; Monechi, Angori and von Salis 2000). This change is also observed at Site 762, though the crossover is more apparent for the sharp decrease and abrupt extinction in *Fasciculithus* spp., from nearly 34% during the excursion to <0.01% above the recovery. The increase in *Z. bijugatus* may be less pronounced due to its moderate abundance at the base of the section (8.8%, Table 6), though the relative abundance does increase up to 20% within CP9a/NP11 (Figure 4).

Sphenolithus spp. are rare but rebound during the CIE recovery, also showing an inverse relationship to *Fasciculithus* spp., though of lesser magnitude than *Z. bijugatus* (Figure 5). *Sphenolithus* spp. are absent below the CIE and < 0.4% at the base of the excursion, but recover to 3.4% just above the event (Table 6). Similar changes were noted by Bown and Pearson (2009), Jiang and Wise (2009), Agnini et al. (2007a, 2007b), Gibbs et al. (2006a), Tremolada and Bralower (2004), and Bralower (2002). Agnini et al. (2007b) and Bralower (2002) suggest the increase in both *Sphenolithus* and *Zygrhablithus bijugatus* indicates a return to more oligotrophic conditions above the CIE.

Other significant trends include an increase in *Chiasmolithus* spp. (Table 6), also noted in Jiang and Wise (2009). *Ericsonia* spp. increase from ~3% at the base of the CIE to > 10% directly above (Table 6), linked to both the LO of *E. formosa* and an increase in *E. cava,* also noted by Agnini et al. (2007b), Tremolada and Bralower (2004), and Bralower (2002). These authors, as well as Bown and Pearson (2009) and Agnini et al. (2007a), also note a relative increase in *Discoaster* spp. At Site 762, peak abundance of *Discoaster multiradiatus* (~3%) and *Discoaster* spp. (11.4%) both occur during peak $\delta^{13}C$ excursion (412.59 msbf) (Table 6, Figure 5).

In summary, reduced preservation through this interval is indicated by enrichment in, and overgrowth on, dissolution resistant forms, such as *Fasciculithus, Discoaster*, *Toweius,* and *Chiasmolithus* spp. Minimum Shannon diversity and species richness for the entire Eocene section in Hole 762C occur just below the PETM. Both rebound significantly at/just above peak CIE (Table 6, Figure 3), linked to increases in *Coccolithus* spp., *Discoaster* spp., *Sphenolithus* spp., and *Z. bijugatus* (Figures 4, 5). Several additional changes are observed, including key dominance crossovers between *Fasciculithus* spp. and *Z. bijugatus*/*Sphenolithus* spp., as well as long-term decline in *Toweius* spp. Poor core recovery and relatively coarse sample spacing does not permit resolution of the many short-lived species and events identified in other high-resolution, PETM-specific studies; however, observations in Hole 762C indicate that this event can be readily identified through even poorly recovered or coarsely-samples intervals (Jiang and Wise 2009).

ETM2/H1

Though the PETM is the most intensely studied event of the latest Paleocene-early Eocene, it is now known that several less-distinct hyperthermal events occurred through the Ypresian (Bohaty et al. 2009; Sluijs et al. 2008; Nicolo et al. 2007; Lourens et al. 2005; Cramer et al. 2003). The most pronounced of these is the H1 event (Cramer et al. 2003), or ETM2 (Eocene thermal maximum 2) (Sluijs et al. 2008), and the associated clay-rich Elmo horizon (Lourens et al, 2005). This event has an associated

$\delta^{13}C$ excursion ~≥ 1.0 ‰ (Nicolo et al. 2007; Lourens et al. 2005), and is dated to ~53.44 Ma (to Berggren et al 1995; Table 5), which closely correlates to the base of nannofossil zones CP9b/NP11 (53.6 Ma; Berggren et al. 1995). This hyperthermal event is expressed well at Site 762, by a negative $\delta^{13}C$ excursion and rebound of ~0.8‰ (Figure 3) between 398.15-393.80 mbsf, and closely correlates to the base of CP9b (396.62 mbsf) (Figure 2, Table 3). The nannofossil assemblage shows a rapid increase in species richness (63), evenness (0.40) and Shannon diversity (3.20), with peak values (at 394.25 mbsf) coinciding with peak negative shift in $\delta^{13}C$ (0.64‰, 394.85 mbsf) (Figure 3).

Unlike the PETM, few prominent changes in the nannofossil assemblage are observed across the ETM2. A transient decrease is seen in *Coccolithus pelagicus* and *Z. bijugatus* of ≥ 4.0-6.0 % each (Figure 4), as well as a permanent reduction in *Toweius serotinous* (~1-2% to ~0.20 %) prior to extinction. Changes in species richness, evenness, and Shannon diversity in this interval are linked to minor increases (~1-2%) in *Sphenolithus* spp., *Discoaster* spp. (Figure 5), *Umbilicosphaera bramlettei*, *Cruciplacolithus parvus* **n. sp.**, *Neococcolithes protenus,* and members of Pontosphaeraceae immediately above the isotope excursion, as well as by the LOs of *S. radians*, *T. orthostylus*, and *Discoaster robustus*.

ETM3/"X"-event/Event "K"

Warming is associated with another carbon excursion, the ETM3. Originally identified by Röhl et al. (2005) as the "X" event, this hyperthermal is correlated to foraminiferal zone P7 and nannofossil zone CP10. The ETM3 is placed in Chron C24n.1n (52.65-53.00 Ma) by Agnini et al. (2007) and by Galeotti et al. (2010). The date provided (Table 4) is based on the relative placement of this event in Chron C24n.1n within the Contessa Road Section, as well as the association by Galeotti et al. (2010) of the isotopic excursion with the LO of D. *lodoensis* (identified at 372.35 and 373.01 msbf in Hole 762C, respectively).

Species richness remains high through the ETM3, with 66 and 61 species identified in the nannofossil samples immediately above (371.49 msbf) and below (373.01 msbf) the isotopic excursion,

respectively. This interval shows the highest Shannon diversity of the Ypresian (3.389, 371.49 msbf), and assemblage evenness is high (0.449, 371.49 msbf), approaching the maximum seen in the EECO (Figure 3). A significant drop is observed in both Shannon diversity and evenness immediately above the $\delta^{13}C$ excursion, to 2.955 and 0.320, respectively. *Discoaster* spp. increase from ~2.0% below the ETM3 to 6.7% during the event, beginning a general rise in the genus through the remaining Ypresian that peaks at the end of the EECO (Figure 5). A peak in warm-water taxa (8.6% to ~14.5%, Figure 6) is also associated with this rise in *Discoaster* spp. Holococcolith abundance also increases just above the ETM3 (Figure 6), from 10.8% (371.49 msbf) to ~18.0% (370.75, 370.00 msbf).

The most significant change in the nannofossil assemblage is the high species turnover near this event relative to background rates, particularly originations. Six species show LOs at 373.01 msbf (*Chiphragmolithus barbatus*, *C. calathus*, *Discoaster gemmifer*, *D. kuepperi*, *D. lodoensis*, *Neococcolithes dubius*) while five have LOs at 371.49 msbf (*Ch. grandis*, *D. germanicus*, *D. septemradiatus*, *P. larvalis*, *G. gammation* (LCO)). This is in significant contrast to the rate of 0-2 species for several samples above and below this interval. This increased rate of speciation is of particular interest because, unlike the higher rates associated with the PETM and EECO, this event has no stratigraphic hiatus associated with it at Site 762. While the increased turnover at the PETM and EECO likely has a large environmental component, it is difficult to unravel this true turnover from the apparent turnover that occurs across a hiatus.

Early Eocene Climatic Optimum (EECO)

Temperatures continued to increase through the early Eocene, peaking in the late Ypresian with the Early Eocene Climatic Optimum (EECO). Minimum $\delta^{18}O$ values occur between ~52-50 Ma (Zachos et al. 2001; Bohaty and Zachos 2003; Tripati et al. 2003), within nannofossil biozones CP10-11 (Ogg Ogg and Gradstein 2008). Following the initial rebound above the PETM, nannofossil diversity and species

richness show a long-term, sustained increase through much of the early Eocene ($Max_{diversity}$ = 3.39; $Max_{richness}$ = 66; 371.49 mbsf)(Figure 3).

Early Eocene peaks in nannofossil species richness (μ = ~60), evenness (0.485) and Shannon diversity (μ =3.13) occur within the EECO (~331.0-352.0 msbf) at Site 762 (Figure 3). Maximum nannofossil diversity (3.32, 335.03 msbf) occurs near the end of this warm interval, followed by a rapid and sustained decline. There is significant turnover in the nannofossil assemblage associated with the end of the EECO as defined here at Site 762. A significant drop in diversity (3.317 to 2.961, Figure 3) is linked to 13 extinctions but only three LOs (333.52-332.75 mbsf); however, the end of this event may be affected by core recovery or truncated by a stratigraphic hiatus (Hiatus B), indicated by the thinness of CP11 and absence of NP13, discussed in the biostratigraphy section, above.

The most distinguishing event through the EECO is the dominance shift in the background assemblage, from *Toweius* spp. in the lower Eocene to *Reticulofenestra/Dictyococcites* spp. in the middle and upper Eocene. This crossover is closely associated with the EECO in Hole 762C, and is linked by a substantial acme in *Discoaster* spp. (Figure 7). These transitions from *Toweius* to *Discoaster* to *Reticulofenestra*/*Dictyococcites* spp. represent two assemblage turnovers that closely approximately the base and top of the EECO interval, respectively, as defined chemically and biostratigraphically at Site 762.

Toweius spp. show a steady decline through the Ypresian, from a peak abundance of 28.0% near the PETM (μ = 23.8%) to ~14.4% at the base of the EECO (Figure 5). This decline becomes more rapid at the base of the EECO, dropping to < 1.0% by the top of the interval, with extinction shortly above. This trend is concurrent with a notable shift in *Discoaster* spp. mean abundance from 8.6% below the basal EECO boundary to 15.1% through the event (Max. = 18.6%). The EECO acme in *Discoaster* spp. is primarily linked to peaks of both *D. lodoensis* (μ = 11.7%; Max. = 14.2) and *D. kuepperi* (μ = 5.6%, Max. = 6.8%).

The LO of the *Reticulofenestra*/*Dictyococcites* group is observed just above the base of the EECO, but remains extremely rare through much this interval (μ = 0.8%; Max. = 1.9%) (Figure 7). An abrupt, but sustained, increase occurs across the upper EECO boundary, from 7.8% to 33.6% just above, and is concurrent with an abrupt and sustained decline in *Discoaster spp*., from 16.6% at the upper EECO boundary to 8.8% above (Figure 7). Abundance of *Reticulofenestra*/*Dictyococcites* continues to increase through much of the Lutetian (μ = 40.4%; Max. = 56.4%). This *Discoaster* acme linking the *Toweius* and *Reticulofenestra/Dictyococcites* assemblages is also seen in the Possango (Italy) section from which Agnini et al. (2006) suggest that warm, oligotrophic conditions originally favor *Discoaster* spp., but a collapse in surface water stratification later favors the more mesotrophic to eutrophic *Reticulofenestra* group.

In addition to the *Toweius-Discoaster-Reticulofenestra* crossovers associated with the EECO, several changes are observed in other nannofossil taxa through the interval. *Sphenolithus* spp. decreases from μ = 5.5% (Max. = 6.6%) through this interval to 2.2% at the end of the EECO (Figure 5), linked to the Eocene peak (μ = 2.3%) and decline (μ = 0.8%) of *S. radians*. *Zygrhablithus bijugatus* increases through CP10-11 with peak abundance through the EECO (μ = 16.2%; Max. = 19.2%), but declines through much of the Lutetian (μ =10.7%) (Figure 4). The LO of *Coccolithus crassus* occurs during the EECO and rapidly increases (μ = 6.3%; Max. = 8.6%) within this interval. This species shows an abrupt decline just above the upper boundary (0.8%) before rapid extinction, suggesting an affinity for warm temperatures or oligotrophic conditions.

The nannofossil assemblage shows a sustained increase in warm water taxa (Table 7) from the ETM2/H1 through the Ypresian, with peak abundance for the Eocene within the upper EECO (μ = 24.4%; Max. = 28.8%) (Figure 6). Abundance of warm water taxa drops rapidly above the EECO to 16.1%, and continues to decline in the Lutetian. Cool water taxa (Table 7) show a short pulse at near the top of the event (Figure 6), linked to an increase in *Chiasmolithus* spp., particularly large species such as *Ch. grandis* and *Ch. californicus*, but do not show a significant increase through the Lutetian.

Campylosphaera dela, Calcidiscus pacificanus and *Girgisia gammation* also increase to μ = 2-3% through the EECO but drop to μ = ≤ 1.0% at or just above the upper boundary. These taxa may have affinity to either warm water or oligotrophic nutrient conditions; however, this suggestion would require further study in sections where these taxa show greater abundance.

Middle Eocene cooling

The end of the EECO marks the beginning of long term cooling through much of the Lutetian, with trends in the nannofossil assemblages mirroring the general rise in $\delta^{18}O$ of ~1.2‰ through this time period (Figure 3). A significant, step-wise decline is seen in both Shannon H diversity (3.265 to 2.749) and evenness (0.460 to 0.274) in CP12a-CP13b, which reach a minimum (2.75 and 0.274, respectively) just above the CP14a boundary. Species richness also decreases above the EECO, but appears to rebound more rapidly, due to the diversification of the *Reticulofenestra*/*Dictyococcites* group, which dominates the assemblage through the Lutetian (μ = 46.2%; Max. = 56.6%; Figures 5, 6). Warm water taxa, which peak in the Ypresian, decline above the EECO through the Lutetian (μ = 12.5%; Min.: 8.5%; Figures 5, 6).

Middle Eocene Climatic Optimum (MECO)

The Middle Eocene Climatic Optimum (MECO) was a transient warming event in the late middle Eocene (~40.0 Ma), superimposed on a long-term middle and late Eocene cooling trend (Bohaty et al. 2009; Jovane et al. 2007; Bohaty and Zachos 2003). Recent work by Bohaty et al. (2009) correlated the MECO to two nannofossil events: 1) the LO of *Dictyococcites scrippsae* at low latitudes and 2) the LO of *Cribrocentrum reticulatum* at southern high-latitude sites. The LO of *D. scrippsae* cannot be used as a proxy for the MECO at Site 762 due to differing taxonomic concepts, and the known latitudinal diachroniety of *Cr. reticulatum* (discussed above) at this mid- to low-latitude site also prohibits use as a proxy for this event. Despite these restrictions, the general isotopic pattern can be identified: A long term

increase in $\delta^{18}O$ in the middle Eocene, followed by a rapid decrease of ~1.0‰ (Figure 3). The long Lutetian cooling shows evidence of reversal at Site 762 with a -0.66 ‰ shift in $\delta^{18}O$ within CP14a.

The decrease in $\delta^{18}O$ coincides with a rapid increase in Shannon diversity (2.89 to 3.33) and evenness (0.306 to 0.489) (Figure 3). This transition initiated the second sustained period of high diversity in the Eocene, which gradually deteriorated through the Bartonian and Priabonian. Warm taxa increased through the event (*Discoaster, Sphenolithus* spp.: Figure 5; *Ericsonia formosa*: Figure 4) with peak abundance at the end of the MECO (18.2%, Figure 6), but underwent a slow decline through the remaining interval (Figure 6). Similar to the EECO, cool taxa exhibited a short pulse at near the top of the event, linked to the LO of *Reticulofenestra daviesii* (Figure 6). *Reticulofenestra* spp. and *Dictyococcites scrippsae* both declined near the MECO (Figure 5). Abundance trends of *D. scrippsae* near the EECO and MECO suggests a cool affinity for this species.

Late Eocene cooling

In general, the Bartonian and Priabonian are marked by global cooling. The peaks in diversity, evenness, and species richness that occur near the MECO turn to a long-term decline through the CP14a-16a (Figure 3) and correlate to a long term global shift in $\delta^{13}C$ and $\delta^{18}O$ (Salamy and Zachos 1999; Zachos et al. 2001). At least two distinct phases of warming are superimposed on this long term trend. Jovane et al. (2007, fig 10) show shifts in $\delta^{18}O$ (~ -1.0‰) and $\delta^{13}C$ (~ 0.7‰) at the Contessa Highway Section (Italy) between ~37-36.5 Ma, with the main warming occurring over ~2.0 My. Bohaty and Zachos (2003, fig.2) show similar $\delta^{18}O$ and $\delta^{13}C$ trends in the Southern Ocean, with an initial rise beginning ~37 Ma and ending ~1.5 My later. These dates correlate to upper CP15a-lower CP15b, which coincides with a conspicuous peak in $\delta^{18}O$ (-0.1 ‰ to -0.6‰) at Site 762 (~232.0-213.0 mbsf; Figure 3).

This isotopic shift actually corresponds to a slight drop in diversity, evenness and species richness at Site 762 (Figure 3). Smaller scale warming events such as these may have acted to temporarily suspend or reverse the middle to late Eocene trend; however, the late Eocene (Priabonian) warming does not

appear to reverse the long term decreases in diversity of the nannofossil assemblage seen through the late Eocene (Figure 3).

The abundance of *Sphenolithus* spp. declined through the Bartonian cooling particularly in CP14b-early CP15a (μ = 2.7%; Min. = 1.4%), but showed only a modest increase in association with the late Eocene warming (Figure 5). *Ericsonia formosa* declined above the MECO through the Bartonian (μ = 2.0%), but showed a notable peak through the late Eocene warming (μ = 3.7%; Max. = 6.2%) (Figure 4). *Dictyococcites bisectus* and *D. stavensis* appeared in the Bartonian, with peak abundance through the late Eocene warming (μ = 14.3%; Max. = 19.4%) but declined significantly above the event (μ = 5.0%, Min. = 3.1%). Peak abundance near the middle-late Eocene boundary is seen by Villa et al. (2008), and Wei and Wise (1990b, fig. 12) also show that *D. bisectus* is significantly more abundant below 40° latitude. These patterns of abundance, with respect to late Eocene warming and other warm-water taxa, suggests that *D. bisectus* and *D. stavensis* had an affinity for warmer conditions. Conversely, the warm-water *Discoaster* spp. increased through the Bartonian cooling (μ = 6.5%; Max. = 9.4%) and decreased through the late Eocene warming (μ = 3.4%; Min. = 1.6%). This is linked to peak abundance of *D. barbadiensis, D. saipanensis,* and *D. nodifer* in the Bartonian (μ = 1.7%, 2.2%, and ~1.0%, respectively), declining by 0.5-1.5% each through the Priabonian. Lower abundance during warm intervals may indicate an oligotrophic response to more mesotrophic to eutrophic conditions through this interval at Site 762. *Cyclicargolithus floridanus* is associated with high productivity (Aubry 1992; Monechi, Buccianti and Gardin 2000). This species was most abundant through CP15a (μ =7.5%) reaching a peak at the base of the late Eocene warming (11.0%), followed by a significant decline through this period. Peak abundance is not centered around the late Eocene warming and $\delta^{18}O$ excursion, and is not likely controlled directly by temperature, but suggests more mesotrophic to eutrophic conditions.

Cool taxa declined through the late Eocene warming (μ = ~1.0%), as indicated by a reduction in both *Reticulofenestra daviesii* and *Chiasmolithus* spp., but rebounded above the event (μ =2.2%) (Figure 6). *Cribrocentrum reticulatum* increased significantly above the MECO, with peak abundance during the

Bartonian cooling (μ = 5.9%; Max. = 10.1%), but decreased rapidly at the start of the late Eocene warming (0.2%) (Figure 4). The abundance of *Lanternithus minutus* declined through the late Eocene warming (μ = 0.7%), but rebounded significantly just above this event (μ = 4.8%; Max. = 8.65%) and through the remainder of CP15b (Figure 4). This pattern of abundance suggests a cool temperature affinity for this species.

"Terminal Eocene event"

Despite the brief late Eocene warming in the Priabonian, climate deterioration continued into the Oligocene, most notably with Oi-1 and the onset of significant ice sheet growth in Antarctica. The Oi-1 is not readily identified at Site 762, as isotopic and biostratigraphic data end near this interval. Nevertheless, some of the preceding isotopic shifts and bioevents can be identified. The $\delta^{13}C$ shows a sustained increase of ~1.0‰ just above the CP16a boundary (192.75 mbsf), and coincides with a $\delta^{18}O$ increase of ~0.5‰. A significant drop in Shannon diversity occurred near the top of the section (189.47 mbsf), from an average of 2.9 through CP16a to the lowest diversity (2.674) and species richness (44) since the Ypresian (Figure 3). This is attributed to the decline in *E. formosa*, *C. protoannulus, L. minutus, B. serraculoides,* and *Z. bijugatus*. The sample immediately above this isotopic shift marks the base of the *Clausicoccus* acme observed in Hole 762C (185.01 msbf). Warm water taxa continued to decline through the Priabonian, while cool taxa, particularly *R. daviesii*, show a maximum near this positive $\delta^{18}O$ shift, but quickly decline above this interval (Figure 6).

Dunkley-Jones et al. (2008) show peak abundance of holococcoliths ~0.6 My below the E-O boundary, followed by a significant decline. At Site 762, *L. minutus* decreased from a maximum of 8.6% near the base of CP16a to an upper Eocene minimum of ~1.0% at the base of the *Clausicoccus* spp. acme (Figure 4). Similarly, *Z. bijugatus* declined from an average of 11.2% through CP16a to 5.4% at the base of the *Clausicoccus* spp. acme (Figure 4). This decline in holococcolith taxa (Figure 6) and in Shannon diversity (Figure 3) closely correlate to positive shifts in both $\delta^{18}O$ and $\delta^{13}C$, and may indicate proximity

to the E-O boundary at Site 762. Dunkley-Jones et al. (2008) also define a group of taxa that are abundant below the Oligocene boundary but decline rapidly through the E-O transition, including *C. protoannulus, L. minutus, Z. bijugatus,* and *R. dictyoda.* At Site 762, this group exhibited peak abundance at the base of CP16a (~42%) but declined to 21.2% by the top of the section. This trend also suggests proximity to the E-O boundary at Site 762.

Helicosphaera spp. were quite rare during the late Eocene warming (μ = <0.5%), but began to increase above this event, particularly *H. compacta* (μ = 2.2%). This species showed peak abundance at the excursion (4.0%), with a pattern of abundance similar to *L. minutus* and *Z. bijugatus* (Figure 4). We also observe an interesting pulse of thinly-calcified, indeterminate nannoliths in Hole 762C (Plate 9-6 to 9-13), with maximum abundance in CP16a (μ = 4.2 %, Max. = 5.6%) and a rapid decline (μ = 1.2%) coincident with the base of the *Clausicoccus* spp. acme.

Several lines of evidence suggest that the top of the interval examined in Hole 762C is very near the Oi-1 event, but it cannot be confidently placed. Magnetostratigraphic data for Site 762 terminates in Core 5, with ~14 m of Chron C13r, but does not identify the C13n reversal. Our nannofossil biostratigraphy terminates in Core 3, above the CP16a boundary, but we do not identify the CP16b boundary. It is possible to distinguish the base of the *Clausicoccus* acme, where *Clausicoccus* spp. increase from ~1.0% (190.24 msbf) to 6.1% (184.49 msbf), but our data does not identify the acme top. Isotopic stratigraphy continues through Core 2, showing a positive $\delta^{18}O$ shift of 1.02‰ (189.72-171.28 msbf). In addition, a positive shift in $\delta^{13}C$ of 0.95‰ (194.24-179.73 msbf) precedes a decrease of 0.42‰ (171.28 msbf; top of available data). All available datasets terminate near the Oi-1 event, but it cannot be identified fully.

3.3 - Problem Taxa

There is some debate as to the environmental affinities of *Zeughrablithus bijugatus* and *Cribrocentrum reticulatum* as summarized by Villa et al. (2008, table 3), with respect to temperature, nutrient levels, and water depth. Trends observed at Site 762 are discussed below.

Zeughrablithus bijugatus

Data from Hole 762C suggests a warm-water affinity for *Z. bijugatus*: Abundance curves mirror $\delta^{18}O$, increasing during the warm Ypresian, peaking through the EECO and declining during the Lutetian cooling. Above this level, the response does not appear to be primarily linked to temperature, with abundance increasing through the Bartonian cooling and dropping during the late Eocene warming (Figure 4). The abundance pattern of *Z. bijugatus* is similar to *Discoaster* spp. (Figure 5) and inverse to *Cyclicargolithus floridanus* (Figure 4), suggesting a greater affinity for oligotrophic conditions. The environmental factors that drive changes in abundance of *Z. bijugatus* may be complex, accounting for the significant disagreement between various nannofossil workers (Villa et al. 2008) and likely requires a detailed, species-specific study.

Cribrocentrum reticulatum

The paleoecological summary of *Cr. reticulatum* from Villa et al. (2008, table 3) shows warm to 'not warm' temperature preferences and mesotrophic to oligotrophic nutrient affinities. *Cribrocentrum reticulatum* increases through the MECO, with peak abundance through the Bartonian and lower Priabonian (μ = 5.9%; Max. = 10.1%), dropping rapidly at the base of the Late Eocene warming (0.2%) (Figure 4). This suggests a preference for temperate conditions. The pattern of abundance of this species is also similar to *Discoaster* spp. (Figure 5), with potential for oligotrophic affinities.

3.4 - Summary

Several notable changes are observed in the nannofossil assemblage that correlate closely to short isotopic excursions or long term trends in $\delta^{13}C$ and $\delta^{18}O$ (Figures 3-7). Patterns of nannofossil diversity and evenness broadly mirror the $\delta^{18}O$ curve, and are primarily attributed to changes in paleotemperatures, but also to fluctuations in nutrient levels associated with circulation and thermal stratification of the water column. Warm water taxa dominate through much of the Eocene, showing the most significant decline through the Lutetian. Cool taxa show only a modest increase in the Bartonian and Priabonian, supporting the overall temperate to warm water interpretation of the site.

Increased rates of speciation and extinction are associated with the PETM and the end of the EECO. These periods of increased turnover are highlighted by events such as the *Fasiculithus*/*Zygrhablithus* crossover at the PETM and by the *Toweius*/*Discoaster* and *Discoaster*/*Reticulofenestra* assemblage turnovers near the base and top of the EECO, respectively. A significant number of bioevents have been identified across the PETM in high-resolution studies, and data from Site 762 and Jiang and Wise (2009) suggest that many of these key changes can be identified in even coarsely sampled or poorly recovered intervals. Though the dominance reversal of *Toweius* and *Reticulofenestra* is well known, the *Discoaster* acme that links these dominant assemblages, identified at Site 762 and Possango (Agnini et al. 2006), indicates two potentially global and synchronous nannofossil assemblage turnovers associated with the EECO. While several isotopic events correlate to significant changes in the nannofossil assemblage, relatively modest changes were observed across the ETM2, ETM3 or MECO events. This may be a true representation of the nannofossil response, but is likely muted by the moderate sample spacing, requiring a higher-resolution sample interval to identify the changes across these short events.

Patterns of abundance of several taxa suggest that changes in the nannofossil assemblage in the early Eocene were influenced primarily by changes in temperature. Above the MECO abundance

patterns of some key taxa, such as *Discoaster* spp. and *C. floridanus*, suggest that the assemblage was also affected by more meso- to eutrophic nutrient levels. Peaks in cool water taxa, holococcoliths, and thinly-calcified indeterminant nannoliths are observed in the Priabonian. Further investigation may reveal significant paleoecological relationships or information on paleoenvironment and nannofossil calcification.

Chapter 4 - SYSTEMATIC PALEONTOLOGY

Several new taxa were identified during this study including one genus (*Hexadelus*), eight species (*Calcidiscus ellipticus*, *Cruciplacolithus nebulosus*, *C. opacus*, *Cyclicargolithus parvus*, *Hayella ovata*, *Markalius latus*, *Pedinocyclus annulus*, *Hexadelus archus*) and at least two species variants (*Hayella simplex* var. *petalus*, *Pedinocyclus larvalis* var. *minimus*). It is still unclear whether these variants represent 'normal' phenotypic variation, a preservational artifact, or are unique and distinct species.

Systematic descriptions are located within Appendix A. Holotype and paratype materials and photographs, are located within the collections of the ODP Micropaleontological Reference Center at the University of Nebraska State Museum (UNSM). Species description uses terms recommended by Young et al. (1997). The appendix follows the higher taxonomic organization of Young and Bown (1997) and Young et al. (2003).

Chapter 5 - CONCLUSIONS

Numerous recent advances in our knowledge of Eocene calcareous nannofossil biostratigraphy, taxonomy, abundance trends, and paleoecology provide an opportunity to reevaluate the Eocene biostratigraphic succession and its relationship to long-term assemblage changes at Site 762. This research was conducted to fulfill a need for a continuous Eocene calcareous nannofossil reference section,

containing range and abundance data for a vast number of Eocene species, relative to the preexisting CP and NP biostratigraphic zonation schemes.

Cross-correlation between the CP and NP standard nannofossil zonation schemes identified three stratigraphic hiatuses at Site 762: Hiatus A (CP8b) occurs across the Paleocene-Eocene boundary. The highly skewed assemblage in CP8a suggests dissolution in association with the PETM. Hiatus B (NP13) indicates a stratigraphic break in the upper Ypresian, closely correlated to the EECO. Hiatus C is identified by the absence of CP13c/NP15c and the convergence of the LOs of *Reticulofenestra umbilica* and *Nannotetrina fulgens* with the HO of *Chiasmolithus gigas*. A paleogeographic and stratigraphic summary of the northwestern Australian margin (Gradstein 1992) suggests an erosional disconformity on portions of the central Exmouth Plateau in the middle Eocene, though Site 762 was thought to show continuous deposition. Results from this study suggest that at least part of the stratigraphic record is affected by erosion or non-deposition on the central Exmouth plateau.

Most taxa in the CP and NP zonation schemes represent highly useful and reliable bioevents; however, comparison of our data to both the Site 762 nannofossil biostratigraphy of Siesser and Bralower (1992) and to other research highlights several problem taxa where rarity or potential diachroniety inhibits (or prohibits?) their application at many sites. The rarity of some taxa, such as *Chiasmolithus grandis* and *Ch. gigas*, was overcome by increasing the number of FOVs; however some marker taxa were sporadic (*Discoaster bifax)* or absent (*Blackites gladius*) at Site 762 and could not be applied biostratigraphically. Comparison of the range of *Discoaster sublodoensis* (CP12a/NP14a) from several sites suggests this bioevent is inconsistent and should be applied tentatively.

Well-calibrated alternative bioevents are needed to act as proxies for rare and or/diachronous marker taxa. Some species already show great potential as proxy events, such as the LO of *S. radians*, while others, such as the LOs of *D. bisecta* and *S. spiniger*, will require additional investigation and calibration. These secondary markers need not be synchronous with the primary marker, as long as the

relative offset between events is understood across both paleolatitude and paleodepth. The notably diverse and robust Eocene assemblages shown at Site 762 and by Bown and others (2007, 2006, 2005) suggests a wealth of potential bioevents, from both well-known taxa and in the >70 recently identified Eocene species, including eight new species and one new genus in the present research. The potential to increase the biostratigraphic resolution of the Eocene will be further influenced by the development of high-precision orbital biochronology.

Advancements in global isotope stratigraphy since the original expedition allows the calcareous nannofossil data from Exmouth Plateau to be correlated to $\delta^{13}C$ and $\delta^{18}O$ data from Site 762. These data were compared to the isotope records generated by previous workers, to examine the relationships between nannofossil turnovers and assemblage shifts with known climate variability throughout the Eocene. Several changes are observed in the nannofossil assemblages that closely correlate to both short isotopic excursions and long term trends in $\delta^{13}C$ and $\delta^{18}O$ (Figures 3-7), including the PETM, ETM2, ETM3, EECO, MECO, a period of late Eocene warming, and the Oi-1 isotopic events. Increased rates of nannofossil turnover as observed primarily at the PETM and during the EECO, but also the ETM3 event. Arguably the most significant turnovers occur near the base and top of the EECO, among the *Toweius, Discoaster and Reticulofenestra* groups, also documented at Possango (Italy) (Agnini et al. 2006). Patterns of nannofossil diversity, evenness, and species richness broadly mirror changes in $\delta^{18}O$, with highest diversity during warmer periods. This reflects the affinity of calcareous nannoplankton for stable, stratified surface water, allowing niche partitioning within this generally oligotrophic group.

Though nannofossil abundance patterns appear to be primarily temperature driven through the Ypresian and Lutetian, abundance trends of *Discoaster* spp. and *Cyclicargolithus floridanus* suggests the influence of meso- to eutrophic nutrient levels in the Bartonian and Priabonian. Despite the general cooling and climate deterioration through the Eocene, nannofossil diversity and species richness remains relatively high through the late Eocene at Site 762. The relationships between temperature and tropic affinity can be difficult to unravel within a nannofossil assemblage; however, there is significant evidence

to suggest that these communities were greatly affected by both shorter term environmental perturbations and long term climate change, with originations, extinctions, and dominance shifts that permanently alter the structure of the nannoplankton community. Significant advancements continue to be made in calcareous nannofossil biostratigraphy, taxonomy, and community structure, even within relatively well-understood geologic time periods. Such studies contribute significantly to our knowledge, but also highlights the need for continuing research in both paleoecology and well-calibrated nannofossil biochronology.

Section II - A new calcareous nannofossil species of the genus *Sphenolithus* from the Middle Eocene (Lutetian) and its biostratigraphic significance

Chapter 1 - INTRODUCTION

A new species of calcareous nannofossil, *Sphenolithus perpendicularis* sp. nov. was identified during a high resolution biostratigraphic study of Eocene open-ocean sediments from Ocean Drilling Program (ODP) Leg 122 Site 762C (Figure 1). *Sphenolithus perpendicularis* sp. nov. shows a unique morphology and is moderately abundant over its notably short stratigraphic range, giving potential for use in nannofossil biostratigraphy. This utility is enhanced particularly in sections where *Nannotetrina* spp. are rare to absent, as is the case at Site 762C. *Sphenolithus perpendicularis* sp. nov., along with related species *S. furcatolithoides* and *S. coniculus* show considerable potential as alternate subzonal markers within CP13 (of Okada & Bukry, 1980) (equivalent to NP15 of Martini, 1971).

Chapter 2 - MATERIALS AND METHODS

The primary locality in this study is ODP Leg 122 Site 762C, located on the central Exmouth Plateau (19°53.23S, 112°15.24E), separated from the Australian Northwest Shelf by the Kangaroo Syncline (von Rad *et al*., 1992). Eocene pelagic sediments from this locality consist of white to green-grey, calcareous oozes, chalks, and marls, indicating a mature, open-ocean setting (von Rad *et al*., 1992). Site 762C was drilled in 1360m of water, with decompacted burial curves signifying little change in depth since the time of original deposition (Haq *et al*., 1992). Calcareous nannofossils are moderately to well preserved, with deposition well above the carbonate compensation depth (CCD). Secondary localities used in this study include Deep Sea Drilling Program (DSDP) Leg 77 Site 538A (Buffler *et al*., 1984) in

the eastern Gulf of Mexico (23°50.95'N, 85°09.93W), and ODP Leg 159 Site 960A (Mascle *et al*., 1996), Ivory Coast, Ghana (3°34.979'N, 2°44.009'W) (Figure 1).

Smear slide preparation for Site 762C followed standard techniques, as described by Bown & Young (1998) and were mounted using Castolite AP Crystal Clear Polyester Resin. Smear slides from Sites 538A and 960A were prepared previously for the University of Nebraska-Lincoln Micropaleontology Repository using the double slurry method (Watkins & Bergen, 2003) and mounted with Norland 61 optical adhesive. Smear slides were examined at 1250x magnification with an Olympus BX51 under plane parallel light (PL), cross-polarized light (XPL), and a one-quarter λ mica interference plate. Univariate analysis of key morphological characteristics was conducted using PAST (Hammer *et al.,* 2001).

Chapter 3 – *Sphenolithus* ABUNDANCE AND DISTRIBUTION

The relative abundance of *Sphenolithus perpendicularis* sp. nov. was documented throughout its observed range in Core 16 of Site 762C (Figure 11). Though numerically few (1 specimen per 2-10 fields of view), this species shows a notable increase in abundance near the central portion of its range (Figure 11). The lowest occurance (LO) of *S. perpendicularis* sp. nov is located near the base of biostratigraphic subzone CP13a (NP 15), marked by the LO of *Nannotetrina fulgens (*syn. *N quadrata, N. alata)* (Figure 12). The highest occurance (HO) is located near the top of subzone 13a, marked by the LO of *Chiasmolithus gigas*.

Following initial identification at Site 762C, *S. perpendicularis* sp. nov. was also observed at DSDP Leg 77 Site 538A-17-4-(111-113cm) in the eastern Gulf of Mexico, as well as at ODP Leg 159Site 960A-14CC along the Ivory Coast, Ghana (Figure 1). The biostratigraphic zonation of these samples were derived from Lang & Watkins (1984) and Shafik *et al*. (1998), respectively. Presence of *S. perpendicularis* sp. nov. in the Indian and Atlantic Oceans, as well as the Gulf of Mexico, indicates a

widely distributed species; however, all sites were located below 25° paleolatitude, which may indicate a restriction to tropical to sub-tropical latitudes.

Chapter 4 – *Sphenolithus* MORPHOLOGY AND LINEAGE

Sphenolithus perpendicularis sp. nov. consists of a small to medium sphenolith base with two tapering, apical spines, that diverge to ~90° just above the basal cycles. Standard sphenolith morphological terms are described in Figure 13. Though *Sphenolithus perpendicularis* sp. nov. shares a dual apical spine with *S. furcatolithoides*, these species differ in significant ways: *S. perpendicularis* sp. nov. shows a wide angle of divergence ($\mu = 96.1°$, N = 30) between the apical spines, which occurs just above a more prominent lateral cycle, and appears stratigraphically restricted to subzone CP13a. *Sphenolithus furcatolithoides* shows a distinctly acute angle of divergence that occurs more distally from a reduced lateral cycle. In addition, *S. furcatolithoides* does not appear until CP13b at Site 762C. As the LO of *S. furcatolithoides* is shown near the base of NP15 (CP13) in Perch-Nielsen (1985, fig. 69), *S. perpendicularis* sp. nov. has likely been grouped with the former, though it is now apparant that these two distinct species show little, if any, stratigraphic overlap. The precise degree of overlap cannot be determined from Site 762C due to only partial recovery near the CP13a-CP13b boundary. The true stratigraphicv relationships will likely be refined with a more continuous section at the CP13a/13b boundary.

The morphological trends from *S. perpendicularis* to *S. furcatolithoides* continues with *S. cuniculus*, whereby the base is further reduced, the angle between the apical spines becomes more acute, and divergence of the spines occurs more distally than in *S. furcatolithoides*. Key characteristics used to identify these three species can be seen when aligned at 0° as well as at 45° under cross-polarized light, and are shown in Figure 14 and Plate 10.

Perch-Nielsen (1985, fig. 69) hypothesized the evolution of *S. furcatolithoides* from the *S. annarhopus- S. orphanknollensis-S. spiniger* lineage. Evidence from this study indicates that *S. furcatolithoides* does not arise directly from *S. spiniger*, but rather from the short-lived *S. perpendicularis* sp. nov. (Figure 15). If *S. perpendicularis* sp. nov. is an ancestral species of *S. furcatolithoides,* then this new species may also be related to this lineage. This relationship would require some reorganization of the crystal units, so that the small central spine of *S. spiniger* is further reduced and two divergent units, birefringent at 0°, are enlarged. This issue is unlikely to be resolved without further investigation using a scanning electron microscope (SEM).

Sphenolithus perpendicularis sp. nov. is also morphologically similar to *S. capricornutus* in that both bear widely divergent apical spines that are highly birefringent when aligned with the polarizers. There are notable differences between these species when oriented at 45° (Figure 14), with *S. perpendicularis* sp. nov. having four birefringent crystals in the proximal and medial cycles and *S. capricornutus* having only two crystals birefringent, in the proximal cycle only. In addition, there is a prominent stratigraphic separation of more than 15 Myr.: *S. perpendicularis* sp. nov. appears restricted to CP13a (NP15) (Middle Eocene; Lutetian), while *S. capricornutus* first appears in the latest Oligocene (Chattian), in CP19b (NP25). If *S. perpendicularis* sp. nov. does indeed develop from *S. spiniger*, and the remainder of the lineage given by Perch-Nielsen (1985) is correct, then the apical spine morphology associated with *S. perpendicularis* sp. nov. and *S. capricornutus* must have developed iteratively within two distinct lineages.

Chapter 5 - *Sphenolithus* BIOSTRATIGRAPHIC SIGNIFICANCE

Currently nannofossil biozone CP13 is divided into three subzones, where the LO of *Nannotetrina fulgens*, the LO of *Chiasmolithus gigas* and the HO of *C. gigas* mark the bases of CP13a, CP13b, and CP13c, respectively (Figure 12; Table 8). As stated above and as noted by Perch-Nielsen

(1985), *N. fulgens* is rare to absent in many sections, often reducing its biostratigraphic utility. As a result, many nannofossil workers employ the HO of *Rhabdosphaera inflata* as a secondary marker for the base of CP13a. Although this has provided a useful alternative, *R. inflata* can also be rare, leading to an ambiguous HO. *Chiasmolithus gigas* may also be rare in some localities, such as Site 762C.

When historic markers are rare to absent *S. perpendicularis* sp. nov.*, S. furcatolithoides,* and *S. cuniculus* may prove to be useful substitutes. The LO of *S. perpendicularis* sp. nov. closely approximates the base of CP13a, as it coincides with the LO of *N. fulgens* and is just above the HO of *R. inflata* at Site 762C (Figure 12; Table 8). The HO of *S. perpendicularis sp. nov.* occurs just below the LO of *C. gigas* at the base of CP13b, which also marks the LO of *S. furcatolithoides*. Bown (2005, fig. 1) also show the LO of *S. furcatolithoides* within CP13b, though above the LO of *C. gigas*. The LO of *S. cuniculus* occurs in CP13b, though near the top of this subzone. This range was confirmed by the short overlap with *C. gigas,* facilitated by the highly expanded section at Site 762C. A short stratigraphic overlap was also observed between *S. furcatolithoides and S. cuniculus.* This overlap of *C. gigas*, *S. furcatolithoides,* and *S. cuniculus* can be used to identify the uppermost portion of CP13b. The HO of *S. furcatolithoides* occurs j ust slightlyabove the HO of *C. gigas* at Site 762C, so that only *S. cuniculus* remains throughout CP13c. In summation, the stratigraphic data provided at Site 762C (Figure 12; Table 8) indicates potential for secondary markers, using *S. perpendicularis* sp. nov.*, S. furcatolithoides*, and *S. cuniculus* as a means to approximate subzones within CP13.

Chapter 6 – *Sphenolithus perpendicularis* n. sp. SYSTEMATIC PALEONTOLOGY

All figured specimens and type species are housed in the Micropaleontology Collections at the University of Nebraska-Lincoln. Species description uses terms recommended by Young *et al*. (1997). Basic Sphenolith terminology is illustrated in Figure 13.

Order DISCOASTERALES Hay, 1977

Family SPHENOLITHACEAE Deflandre, in Grassé, 1952

Genus *Sphenolithus* Deflandre, in Grassé, 1952

***Sphenolithus perpendicularis* sp. nov.**

Pl. 1, figs. 1-6

Derivation of name: From the Latin *perpendicularis*, referring to the near-perpendicular angle between the apical spines immediately above the proximal base.

Diagnosis: Sphenolith with a small- to medium-sized base, bearing two tapering, apical spines that diverge to ~90° just above the basal cycles.

Description: Proximal cycle consisting of about 10 elements, greater than half the length of the base, supporting a lateral cycle that is equal to or less than the width of the proximal cycle, giving a generally square outline. The base supports two prominent apical spines centered about the median axis, which are widely divergent just above the base. Measurement of 30 specimens yields a mean angle of divergence of 96.1°. These spines may be more than twice the length of the base in well preserved specimens, but may break or dissolve in more poorly preserved forms. When the long axis is oriented at 0° under cross-polarized light, the outer elements of the proximal base, upper lateral cycle, and apical spines are highly birefringent. When oriented at 45° the central elements of the proximal base and the lateral cycle are highly birefringent, with the prominent apical spines being extinct (Figure 14). Specimens may also show an enlarged element in the upper cycle, centered about the median axis, which projects above the base between these larger spines. In less well preserved specimens this enlarged element may approximate the length of the spines, giving specimens a more tricuspid appearance. Imaging of these specimens was difficult due to poor preservation and high birefringence.

Differentiation: *Sphenolithus perpendicularis sp. nov.* can be differentiated from *S. capricornutus* by the birefringence pattern observed at 45°, as shown in Figure 14. These species can be further distinguished

by a prominent stratigraphic separation of more than 15 Myr. *Sphenolithus perpendicularis sp. nov.* may be differentiated from *S. furcatolithoides* by the significantly wider angle of divergence of the spines. In addition, there appears to be little, if any, stratigraphic overlap of these two species.

Dimensions: (N=30 for base width, height, and interior angle). Base Width: Min.: 3.2 µm; Max.: 4.8 µm; Mean: 4.0 µm; Std. Error: 0.08; Variance: 0.21. Base Height: Min.: 3.2 µm; Max.: 4.8 µm; Mean: 4.0 µm; Std. Error: 0.08; Variance: 0.21. Apical Spine Interior Angle: Min.: 85.5°; Max.: 115.8°; Mean: 96.1°; Std. Error: 1.3; Variance: 0.51. Spine Length: From 2.0 µm - 8.5 µm; dependant on preservation.

Holotype: Pl. 1, fig. 1. **Paratype:** Pl. 1, fig. 2

Type locality: ODP Leg 122, Exmouth Plateau, Western Australia

Type level: Middle Eocene (Lutetian), Site 762C-16-2-(125-126 cm)

Occurrence: CP13a; 762C-16-4-(45-46) to 762C-15-3-(48-49)

Section III - Eocene Bio-Geochronology of ODP Leg 122 Hole 762C, Exmouth Plateau (Northwest Australian Shelf)

Chapter 1 - INTRODUCTION

The geologic time scale has seen significant evolution since the original interpretation of Hole 762C in 1992. High impact research includes the widely employed geomagnetic polarity time scale of Cande and Kent (1995, CK95) and the resultant integrated magnetobiochronologic scale of Berggren et al (1995, BKSA95). Both of these calibrated scales had significant influence on the geologic time scales of Gradstein Ogg and Smith (2004) and Ogg Ogg and Gradstein (2008). In addition to the increased control of microfossil bioevents and magnetic polarity reversals, there has been significant improvement in the resolution of $\delta^{13}C$ and $\delta^{18}O$ isotope stratigraphy through the Eocene (Bohaty et al. 2009; Cramer et al. 2009; Sluijs et al. 2008; Jovane et al. 2007; Nicolo et al. 2007; Lourens et al. 2005; Bohaty and Zachos 2003; Cramer et al. 2003; Zachos et al. 2001; Salamy and Zachos 1999). This progress within these individual disciplines, and with integration of these different types of stratigraphic data, has changed the way a particular succession may be evaluated. In general, there was a tendency to assume that many deep sea succession were continuous, particularly in passive geologic settings with high accommodation; however, in the last 20 years, particularly since Berggren et al. (1995a), integration of these biostratigraphic, isotopic, and magnetostratigraphic data have shown how incomplete many of deep-sea successions truly are (Florindo and Roberts, 2005; Aubry, 1995; Gradstein, 1992).

Ocean Drilling Program Leg 122 Hole 762C (northwest Australian Shelf) was selected for a previous study of Eocene calcareous nannofossils (Section I) as aspects of the stratigraphic record were well constrained by previous biostratigraphic data (Siesser & Bralower 1992) and depositional models (Golovchenko et al. 1992; Haq et al. 1992), which proposed an essentially complete Eocene record. Reexamination of the calcareous nannofossil biostratigraphy (Section I) showed several potential hiatuses

within this 'continuous' section. Attempts to ameliorate these issues through cross-correlation of planktonic foraminiferal P-zones, magnetostratigraphic reversals and isotopic excursions further supported the presence of these hiatuses. The present research was conducted to fulfill the need for a new, integrated age model for Hole 762C.

Biostratigraphic, magnetostratigraphic, and isotopic data were published in the Leg 122 *Initial Reports* (Haq et al. 1990) and *Scientific Results* (von Rad et al. 1992); however, these data sets have not been fully integrated to produce a robust chronostratigraphic framework.

Galbrun (1992) used calcareous nannofossil data of Siesser and Bralower (1992) to guide the magnetostratigraphic interpretation, but issues of core recovery (and undetected hiatuses) limited this interpretation. As noted by Berggren, et al. (1995b), Hole 762C does represent a well preserved and expanded Eocene section; however, data from this site was not used in calibration of the Berggren et al. (1995b) integrated magnetobiochronologic scale (IMBS) (hereafter referred to as BKSA95), as the authors believed the data of Galbrun (1992) should be reinterpreted. Though some issues do exist with the interpretation of Galbrun (1992), we believe many of these can be resolved with integration of additional nannofossil events, as well as planktonic foraminiferal and $\delta^{13}C$ and $\delta^{18}O$ data from Hole 762C.

Recent and substantial interest in the chemostratigraphy of the Cenozoic has produced high-resolution $\delta^{13}C$ and $\delta^{18}O$ isotopic records for the Eocene (Galeotti et al. 2010; Bohaty et al. 2009; Pearson et al. 2008; Jovane et al. 2007; Lourens et al. 2005; Bohaty and Zachos 2003; Cramer et al. 2003; Zachos et al. 2001, others). Several isotopic excursions identified in these records have been linked to significant short- and long-term paleoenvironmetnal changes. When Hole 762C was originally drilled in 1990 these distinct $\delta^{13}C$ and $\delta^{18}O$ excursions, and the associated environmental events, were just recently described (PETM), or had not yet been identified (ETM2, Eocene thermal maximum 2). Today these events are not only readily identified and better understood, but have been dated by several groups of researchers,

providing another set of calibration points that can be integrated with magnetostratigraphic and biostratigraphic data.

In general, key events near the base (PETM, Paleocene-Eocene thermal maximum) and top (Oi-1) of the Eocene are fairly well understood; however, the general magneto-biochronology of this epoch is still being developed. In addition, the relationships among paleontologic, magnetostratigraphic, and isotopic events, as well as their relationships to local and regional hiatuses, are still being determined. Integration of various data sets from Leg 122 Hole 762C may help to increase this understanding, particularly in the eastern Indian Ocean.

Here we reinterpret the original magnetostratigraphy from Hole 762C (Galbrun 1992) and integrate these data with biostratigraphic (Section I) and isotopic data sets (Thomas Shackle ton and Hall 1992), in order to develop a more robust geochronology for this locality. Though no stratigraphic breaks were originally identified in Hole 762C, this new interpretation suggests at least four hiatuses, within magnetozones C20n-C20r, C21n-C21r, C22r, and C24r, each 1-2 My in duration. Sedimentation rates derived from this revised age model are used to date significant nannofossil events, and these are compared to dates provided by, or derived from, several additional localities.

Chapter 2 - SETTING AND STRATIGRAPHIC CONTEXT

2.1 - ODP Leg 122 Hole 762C

ODP Leg 122 Hole 762C (19°53.23S, 112°15.24E) is located on the central Exmouth Plateau (northern Carnarvon Basin, Australia) and is separated from the Australian Northwest Shelf by the Kangaroo Syncline (von Rad et al. 1992) (Figure 1). Though rifting stretched the site in its early history, the plateau has been relatively inactive since the mid-Cretaceous. The plateau shows fairly uniform

thermal subsidence, with decompacted burial curves showing little change in depth since the time of original deposition (Haq et al. 1992).

Hole 762C was drilled in 1360m of water with ~ 240 m of Eocene sediments penetrated in Cores 3-29, ~180-422 meters below sea floor (mbsf). Core recovery varies considerably throughout this interval, ranging from 12 to ≥ 100%, with an average recovery of ~67% (Figure 16). Original estimates of sedimentation rates were 1-2 cm/ky in the early and late Eocene, slowing to < 1.0 cm/ky in the middle Eocene (Haq et al. 1990). Eocene pelagic sediments from this locality indicate a mature, open-ocean setting (von Rad et al. 1992), and are divided into three lithologic subunits: Unit II [3-3-(0 cm)-12-1-(0 cm)] is composed of white nannofossil chalk and extends from 181.5-265.0 mbsf. Unit IIIA [12-1-(0 cm)-26-10-(0 cm)] extends from 265.0-398.0 msbf and is composed of light green-grey and white nannofossil chalk with foraminifera. Unit IIIB [26-10-(0 cm)-29-1-(50 cm)] extends from 398.0-554.8 msbf and consists of light green nannofossil chalk. Both clay content and bioturbation increased downward toward the Lower Eocene.

2.2 - Additional Sites

The dates of calcareous nannofossil events derived from Hole 762C are compared to several additional global localities, particularly for bioevents that have not been calibrated in the BKA95 model. Localities were selected based on a well preserved and diverse nannofossil assemblage that provided good biostratigraphic control and the quality and completeness of magnetostratigraphic data. In an attempt to avoid difficult or ambiguous correlations, we avoid localities with issues that may compromise the stratigraphic interpretation, such as poor nannofossil preservation, weak magnetization, poor core recovery, or identified hiatuses. Localities were also selected for a broad global distribution, at various paleolatitudes and from several ocean basins. These additional localities are discussed briefly below.

The classic Italian sections of Possango, Bottaccione and Contessa Highway are included for comparison of nannofossil events to outcrop data. Biostratigraphic and magnetic polarity data for the

Possango section (45°50’02’’N, 11°31’01’’E) is from Agnini et al. (2006). Magnetostratigraphic data for the Bottaccione section is from Napoleone et al. (1983) and from Lowrie et al. (1982) for the Contessa Highway section. Calcareous nannofossil data for the Bottaccione and Contessa Highway sections are from Monechi and Thierstein (1985). Additional land-based correlations are derived from the southern Pyrenean foreland basin for C13r-C17n.1n (Cascella and Dinarès-Turell 2009), and from the New Jersey coastal plain for C21n-23n (Miller et al. 1990).

ODP Hole 1051A (Blake Nose) is located in the northwestern Atlantic Ocean (30°03.174’N, 76°21.458’W), and was drilled during Leg 171B. Calcareous nannofossil data are from Mita (2001) with magnetostratigraphic correlations of Ogg and Bardot (2001). Biostratigraphic data from Chrons C21n, C21r and C22n (~Cores 37-42) were not included due to a likely hiatus and ambiguity in polarity zone boundaries. ODP Site 1262 (Walvis Ridge) was drilled during Leg 208, and is located in the southeastern Atlantic Ocean, off the northwestern flank of Walvis Ridge (27°11.15´S, 1°34.62´E). The relative placement of bioevents within the magnetostratigraphic framework is from Agnini et al. (2007, table 1). ODP Hole 1090B (Agulhas Ridge) was drilled during Leg 177 and is located in the southeast Atlantic sector of the Southern Ocean (42°54’S, 8°53’E). Calcareous nannofossil data for this Site are by Marino and Flores (2002a, b), with depth of polarity zones from Channell et al. (2003). Data are integrated through C18n?, where magnetostratigraphy becomes more ambiguous (Channell et al. 2003, fig. 4).

Deep Sea Drilling Program (DSDP) Site 577 was drilled during Leg 86 and is located in the northwestern Pacific Ocean (32°26.51'N; 157°43.40'E). Calcareous nannofossil data are provided by Monechi (1985) with magnetostratigraphic data from Bleil (1985). Events are calibrated only from C24n-C25n, as depths of polarity reversals become ambiguous above this interval. ODP Sites 1218 (8°53.378´N, 135°22.00´W) and 1215 (26°01.77´N, 147°55.99´W) were drilled during Leg 199 in the central equatorial Pacific Ocean. Magnetic reversal calibration and biostratigraphic data for Site 1218 are both provided by Pälike et al. (2006). Calcareous nannofossil data for Holes 1215A-B are by Raffi et al. (2005) with depths of paleomagnetic reversals by Lyle et al. (2002). ODP Hole 1123C (Eastern New

Zealand) was drilled during Leg 181 and is located in the southwest Pacific (41° 47.147'S, 171° 29.941'W). Calcareous nannofossil data are derived from McGonigal and Di Stefano (2002) with magnetostratigraphy for Hole 1123C from the Leg 181 Shipboard Scientific Party (2000).

ODP Hole 1172A (East Tasman Plateau), located in the Southern Ocean (43°57.5854´S, 149°55.6961´E), was drilled during ODP Leg 189. Calcareous nannofossil and magnetostratigraphic data are from Wei, McGonigal and Zhong (2003) and Stickley et al. (2004). ODP Leg 113 Hole 689B (Maud Rise) is located in the eastern Weddell Sea (64°31.009'S, 3°5.996'E). Calcareous nannofossil data are from Wei and Wise (1990), with magnetostratigraphic data of Florindo and Roberts (2005).

Chapter 3 - DATA AND METHODS

3.1 - Magnetostratigraphy

The magnetic polarity data for Hole 762C are provided by ODP Leg 122 Scientific Results, which gives detailed sampling, laboratory, and analytical procedures (Galbrun, 1992). The polarity reversals and original magnetostratigraphic interpretation of Galbrun (1992) are provided in Figure 16. Poor core recovery in several sections creates ambiguous magnetostratigraphic patterns and greatly limits interpretation. Though the original interpretation does use nannofossil biostratigraphy to aid correlation of the magnetic polarity sequence, several issues exist with this original age model. Berggren, et al. (1995b) note that Hole 762C represents a well preserved and expanded Eocene section; however, despite Hole 762C's stratigraphic 'potential', data from this site was not used in the calibration of the BKSA95 IMBS. The authors question the original interpretation of Galbrun (1992), noting that "the magnetobiostratigraphic correlations in the site appear to be rather ambiguous" (Berggren, et al., 1995, p. 184). Despite the intermittent core recovery through Eocene sediments at Hole 762C, it is possible to generate a relatively robust age model with integration of additional stratigraphic data. This revised magnetostratigraphy for Hole 762C is discussed in the interpretation section below.

3.2 - Nannofossil Biostratigraphy

The detailed biostratigraphy, assemblage data, dominance trends, and systematic paleontology for Hole 762C have been examined in Section I, which provides information in nannofossil sample selection, preparation, and data collection. Sample interval and depth data for nannofossil biostratigraphy are provided in Table 1 for Cores 3-29. Nannofossil data for Core 2 is from Siesser & Bralower (1992). Core samples and smear slides are located within the collections of the ODP Micropaleontological Reference Center at the University of Nebraska State Museum (UNSM).

Two well known biozonation schemes are widely employed in Paleogene calcareous nannofossil biostratigraphy. Data from Section I includes both the low-latitude CP Zonation of Okada and Bukry (1980, with select subzones and secondary markers of Perch-Nielsen, 1985) and the cosmopolitan to high-latitude NP Zonation Martini (1971, with select subzones of Aubry, 1991). Strict application of some zonal boundaries was not possible, due to rarity or absence of some marker taxa (*Rhabdosphaera gladius, Discoaster bifax, Nannotetrina alata*). The CP and NP nannofossil biostratigraphy at Hole 762C is illustrated in Figure 16, and sample depths of key nannofossil marker taxa are summarized in Table 3. Biostratigraphic events will be referred to as lowest occurrence (LO), lowest consistent occurrence (LCO), highest occurrence (HO), highest consistent occurrence (HCO), acme beginning (AB), acme end (AE), abundance increase (INC) and cross-over (CO) (dominance reversal).

Concurrent application of both zonation schemes with the new data set (Section I) identifies zones and subzones that are absent from both the NP and CP zonation schemes: 1) Subzone CP8b is absent from Hole 762C, as both the primary marker (LO *Campylosphaera eodela*) and the secondary marker (LO *Rhomboaster* spp.) are concurrent with the biomarker for CP9a (LO *Discoaster diastypus*) (28-1-59 cm, 412.59 mbsf). This missing subzone is linked to an hiatus associated with the PETM. 2) NP13 is marked by the HO of *Tribrachiatus orthostylus* (also the 2° marker for CP11 (Perch-Nielsen, 1985)*;* however, there is no apparent separation between this biohorizion and the base of NP14a (LO

Discoaster sublodoensis), as both events were observed in the same sample. In fact, extrapolation upward and downward for the HO and LO, respectively, creates a depth cross-over as shown in Table 3. While it is quite possible that the LO of *D. sublodoensis* occurs 'early' at this locality, creating convergence, this relationship is also likely related to a hiatus within this interval. 3) CP13 is divided into subzones CP13b and CP13c by the LO and HO of *Chiasmolithus gigas*, respectively, and these subzonal markers are often similarly applied to NP15. Zone NP15c is severely reduced and subzone CP13c is absent from Hole 762C. The HO of *Ch. gigas* (14-6-50, 292 mbsf) shows very little stratigraphic separation from either the HO of *N. fulgens* (14-5-115, 291.15 mbsf) or the LO of *R. umbilica* (14-6-50, 292.00). The relative depths of these three bioevents strongly suggest a hiatus in this interval. These issues are considered when integrating various data sets, as well as in the final age model. Calcareous nannofossil tie-points used in the revised age model are summarized in Table 9.

3.3 - Planktonic Foraminifera Biostratigraphy

The original planktonic foraminiferal biostratigraphy for Hole 762C (Shipboard Scientific Party, 1990) was conducted at coarse sample spacing of one sample [CC]/core, or approximately every 10 m. Such resolution does not allow these bioevents to be used as calibrated tie points within the final age model; however, the planktonic foraminiferal P zonation (Berggren and Miller, 1988; Berggren and Pearson, 2005) as applied at Hole 762C can help guide the correlation of a particular polarity reversal to the GPTS. This data has given significant support to the present interpretation, based primarily on higher resolution nannofossil biostratigraphy. Core-scale resolution of planktonic foraminiferal P zones is shown in Figure 16. Specific intervals or correlations used to aide in magnetostratigraphic interpretations are discussed below.

3.4 - Isotope Stratigraphy

Stable isotope stratigraphy provides another valuable set of tie-points in our revised age model for Site 762, with bulk analysis of $\delta^{13}C$ and $\delta^{18}O$ provided by Thomas Shackleton and Hall (1992).

Significant advancements have been made in Paleogene isotope stratigraphy since the time of the original publication. The development of high-resolution global $\delta^{13}C$ and $\delta^{18}O$ records allows identification of several well-calibrated excursions through the Eocene (Bohaty et al. 2009; Cramer et al. 2009; Sluijs et al. 2008; Jovane et al. 2007; Nicolo et al. 2007; Lourens et al. 2005; Bohaty and Zachos 2003; Cramer et al. 2003; Zachos et al. 2001; Salamy and Zachos 1999). This plethora of research has also generated multiple names for one isotopic event, which are summarized in Sluijs et al (2008). For brevity, only the first of the several names provided in Table 10 will be used in discussion.

Many of the paleoenvironmetnal events recorded globally in $\delta^{13}C$ and $\delta^{18}O$ data have been correlated to nannofossil biostratigraphy and magnetostratigraphy, and can provide well calibrated dates (Table 10). The dates applied to several isotopic excursions were derived by the original authors using GPTSs such as the Cande and Kent (1995, hereafter CK95). The original dates for such isotopic excursions have been recalibrated to the timescale of Ogg Ogg and Gradstein 2008. Though the sampling spacing of stable isotopic data from Hole 762C was quite coarse (~2/core, Cores 2-17, 28-29; ~1/core, Cores 18-27) (Thomas Shackleton and Hall, 1992, table 1), high-resolution $\delta^{13}C$ and $\delta^{18}O$ records are available from other localities and studies (Cramer et al. 2009; Nicolo et al. 2007; Bohaty and Zachos 2003; Zachos et al. 2001, others). Those additional records allow us to identify key isotopic excursions and to make relatively robust correlations, even when faced with limited data sets such as those from Hole 762C. Not all global paleoenvironmetnal events can be identified in the isotopic records from Hole 762C, such as some short-lived hyperthermals (Nicolo et al. 2007; Lourens et al. 2005); however, several events are identified by comparing the isotopic excursion patterns to the magnetostratigraphy and nannofossil biostratigraphy. These events, as well as the criteria used to identify them in Hole 762C, are summarized below (see also Table 10 and Figure 16).

The age assigned to the PETM at Site 762 is derived from Cramer et al. (2003), as the Chron C25n/C24r boundary age – 0.924 My. The depth of the ETM2 (Eocene thermal maximum 2) in Hole 762C was determined by both the magnitude of the CIE (~1.0‰, Cramer et al. 2003), and by correlation

to nannofossil zone CP9b/NP11 boundary. Two dates are provided in the literature for the ETM2 event, though very closely spaced (Table 10): The upper date is derived by determining the relative placement of the Elmo horizon (Lourens et al. 2005) within Chron C24r at Site 1262 (~115.5-153.5 mcd) (Bowels, 2006), then converting that relative placement to the Ogg Ogg and Gradstein 2008 GPTS. This retains the relative placement of this excursion by Lourens, et al. (2005) below the Chron C24r/C24n polarity reversal. The lower ETM2 date is derived by Cramer et al. (2003), placed between the Chron C24r/C24n reversal and the base of NP11. We identify the ETM2 excursion below the Chron C24r/C24n reversal in Hole 762C, so apply the date provided by Lourens et al. (2005). The ETM3 was originally described as the "X" event by Röhl et al. (2005), and is correlated to foraminiferal zone P7 and nannofossil zone CP10. Both Agnini et al. (2007) and Galeotti et al. (2010) identify the ETM3 event in Chron C24n.1n (52.65-53.00 Ma) at Contessa Highway. The date we apply the EMT3 in Hole 762C (Table 10) is based on those correlations to Chron C24n.1n, as well as the association by Galeotti et al. (2010) of the ETM3 with the LO of *D. lodoensis* within Chron C24n.2r (53.23 Ma 2008 GPTS; 52.85 Ma, BKSA95), also observed in Hole 762C.

A significant warming trend occurred from the late Paleocene through the early Eocene. This global warmth peaked with the EECO (Early Eocene climatic optimum), ending at ~49.8 Ma (Chron C22r) (Bohaty and Zachos 2003). Delineating the termination of a long term trend can be difficult, with much greater stratigraphic freedom than the short lived hyperthermals discussed above. Placement of the EECO in Hole 762C is guided by recent isotopic curves of Cramer et al. (2009), who identified the end of the EECO just past the peak negative $\delta^{18}O$ excursion, on the falling limb of the curve. The age applied to the end of the Late Eocene warming in Hole 762C was derived from Vonhof et al. (2000), who dates the base of the "Vonhof" cooling event (Bohaty and Zachos 2003) at 35.5 Ma ($^{40}Ar/^{39}Ar$), correlating to nannofossil zones CP15/NP18. Global isotopic trends from Bohaty and Zachos (2003, fig. 2) show a direct transition from the late Eocene warming trend into the "Vonhof" cooling event, and we adopt a similar convention in Hole 762C (Table 10, Figure 16).

Chapter 4 - RESULTS

4.1. - Revised Magnetostratigraphy

Despite the presence of a thick and expanded Eocene section at Site 762, intermittent core recovery (and several hiatuses) impedes direct correlation between the polarity reversals observed and the idealized polarity pattern the GPTS. The original magnetostratigraphy of Galbrun (1992) used nannofossil biostratigraphy of Siesser and Bralower (1992); however, here we present a reinterpreted magnetostratigraphy for the Eocene section of Hole 762C, facilitated by the integration of a revised calcareous nannofossil biostratigraphy (Table 3), planktonic foraminifera, and isotopic data, calibrated to the GPTS of Ogg Ogg and Gradstein (2008).

Correlations among calcareous nannofossils, planktonic foraminifera, $\delta^{13}C$ and $\delta^{18}O$ isotopic excursions, and magnetic polarity reversals observed at Site 762 are summarized in Figure 16. The polarity reversal pattern (center) is shown against the original magnetostratigraphic interpretation of Galbrun (1992) (left), in comparison to the revised interpretation of this study (right). Sampling intervals for magnetic polarity data are provided in Galbrun (1992, appendix B). Primary evidence used in the interpretation of each magnetochron is discussed below. These revisions allow adjustment of magnetostratigraphic tie-points, with these reversals integrated into the revised age model (Table 11).

Polarity zones and GPTS Chron designations are discussed by core and illustrated in Figure 16. The reinterpretation was more simplistic through the Ypresian and Priabonian, but became increasingly difficult in the Lutetian and Bartonian. This is related to both the quality and quantity of stratigraphic data at various intervals, as well as ambiguity through intervals with poor core recovery and/or stratigraphic hiatuses. This portion of the section was constrained as much as possible by all available data, as well as confidence in the reinterpretations above and below.

Core 5-6: Though attributed to Chron C13r by Galbrun (1992), this interval is now identified as C15r: Several bioevents correlated to Chron 13 are observed above this interval, including the HOs of

Discoaster saipanensis and *D. barbadiensis* in Core 4 (Table 9), and the *Clausicoccus* spp. AB in Core 3. Significant positive isotopic shifts are seen in Core 3 (Figure 16), and likely represent the first step of Oi-1 (Pearson et al. 2008), also correlated to Chron C13r. Several lines of evidence also suggest a positive correlation to Chron C15r, including the HCO of *Cribrocentrum (Reticulofenestra) reticulatum* in Core 5 (HO = Core 4) and the HO of planktonic foraminifera *Turborotalia pomeroli* within sample 762C- 5x-CC.

Core 7: Correlated to Chron C15n in Galbrun (1992), this section is reinterpreted as Chron C16n, based on the LO of *Isthmolithus recurvus* (Table 9). This adjustment also brings the LO of *Reticulofenestra oamaruensis* into better agreement with its calibration to Chron C16n. Though the event is still observed slightly above Chron C16n, this may be due to the mid-latitude paleogeography of Site 762. In addition, a notable period of Late Eocene warming terminates with the "Vonhof" cooling event (Zachos, et al. 2001; Vonhof, et al. 2000), calibrated to Chron C16n, identified as a $\delta^{18}O$ isotope shift within Core 762C-7 (Figure 16, Table 10).

Core 8: Originally attributed to Chron C16n, this study finds greater stratigraphic agreement with assignment to Chron C17n, due to the HOs of both *Ch. grandis* and *Ch. oamaruensis* (Table 9).

Core 10: Core 10 has been correlated to planktonic foraminiferal zone P14, which is limited to Chron C18. Though this designation comes only from sample 762C-10x-CC, it indicates that at least some of this core must belong to Chron C18, suggesting that the polarity reversal captured in this section is correlated to the Chron C18n/17r boundary (Figure 16).

Core 11: This normal polarity zone is attributed to Chron C18, based on the presence of Chron C18, above, and Chron C18 and C19, below.

Core 12-13: This interval retains the original interpretation of Galbrun (1992). The HO of *Ch. solitus*, correlated to Chron C18, occurs within Core 12, as well as the LCO of *C. reticulatum* in Chron C19 (Table 9). Core 12 contains a problematic series of thin magnetic reversals that are difficult to

interpret. These may be due to overprinting of the original magnetic signal, or may represent a condensed section, as derived sedimentation rates drop considerably and this is the only interval with rates < 1.0 cm/ky.

Core 14-16: As in Galbrun (1992), we attribute this interval to Chron C20. This designation is supported by several bioevents, including the LO of *Ch. gigas,* HO of *Ch. gigas*, HO of *N. fulgens,* correlation of planktonic foraminiferal zone P11, and the HO of planktonic foraminifera *Morozovella aragonensis*, all correlated to Chron C20r.

Core 17: This interval is attributed to Chron C21, based on the calibration of LO of *Rhabdosphaera (Blackites) inflata* to Chron C21r in the BKSA95, as well as observation in Chron C21n at both Bottaccione (Monechi and Thierstein 1985) and at ODP Site 1051 (Table 12). When this interval is assigned to Chron C21n, the midpoint for the LO of *N. fulgens* may also then occur within its calibrated magnetozone (Chron C21n, BKSA95) (Figure 16).

Core 18-19: Attributed to Chron C21 by Galbrun (1992), this section is now correlated to Chron C22. The *Discoaster* spp. AE is observed in this interval, correlated to Chron C22r by Agnini et al (2006). Core 19 also contains significant positive isotopic shifts: $\delta^{13}C$ increases by 0.71‰ (341.82-336.72 msbf) while $\delta^{18}O$ increases by 0.5‰ (343.21-336.72 msbf) toward a sustained low through the Lutetian (Figure 16). This shift likely represents the end of the EECO, also calibrated to Chron C22r (Bohaty and Zachos 2003).

Core 20-22: The authors agree with Galbrun (1992) with correlation of Core 22 to Chron C23r; however, the original interpretation of Cores 20-21 to Chron C22 is amended in this study to also correlate to Chron C23 (Figure 16). The LO of *Coccolithus crassus*, reported from Chron C23n from several European sections (Table 12), is observed in this interval (Figure 16, Table 9). The *Discoaster* spp. AB at Site 762, discussed in Section I is correlated to Chron C23n by Agnini et al (2006). This

reinterpretation is also supported by planktonic foraminiferal data, with the co-occurrence of *Morozovella formosa* and *M. aragonensis* limited to Chron C23n.

Core 22-25: The present analysis agrees with Galbrun (1992) with correlation to Chron C24n. This interpretation is supported by nannofossil data (LO *Discoaster lodoensis*, LO *Girgisia gammation*), planktonic foraminifera data (absence of *Morozovella aragonensis*, with LO in Chron C23r, above) and $\delta^{13}C$ isotopic data (ETM3) (Figure 16).

Core 25-28: The present interpretation is in agreement with Galbrun (1992) with correlation to Chron C24r. Supporting data include several bioevents calibrated to this magnetochron in the BKSA95 (Table 12) (LOs of *D. diastypus, D. barbadiensis, Tribrachiatus bramlettei, T. contortus, T. orthostylus;* HOs of *Fasciculithus* spp. and *T. contortus*; planktonic foraminiferal zone P5) as well as isotopic excursions that have been tied to Chron C24r (PETM and ETM2) (Table 10).

Core 29: As with Galbrun (1992), the upper polarity reversal captured in Core 29 is identified as the Chron C25n/C24r reversal boundary, with the lower correlated to the Chron C25r/C25n reversal. This interpretation is supported by the presence of *Discoaster nobilis*, HO of *Ericsonia robusta*, LO of *D. multiradiatus* and planktonic foraminiferal zone P4.

We demonstrate that the reinterpreted magnetostratigraphy at Hole 762C gives well defined intervals through the Eocene that compare well with the idealized magnetostratigraphy of published GPTSs (Ogg Ogg and Gradstein 2008; Gradstein Ogg and Smith 2004; Cande and Kent 1995), except where hiatuses have been identified, and in the lower Bartonian (Core 12) where magnetic reversal patterns are ambiguous. Micropaleontological data lends high confidence to the magnetostratigraphic interpretation of Cores 5-29 at Site 762; however, poor core recovery, sparse data points and ambiguous polarity reversals decrease confidence within these problem intervals.

4.2 - Age-Depth Plot

Biostratigraphic, isotopic, and magnetostratigraphic data, correlated to the Ogg Ogg and Gradstein 2008 GPTS, are integrated to construct a revised age-depth plot for Hole 762C (Figure 17). Dates of nannofossil bioevents are from BSKA95, recalibrated to Ogg Ogg and Gradstein 2008. Constant sedimentation was assumed between age calibration points. A summary of the primary biostratigraphic, isotopic and magnetostratigraphic tie-points shown in Figure 17 is provided in Tables 3-5, respectively.

Stratigraphic Hiatuses

Integration of biostratigraphy, magnetostratigraphy and $\delta^{13}C$ and $\delta^{18}O$ data from Hole 762C has demonstrated the presence of a least four previously unidentified Eocene hiatuses, illustrated in Figure 17 and summarized in Table 13. These are treated separately, below:

Hiatus A: The shallowest hiatus is identified at 289.75 msbf, at the midpoint between the HO of *N. fulgens* (Table 9) and the Chron C20n/C20r reversal (Table 11). This hiatus also includes the LO of *R.* umbilica and the HO of *Ch. gigas* (Figure 17). This disconformity includes nannofossil zone CP13c/NP15c and portions of both Chron C20n and Chron C20r. The upper and lower age limits for this hiatus are dated to 42.02 and 44.22 Ma, respectively, a duration of ~2.2 My.

Hiatus B: Three of the four hiatuses discussed in this section are readily identified with nannofossil biostratigraphy; however, an additional hiatus was identified based on the relationships between magnetic reversals and sedimentation rate. The normal polarity interval in Core 18 has been attributed to Chron C22, based on the HO of *T. orthostylus* (Table 9), the *Discoaster* spp. AE (Table 12), and isotopic shifts indicating the end of the EECO (Table 10); however, the normal polarity interval in Core 17 has been attributed to Chron C21, based on the LO of *R. inflata* (Tables 3, 6). This interpretation implies that the reverse polarity interval of Chron C21 must occur in the ~1.75 m coring gap at the base of Core 17 (Figures 2, 3). Sedimentation rates must slow significantly to ~0.13 cm/ky to fit a 1.37 My polarity reversal within this coring gap. All derived sedimentation rates through the Eocene at Hole 762C

are > 1.0 cm/ky (less Core 18), with a greater likelihood of a hiatus between these two normal polarity intervals. As all of Chron C21r (47.23-48.60 Ma) is absent, we can first estimate a minimum duration for this hiatus of 1.37 My. This hiatus is placed within the age model (Figure 17) by assuming a minimum duration and assigning top and base dates of Chron 21r to the upper and lower depths of the coring gap, respectively (Table 11). The depth of the disconformity was placed at the mid-point between these two events (321.13 msbf), but also includes the LO of *Rhabdosphaera inflata* (Figure 17). The upper and lower age limits for this hiatus are dated to 47.10 Ma and 48.83 Ma, respectively, for a duration of ~1.7 My.

Hiatus C: The third disconformity is identified at 332.18 msbf, at the midpoint between the HO of *T. orthostylus* (Table 9) and the end of the EECO (Table 10, Figure 16). The upper and lower age limits of this hiatus are dated to 49.79 and 50.71 Ma, respectively (~0.9 My) and includes a portion of Chron C22r. This interval also includes the LO of *D. sublodoensis*, discussed further below.

Hiatus D: The deepest disconformity is identified at 412.78 msbf, at the midpoint between the PETM (Table 10) and a key nannofossil sample interval, containing the LOs of *D. diastypus*, *D. barbadiensis*, *C. eodela*, and *T. bramlettei* (Table 9), as well as the HO of *Fasciculithus* spp. and the LO of *T. contortus* (Table 12). This hiatus includes nannofossil zone CP8a and portions of Chron C24r. The upper and lower age limits of this hiatus are dated to 54.41 and 56.22 Ma, respectively, a duration of ~1.8 My.

4.3 - Sedimentation Rates and Nannofossil Calibration

Identification of these stratigraphic hiatuses, totaling ~6.6 My in duration, allows recalculation of sedimentation rates through the Eocene (Figure 17). These rates are then used to derive the ages of calcareous nannofossil bioevents at Site 762, using the relative placement of the bioevent within a particular magnetochron. Precision decreases with lower core recovery. Error reflects only the stratigraphic resolution around nannofossil sample midpoints, and does not account for error around

magnetic polarity reversals. Extrapolated dates for nannofossil bioevents at Site 762 are provided in Table 12.

Revised sedimentation rates were used to calculate a weighted average for each epoch during periods of deposition. As anticipated, the highest average rates are observed in the Ypresian (~1.95 cm/ky), as this period of global warmth is linked to high rates of productivity. Average sedimentation rates drop considerably in the Lutetian and Bartonian, to ~1.06 and ~1.05 cm/ky, respectively. A partial recovery in sedimentation rates is observed in the Priabonian, increasing to ~1.55 cm/ky. Though slightly elevated during the Ypresian and reduced in the middle Eocene, sedimentation rates at Site 762 are fairly consistent, with an average of ~1-2 cm/ky through most of the Eocene.

The sedimentation rate between hiatuses A and B is shown as a dashed line, representing uncertainty in this calculation, due to the general lack of tie-points, significant error around existing tie-points, and truncation above and below by hiatuses (Figure 17). The rate shown is chosen for its placement just after the Chron C21n/C21r polarity reversal (See hiatus B, above), and is well centered on the only available tie-point within this interval, despite its large sample error. In addition, this rate of > 1.0 cm/ky is in good agreement with the general sedimentation trends observed at Hole 762C.

Comparison to the BKSA95 and auxiliary sites

Several additional Eocene sections (Figure 1) have been included in this study for comparison of nannofossil bioevents to Site 762, as well as the BKSA95 (Table 12). Several studies provide event dates derived directly from the authors' age model (ODP Sites 1262, 1218, 1215, 1172, 1123, and Possango), which were recalculated from the original GPTS (geomagnetic polarity time scale) used in that research to that of Ogg Ogg and Gradstein (2008). Other localities (Bottaccione, Contessa Highway, NJ coastal plain, ODP Sites 1090, 1051, 689, and DSDP Site 577) provided no age estimates for bioevents; at these localities, ages were instead derived by the position of the bioevent within a particular magnetostratigraphic chron.

Several of these studies identify the depth in which particular bioevents were observed; however, the ages of events provided in this study have been derived using the midpoint between the event depth and the sample above (for HOs) or below (for LOs). In some instances, due to the relationship between sample spacing and magnetic reversal depths, the strict use of the midpoint shifts the bioevent into a different polarity zone. By comparison to additional studies we determined the polarity zone in which this event most likely occurs, and extrapolate the midpoint using that reversal depth.

All events have been recalibrated to the GPTS of Ogg Ogg and Gradstein (2008) and are directly comparable. Many studies included in Table 12 are conducted at fairly high resolution. We provide the mean age for events where the total error provided by the original author was ≤ 0.01 Ma, so that 56.64-56.65 Ma = 56.645 Ma. Though most nannofossil bioevents at Site 762 were found to be in close correlation with the BKSA95, six such events show considerable divergence from this IMBS and/or the additional sites shown in Table 12. These bioevents are treated separately, below:

The HO of Sphenolithus radians: Though no date for this bioevent is provided in the BKSA95, dates have been derived from the Bottaccione and Contessa Highway Sections (Table 12). The date derived from Hole 762C is considerably younger (~34.4 Ma) than these Italian sections (38.74 and 39.65 Ma, respectively); however, the range pattern observed at Exmouth Plateau is in good agreement with that shown by Perch-Nielsen (1985, fig. 69), with consistent observation through CP14a/NP16, becoming more rare and sporadic through CP15b/NP19/20.

The LO of Reticulofenestra oamaruensis: This event is dated significantly younger at Site 762 than reported in the BKSA95 (Table 12). *Reticulofenestra oamaruensis*, extremely rare at Site 762, is known to have an affinity to high latitude (Monechi et al 2000; Berggren et al 1995) and this delayed appearance may be due to paleogeographic exclusion. Site 762 is located at mid-paleolatitudes (~40-45°S) during the late Eocene, and the distribution of this species may have expanded into these latitudes during Priabonian cooling (Figure 16).

The LO of Isthmolithus recurvus: Two specimens of *I. recurvus* were identified deeper in the section, with these oldest occurrences dated to 36.37±.12 Ma. The LCO of *I. recurvus* at Hole 762C (36.04±.06 Ma) is in much greater agreement with the calibrated age of the BKSA95 timescale (35.98 Ma). A similar temporal relationship is seen at Site 1090 (Table 12).

The HO of Cribrocentrum (Reticulofenestra) reticulatum: We observe a divergence in the HO and HCO of *C. reticulatum* with respect to the BSKA95 (Table 12). The HO of *C. reticulatum* at 189.86 msbf is dated to ~34.20 Ma; however this species becomes rare and sporadic above 199.00 msbf. The depth for the HCO of *C. reticulatum* fits well within the sedimentation curve, derived using isotopic and magnetostratigraphic tie-points, and so it is this HCO that has been correlated to the BKSA95 at 35.09 Ma.

The LO of Dictyococcites (Reticulofenestra) bisectus: The revised age-model derived for Site 762 yields a significantly older date for both the LO (39.96±.13 Ma, Chron C18r) and LCO (39.11± Ma, Chron C18n.2n) of *D. bisectus* than the LO provided in the BKSA95 timescale (37.68 Ma, Chron C17n.3n). Despite this divergence from the BSKA95, these dates are in good agreement with data from other localities globally, including ODP Sites 1218, 1172, 1090, 1051, Bottaccione, and Contessa Highway, all of which report this species from either Chron C18n or Chron C18r (Table 12). This global agreement suggests *D. bisectus* has good potential as a biostratigraphic marker and should be investigated for consistency in LO and LCO bioevents at these and other sites.

The LO of Discoaster sublodoensis: The LO of *D. sublodoensis* is thought to occur too low in the section at Site 762. The age-depth point for this event falls below the sedimentation curve (Figure 17), and attempts to bring this event into greater alignment with hiatus C results in a poor fit among other biostratigraphic, isotopic and magnetostratigraphic tie-points. Our age estimates give a significantly older date (50.51±.02 Ma, Chron C22r) than that provided in the BSKA95 (49.41 Ma, Chron C22n). Only specimens with five, straight, pointed rays were identified as *D. sublodoensis,* so it is unlikely that these

early forms are misidentified specimens of *D. lodoensis*. A similar distribution to Site 762 is observed at Site 1051, Site 689, Possango, and Bottaccione, with specimens of *D. sublodoensis* identified in CP10 and CP11, prior to the LCO and base of CP12a. These issues may be resolved with a more focused examination of both taxonomy and stratigraphic distribution, particularly at these sites, to better constrain the utility of this marker taxa.

Chapter 5 - DISCUSSION

Sedimentation rates derived from the revised age model at Site 762 show considerable differences to those originally calculated (Shipboard Scientific Party 1990; Haq et al. 1992). Average rates for the Priabonian are comparable between studies (~1.5 cm/ky); however, the original model shows rates of up to ~3 cm/ky in the upper Priabonian, considerably higher than our maximum of ~2 cm/ky. Weighted averages for rates through the Bartonian are also notably higher in the original analysis than in the current results (~2 cm/ky and ~1 cm/ky, respectively). The most striking difference between these analyses is seen in the Lutetian. Though the original model shows sedimentation of ~1-2 cm/ky throughout most of the Eocene, rates drop considerably through this interval to a weighted average of ~0.5 cm/ky. Conversely, our average rate is double this, at ~1 cm/ky. Two hiatuses (A and B) have been identified in the Lutetian, totaling ~4.0 My in duration. This accounts for nearly half of the 8.2 My long epoch, resulting in a doubling of sedimentation rates in the revised age model. Rates for the uppermost Ypresian are also low in the original age model (~0.3 cm/ky; 329.5-332.5 mbsf), to accommodate the ~0.9 My hiatus (332.18 msbf) identified in the revised model. Original sedimentation rates through the remaining Ypresian are comparable to the revised age model, averaging ~2-3 cm/ky, until dropping again near the Paleocene-Eocene boundary (<1 cm/ky). This decrease in the original sedimentation rate is related to a ~1.8 My hiatus identified in the revised age model (412.78 msbf), in association with the PETM.

The revised geochronologic model at Site 762 has produced several notable changes in sedimentation rates through the Eocene. Reanalysis of the nannofossil biostratigraphy and magnetostratigraphy has played a key role; however, these changes are primarily due to incorporation of four stratigraphic hiatuses, totaling ~6.6 My in duration, approximately 25% of the total time originally thought to be represented at this locality. Though no stratigraphic breaks or significant changes in lithology are see in Hole 762C, we interpret these hiatuses as stratigraphic unconformities rather than condensed sections during periods of low sedimentation. While it is beyond the scope of this research to discuss and weigh the numerous mechanisms which may be responsible for creating these disconformities, some comparisons can be drawn between our observations and other research.

Third-order sequence boundary dates of Hardenbol et al. (1998) are contained within the age ranges of the hiatuses identified at Site 762 (Table 13): The Lu3 sequence boundary age (42.98 Ma) is contained within unconformity A (42.02-44.22). The Lu1 sequence boundary age (47.47 Ma) is contained within disconformity B (47.01-48.83). Disconformity C (49.79-50.71 Ma) incorporates the sequence boundary ages of both Yp10 (49.78 Ma) and Yp9 (50.13 Ma). Similarly, disconformity D (54.41-56.22 Ma) contains the sequence boundaries of Yp3-Yp1 (55.19, 55.29 and 55.98 Ma, respectively).

Disconformity D is linked to the PETM (Chron C24r), due to the high relative abundance of dissolution resistant taxa such as *D. multiradiatus*, *S. primus*, and *F. tympaniformis* [Bown and Pearson (2009); Jiang and Wise (2009); Monechi and Angori (2006); Kahn and Aubry (2004)]. Several authors also note a barren interval associated with the CIE, as well as an increase in clay content [Jiang and Wise (2009); Monechi and Angori (2006); Kahn and Aubry (2004)]. Raffi and De Bernardi (2008) provided a synthesis of 18 PETM sites, where the authors attribute these observations to truncation of the basal PETM sequence from acidification and dissolution of carbonate sediments. Similarly, Ali and Hailwood (1995, fig 2) show stratigraphic gaps in mid-Chron C24r across nine sites in SE England, France and Belgium, with these also correlating to disconformity D at Site 762 (Figure 17).

A paleogeographic and stratigraphic summary of the northwestern Australian margin (Gradstein 1992), suggests that at least part of the stratigraphic record in this region is affected by erosion or non-deposition, and suggests links to the Himalayan orogeny, ocean spreading tectonics, and/or and ocean current reorganization. Gradstein (1992) shows a middle Eocene hiatus at the western foot of Exmouth Plateau (Site 766) and on the Argo Abyssal Plain (Site 765). Siesser and Bralower (1992) identify significant gaps in the nannofossil biostratigraphy on the central Exmouth Plateau at Site 763 in the lower and middle Eocene, but continuous sedimentation through this interval at Site 762. Disconformities identified at Site 762 in the present study may be linked to those described by Siesser and Bralower (1992) and Gradstein (1992), and suggests the mechanism was effective over a much larger area, and a wider range of paleodepths across the northwestern Australian margin.

Similarly, an extensive study by Aubry (1995) examined DSDP and ODP Sites in the northern and southern Atlantic Ocean, with these localities showing stratigraphic hiatuses at discrete magnetostratigraphic intervals through the middle Eocene. A striking number of these Sites correlate to unconformities A-C at Site 762: Unconformity A: Chron C20n-C20r - > 20 Sites; Unconformity B: Chron C21n-C21n - > 30 Sites; Unconformity C: Chron C22r - > 20 Sites. Such wide-spread and extensive stratigraphic gaps suggest the deep sea record is not as continuous as once thought, but can contain frequent hiatuses of significant duration. Many stratigraphic sections likely contain such hiatuses, but have not been identified due to the more recent trend toward integrated geochronologic models. Such relationships can be critical to paleoceanographic research, and reexamination of older sedimentation models will likely show additional regions with widespread deep-water hiatuses. Sufficient mechanisms, such as eustacy, tectonics, and ocean current reorganization, can only be determined once such sections are accurately interpreted.

Chapter 6 - CONCLUSIONS

Reexamination of the Eocene calcareous nannofossil biostratigraphy of Hole 762C indicates four stratigraphic disconformities in a section previously described as continuous (Siesser & Bralower 1992; Shipboard Scientific Party 1990). The magnetostratigraphy of Galbrun (1992) was reinterpreted using this revised nannofossil biostratigraphy, as well as planktonic foraminifera data and stable isotopic data, resulting in considerable adjustment to magnetic reversal boundaries (Figure 16). These magnetostratigraphic calibration points, as well as isotopic data and nannofossil bioevents, were combined to produce an integrated age-depth plot, calibrated to the GPTS of Ogg Ogg and Gradstein (2008). We identify four hiatuses of ~1-2 My each in duration. Incorporation of these hiatuses into the depositional model results in a significant increase in sedimentation rates through the Lutetian and portions of the Ypresian. Dates for several nannofossil bioevents are also derived using these new sedimentation rates, and are compared to events from the BKSA95, as well as several, globally distributed sites. Most nannofossil bioevents at Hole 762C are in good agreement with the BKSA95; however, a select number of events at Hole 762C show some offset from that biochronology (LO *R. oamaruensis*, LO/LCO *I. recurvus*, HO/HCO *C. reticulatum*, LO *D. sublodoensis*) or from additional sites (HO *S. radians*), where no date is provided by BKSA95. The most notable and consistent divergence is seen in the LO of *Dictyococcites bisectus*, observed at Site 762 ~2 My before the BKSA95. This early occurrence is also observed at Bottaccione, Contessa Highway, and ODP Sites 1218, 1172, 1090 and 1051. Similar discrepancies are observed for the LO of *Discoaster sublodoensis*, observed at Site 762 ~1 My before the BKSA95, and indicates a need for detailed recalibration of these nannofossil datums.

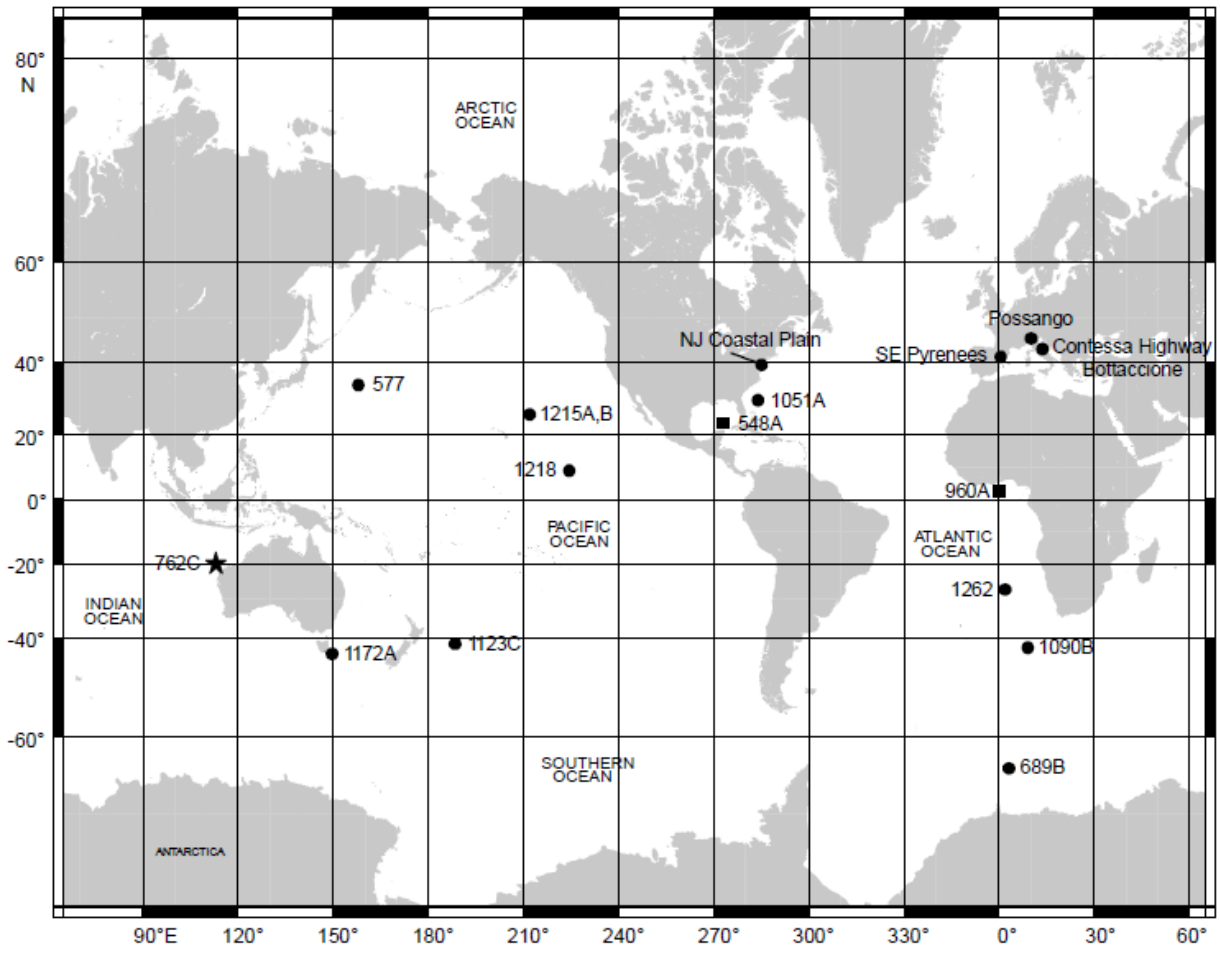

Figure 1 – Site Map: Site map showing the primary locality examined in this research (Star = ODP Site 762C, NW Australian Shelf), as well as additional sites used in Section II (Square) and Section III (Circle).

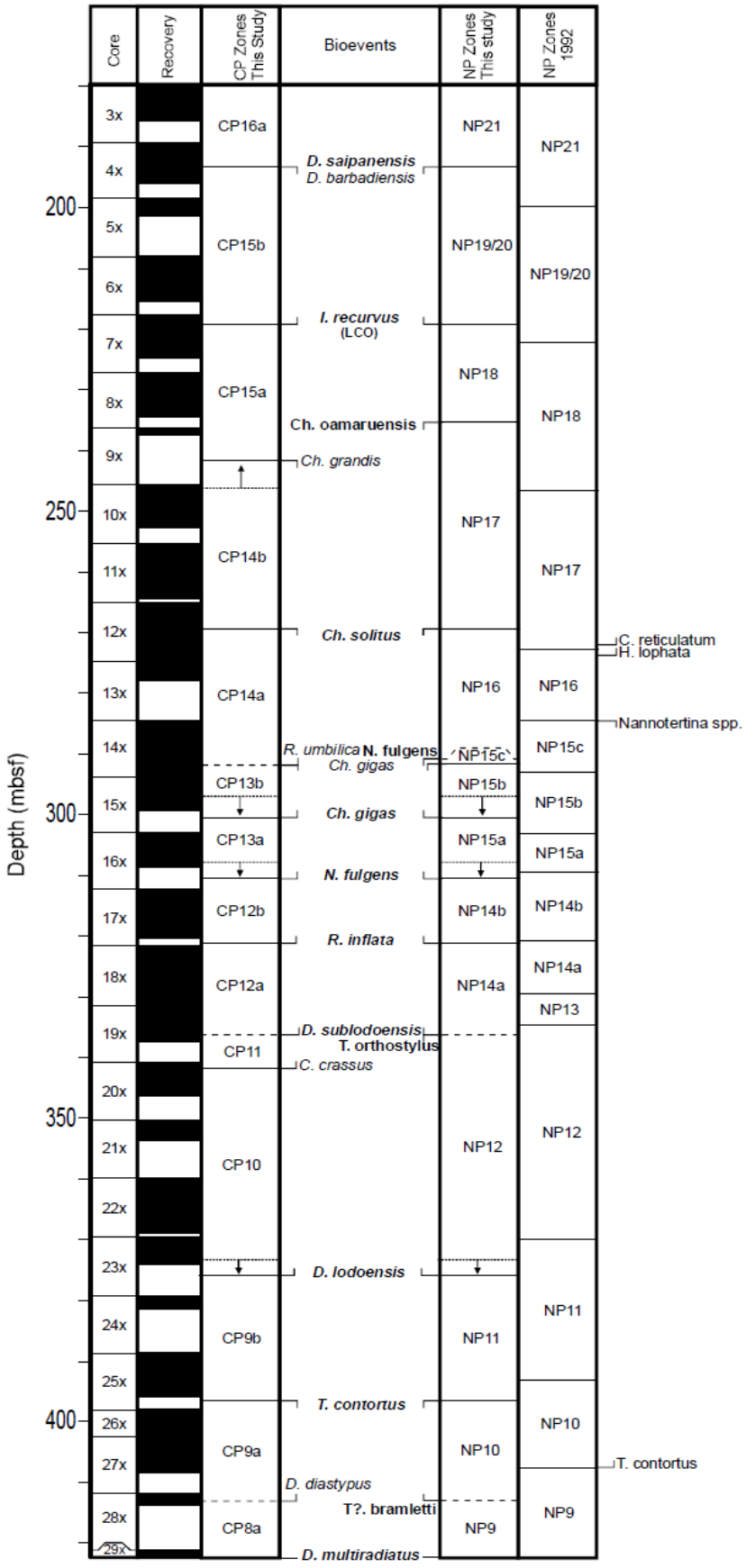

Figure 2 – Nannofossil Biostratigraphy: Calcareous nannofossil biostratigraphy for Site 762C. Depth (msbf), core, and core recovery shown from left. Biomarkers from the CP zonation (Okada and Bukry 1980) are shown in bold. NP zonal markers from Martini (1971) with select subzones of Aubry (1991) shown in italic. Joint markers for CP and NP zones are shown in bold and italic. Original interpretation of Siesser and Bralower (1992) shown at right, with alternate biomarkers of that study at far right. Locations of zonal boundaries reflect the midpoint between the observed event and the sample above (for HOs) or the sample below (for LOs). These values are provided in Table 3. Observed depths are given as dotted lines where coring gaps create > 2 m offset between the observed depth and the extrapolated event midpoint. Biostratigraphic hiatuses are shown as dashed lines.

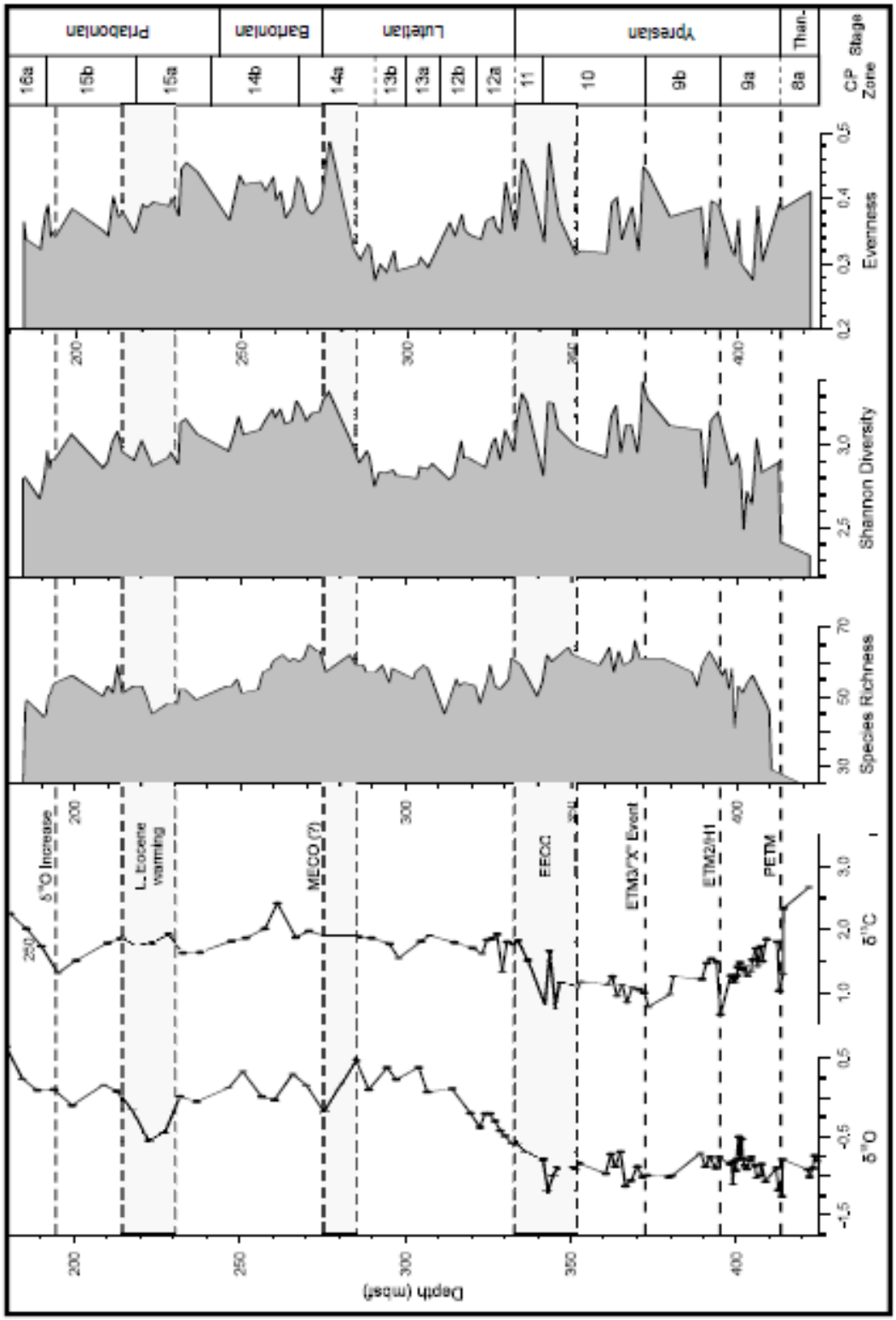

Figure 3 – Isotopic Data and Nannofossil Assemblage Trends: $\delta^{18}O$ and $\delta^{13}C$ isotopic data from Site 762C (Thomas, Shakleton and Hall, 1992), with interpretation of isotopic events shown as dashed lines or shaded boxes. Species richness (S), Shannon diversity (H), and evenness correlated to depth (msbf, left), nannofossil CP zones (right), and geologic epoch (far right) (Ogg ,Ogg and Gradstein 2008).

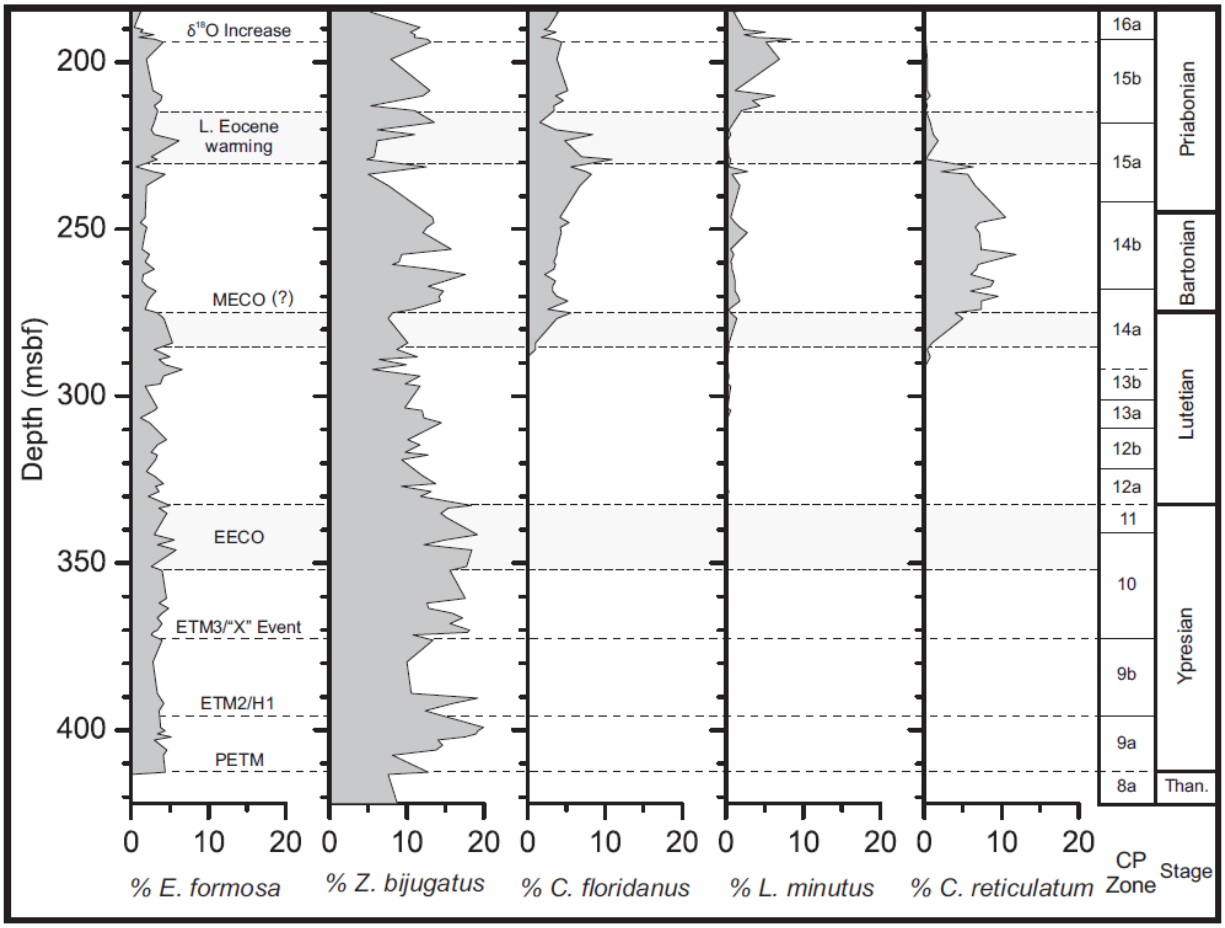

Figure 4 – Nannofossil Species Abundance Trends: Abundance patterns of select nannofossil species correlated to depth (msbf, left), nannofossil CP zones (right), and geologic epoch (far right). Isotopic events identified in Figure 3 shown as dashed lines or shaded boxes. Data is expressed as percentage of 500 specimens.

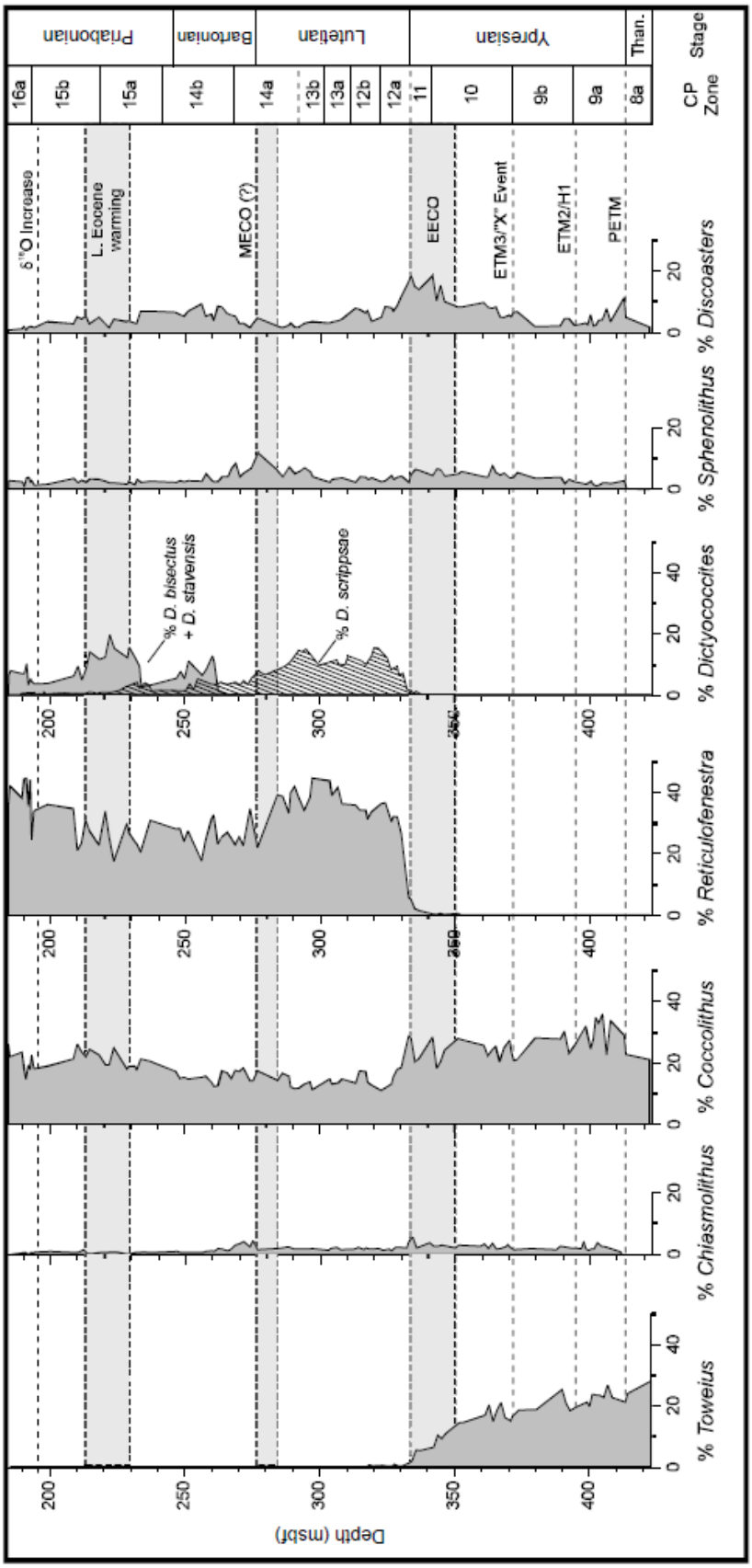

Figure 5 – Genera Abundance Trends: Abundance patterns of select nannofossil genera correlated to depth (msbf, left), nannofossil CP zones (right), and geologic epoch (far right). Isotopic events identified in Figure 3 shown as dashed lines or shaded boxes. Data is expressed as percentage of 500 specimens

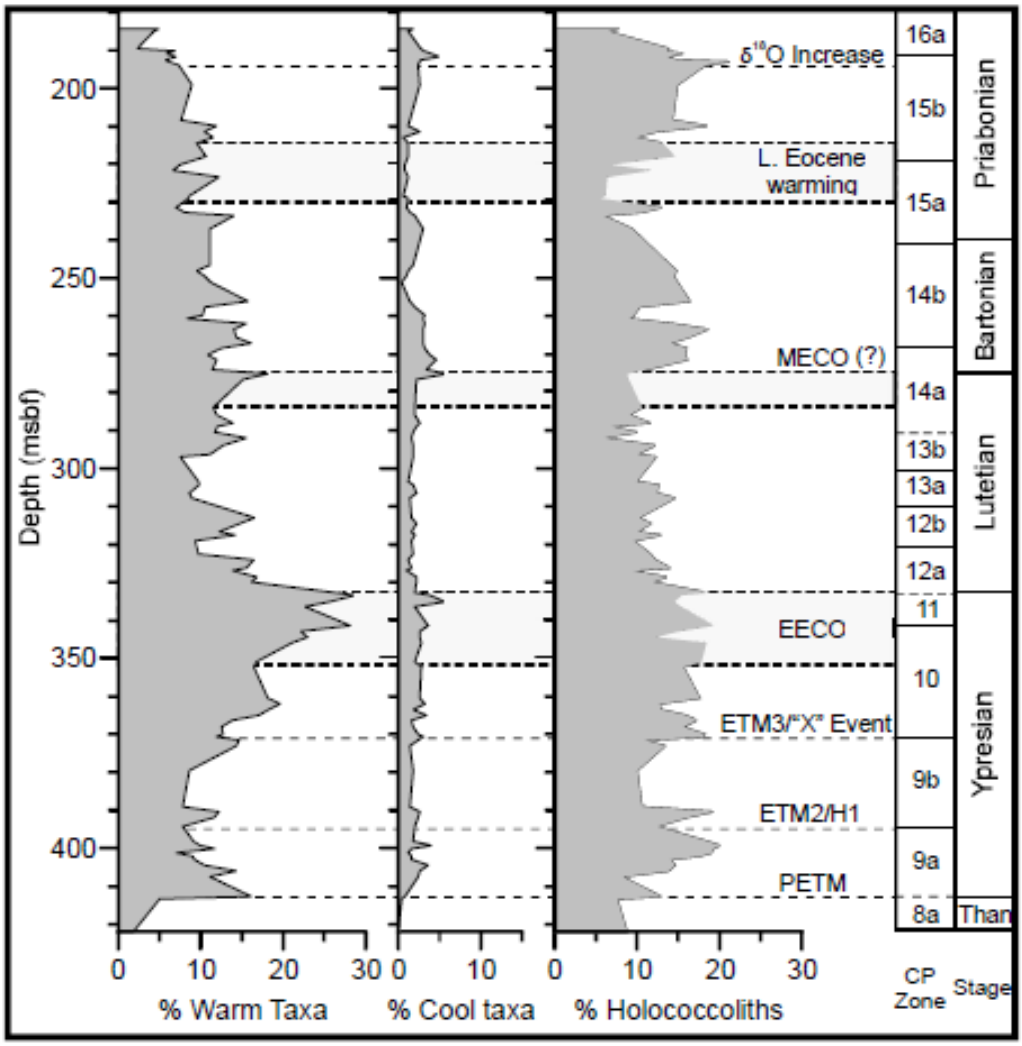

Figure 6 – Warm Taxa, Cool Taxa and Holococcolith Abundance Trends: Abundance patterns of warm taxa (*Discoaster* spp., *Sphenolithus* spp., *Ericsonia formosa*), cool taxa (*Reticulofenestra daviesii, R. hillae*, *Isthmolithus recurvus*, *Chiasmolithus* spp.), and holococcoliths (*Zygrhablithus bijugatus, Lanternithus minutus*) from Site 762C, correlated to depth (msbf, left), nannofossil CP zones (right), and geologic epoch (far right) (Ogg Ogg and Gradstein, 2008). Isotopic events identified in Figure 3 shown as dashed lines or shaded boxes. Data is expressed as percentage of 500 specimens. Groups based on Perch-Nielsen (1985) and a well-researched summary by Villa et al. (2008, table 3).

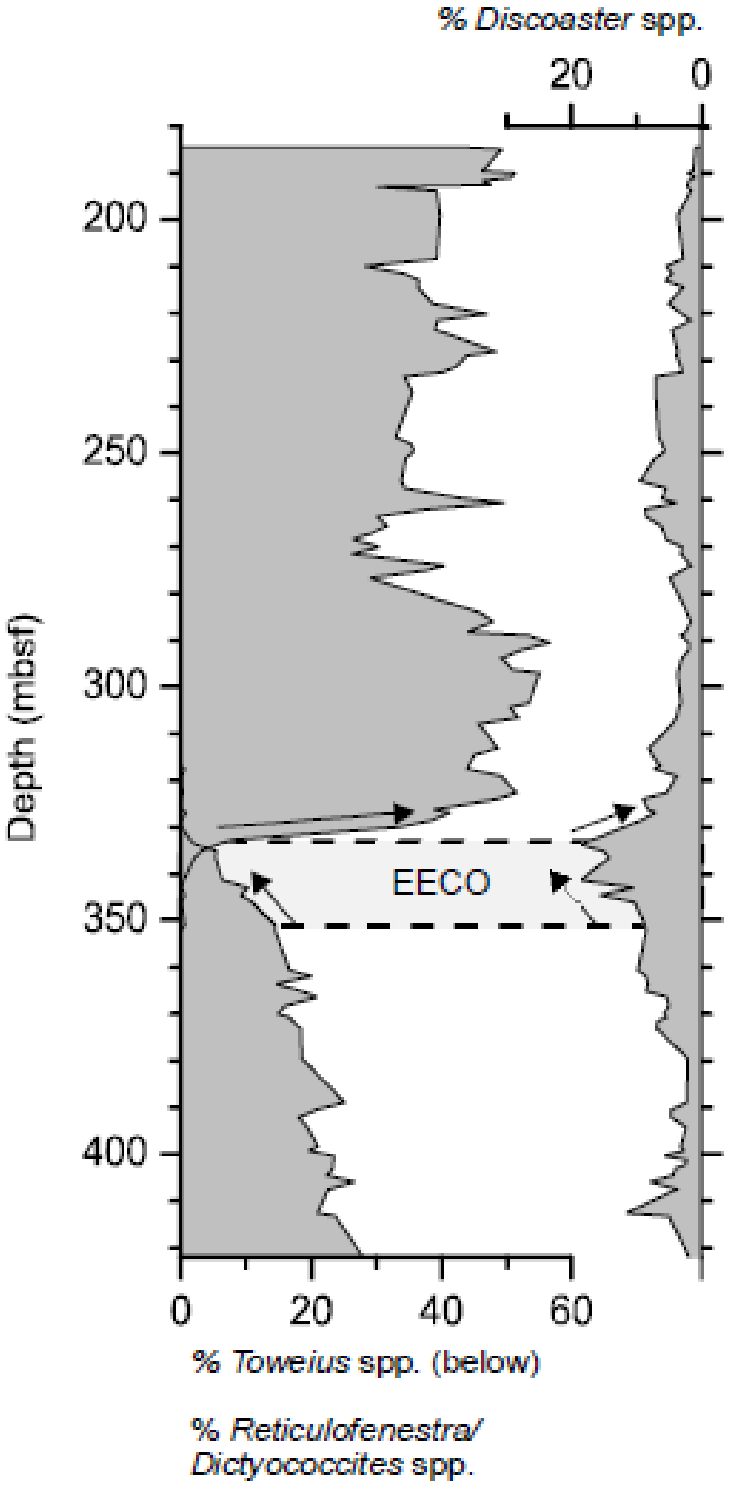

Figure 7 – EECO Nannofossil Assemblage Turnovers: Abundance patterns of key taxa from the lower-middle Ecoene dominance reversals correlated to depth (msbf). *Toweius* spp. plotted on lower left, with *Reticulofenestra* spp. (including *Dictyococcites bisecta, D. stavensis, D. scrippsae*) on upper left. *Discoaster* spp. plotted on right. Major abundance shifts highlighted with arrows in relation to the isotopic shift, related to the end of the EECO.

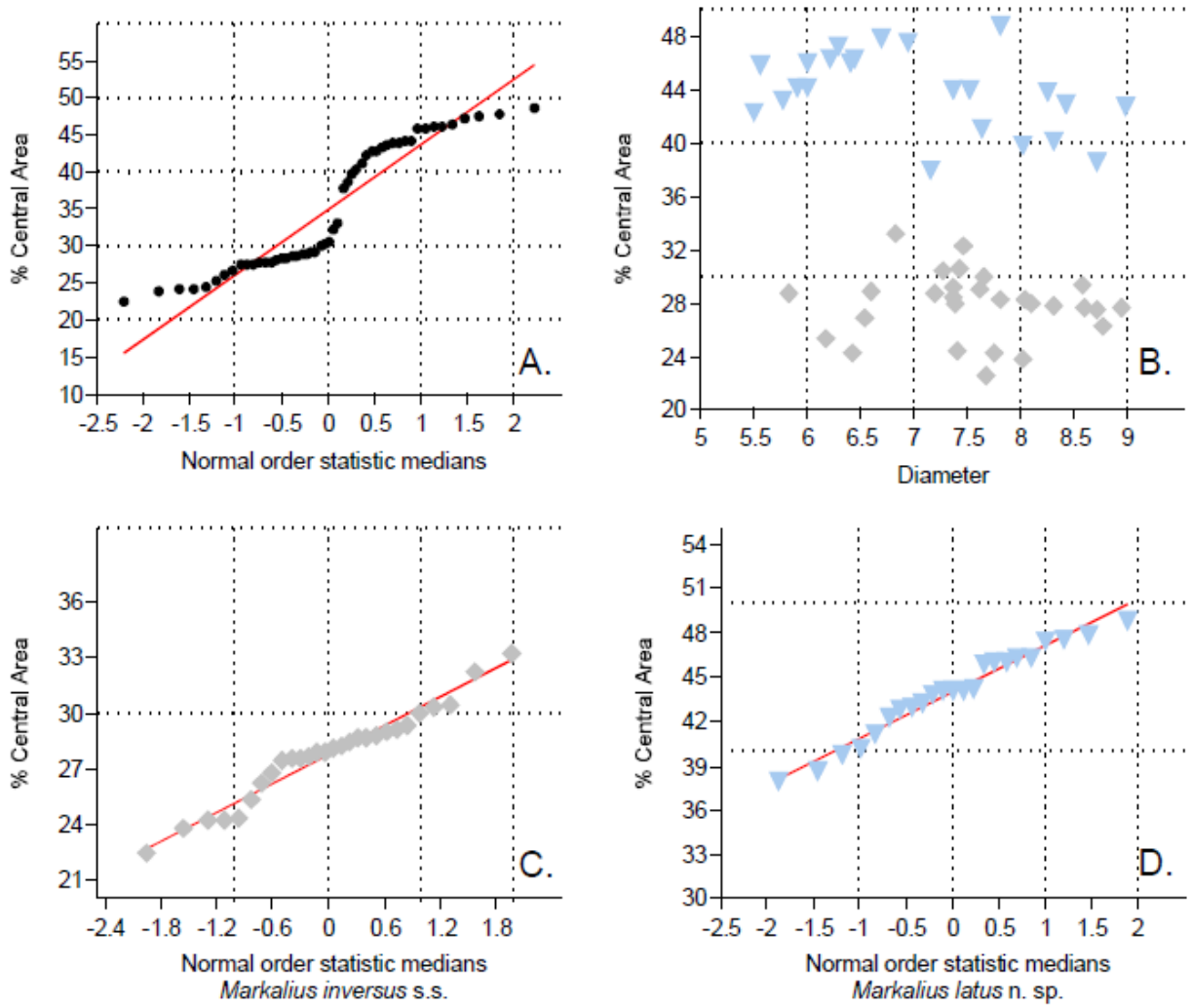

Figure 8 – *Markalius* spp. analysis: Univariate statistical analysis of the genus *Markalius*: A) Non-normal distribution of *Markalius* specimens with respect to size of the CA (central area). B) Distribution of *Markalius* specimens showing clear separation between forms with relatively small CA (< 35%; *Markalius inversus* s.s.) and those with a larger CA (>35%; *Markalius latus* **n.sp.**) (See Appendix). C, D) Near normal distributions of *Markalius* specimens when separated by the relative size of the CA into two distinct populations.

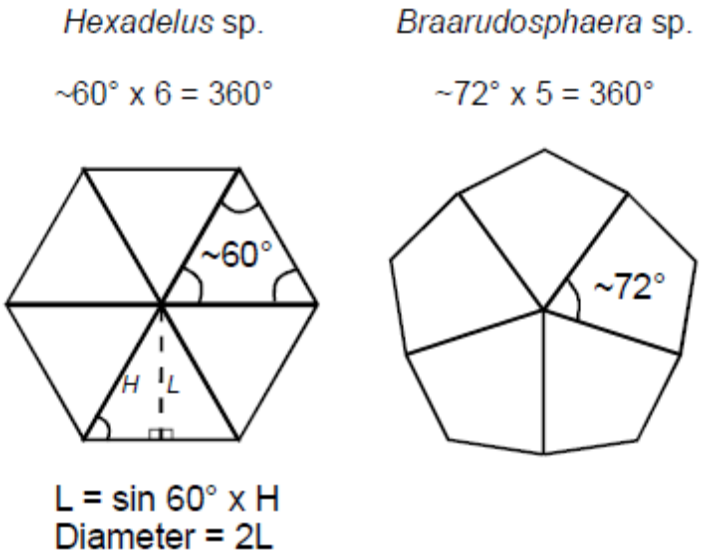

Figure 9 – *Hexadelus* and *Braarudosphaera* Geometries: Stylized figure showing the morphological relationship between disarticulated plates of the pentalith family Braarudosphaeraceae and those of the newly described genus *Hexadelus*. Geometrically, the interior angle of a pentalith must average ~72°, while plates that are 60° require six segments in order to complete a cycle.

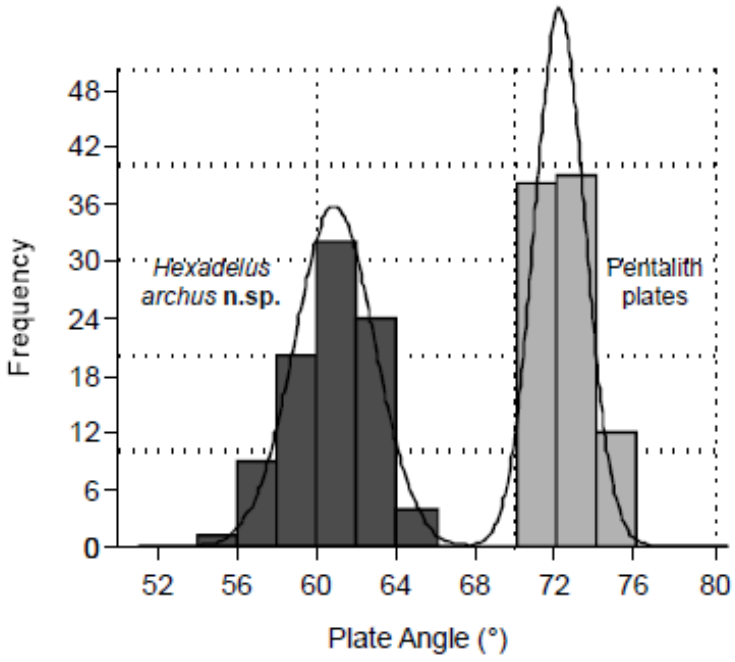

Figure 10 – *Hexadelus* and Braarudosphaeraceae Distribution Curves: Histogram showing the non-overlapping relationship between Braarudosphaeraceae and the type species *Hexalithus archus* **n.sp.**, with respect to the interior angle. Normal distribution curves superimposed. Univariate t-tests show distinct separation between plate geometry of pentaliths and *H. archus* **n. sp**.: At the 95% confidence level, pentalith angle = 71.98-72.52°; *Hexadelus archus* = 60.38-61.23°, $p_{(same\ \mu)} = 9.93\ E^{-100}$, N = 90 each species.

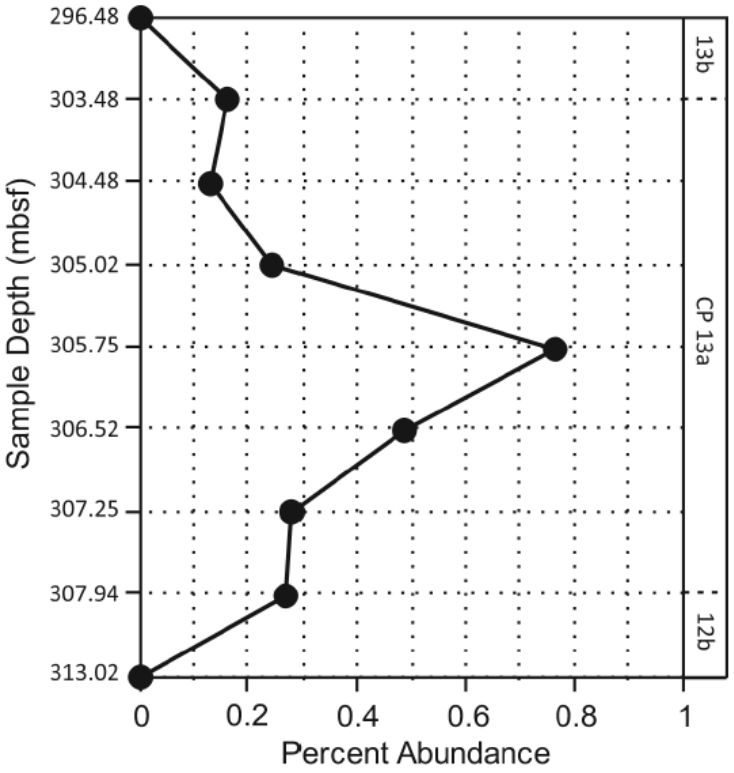

Figure 11 – *Sphenolithus perpendicularis* n.sp. Abundance: Graph showing the percent abundance of *S. perpendicularis* to total nannofossil assemblage (total *S. perpendicularis* per traverse/total nannofossils per traverse x 100). *Sphenolithus perpendicularis* appears to range throughout CP13a.

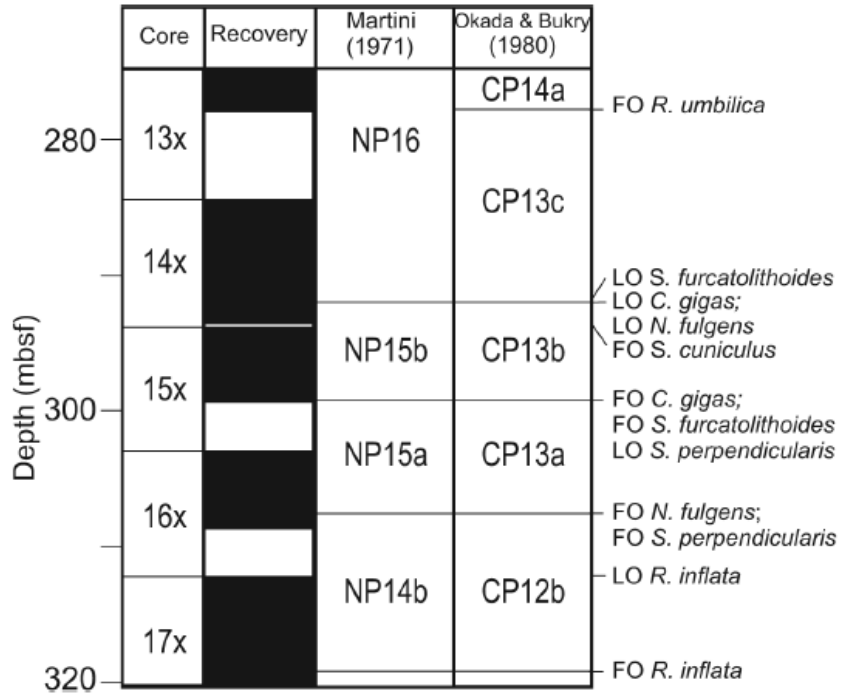

Figure 12 – Observed *Sphenolithus* Ranges : Nannofossil biostratigraphic scheme for the studied interval at Site 762C, showing sample depth, core interval, core recovery, NP markers, and CP markers, along with appearance of key *Sphenolithus* species. See Table 1 for detailed interval data.

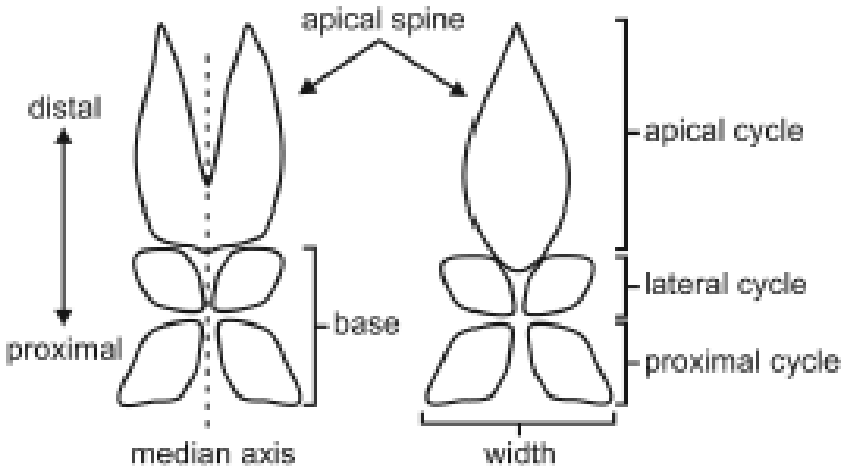

Figure 13 – Sphenolith Morphology: Schematic diagram showing basic Sphenolith morphological terms. See also Young *et al.* (1997, fig. 12) and Perch-Nielsen (1985; fig. 69).

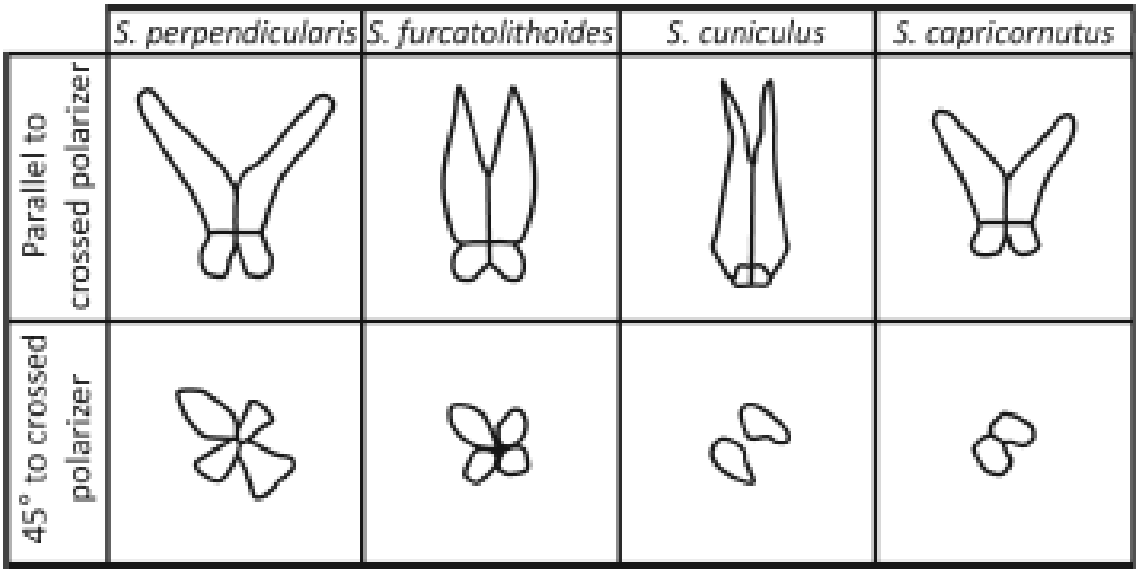

Figure 14 - Sphenolith extinction patterns: Stylized drawing showing birefringence and extinction patterns of *Sphenolithus perpendicularis, S. furcatolithoides, S. cuniculus,* and *S. capricornutus* aligned at 0° and 45° to crossed polarizers.

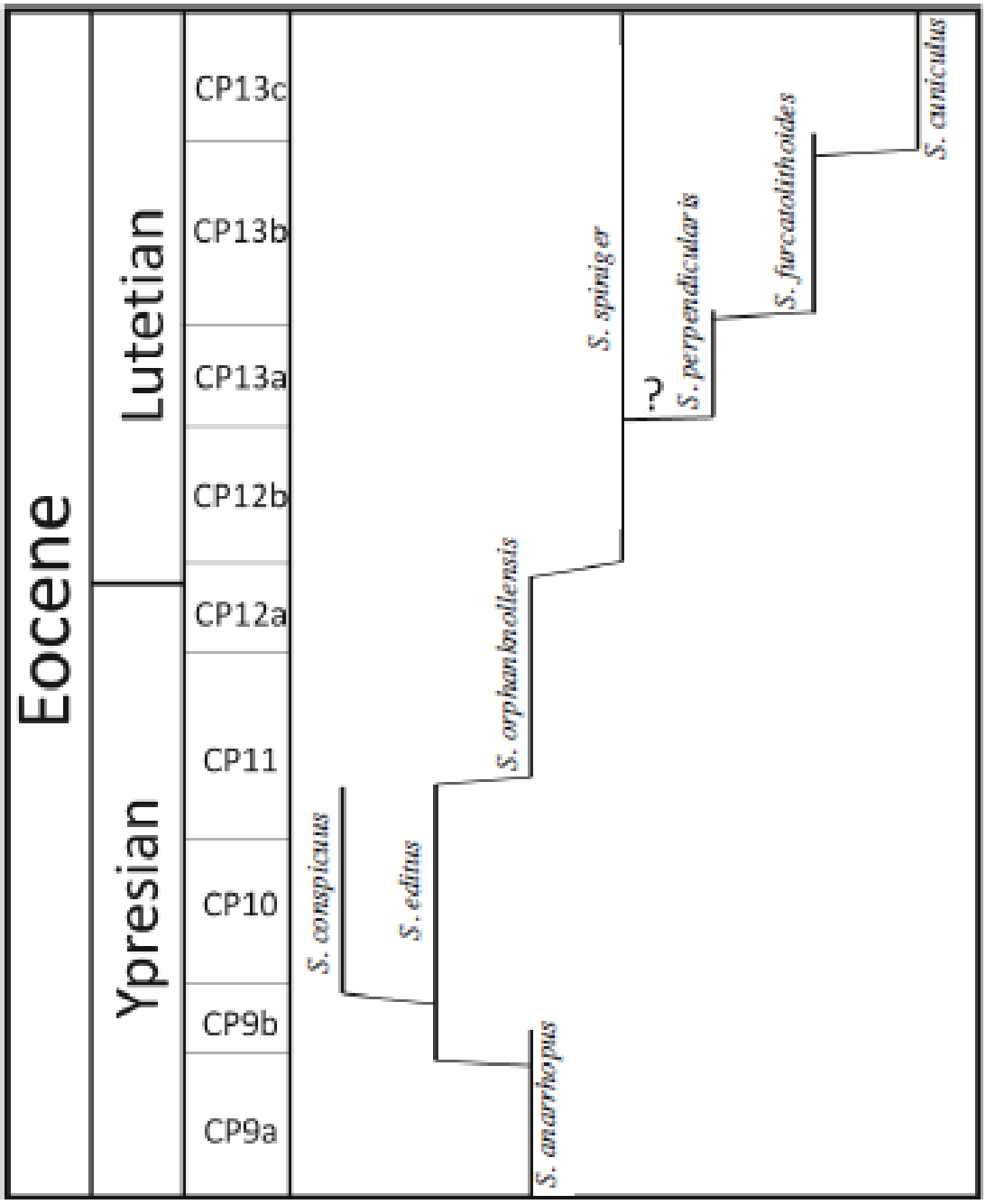

Figure 15 - Proposed Sphenolithus Lineage: Tentative evolutionary lineage of *Sphenolithus,* integrating *S. perpendicularis* and *S. cuniculus,* modified from fig. 69 of Perch-Nielsen (1985).

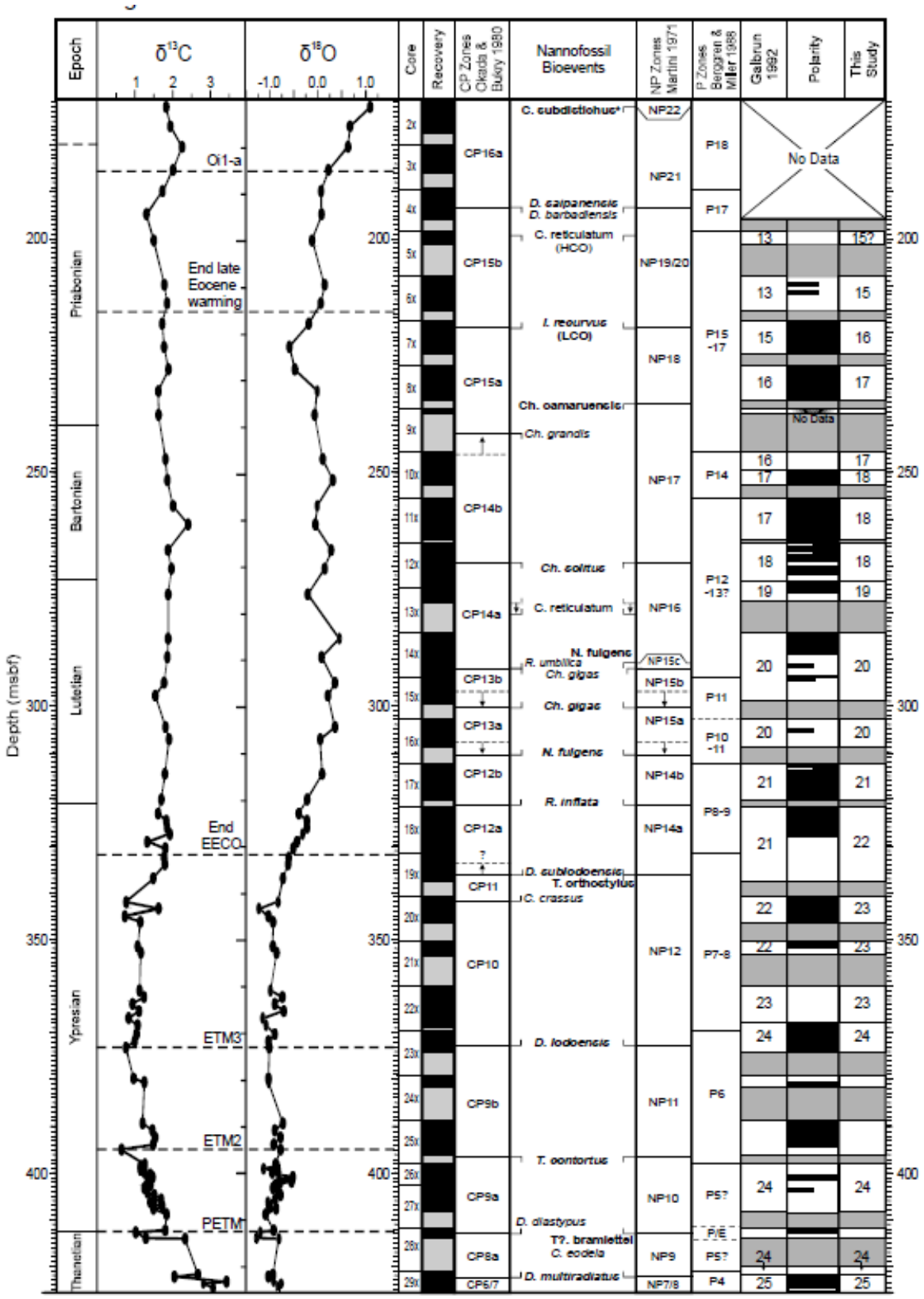

Figure 16 – Stratigraphic Data Correlation at Hole 762C: Correlation of stratigraphic data sets from Site 762C, showing, from left to right, core depth (msbf), $\delta^{13}C$ (‰), $\delta^{18}O$ (‰), core number, core

recovery, calcareous nannofossil CP zonation, nannofossil bioevents, nannofossil NP zonation, planktonic foraminiferal P zonation, magnetostratigraphy of Galbrun (1992), magnetic polarity sequence, and present magnetostratigraphic reinterpretation. $\delta^{13}C$ and $\delta^{18}O$ isotopic data from Thomas Shackleton and Hall (1992), with interpretation of isotopic events shown as dashed lines. Numbered sequence correlates to Table 4 (column 1). CP biomarkers of Okada and Bukry (1980) in bold. NP biomarkers of Martini (1971), with select subzones of Aubry (1991), shown in italic. Joint markers for CP and NP zones shown in both bold and italic. Locations of CP and NP zonal boundaries reflect the midpoint between the observed event and the sample above (for HOs) or below (for LOs). Nannofossil biozone boundaries are shown by solid lines; however, dashed lines are used to show the observed event depth, when sample spacing creates ≥ 2.0 m gap around the bioevent midpoint. Sample depths for nannofossil biostratigraphy provided in Table 2. *Bioevent data from Siesser and Bralower (1992). Coring gaps are shown in grey in both core recovery and magnetic polarity columns. Magnetic polarity indicated by black (white) fill for normal (reverse) polarity. Revised magnetostratigraphy correlated to the GPTS of Ogg, Ogg and Gradstein (2008).

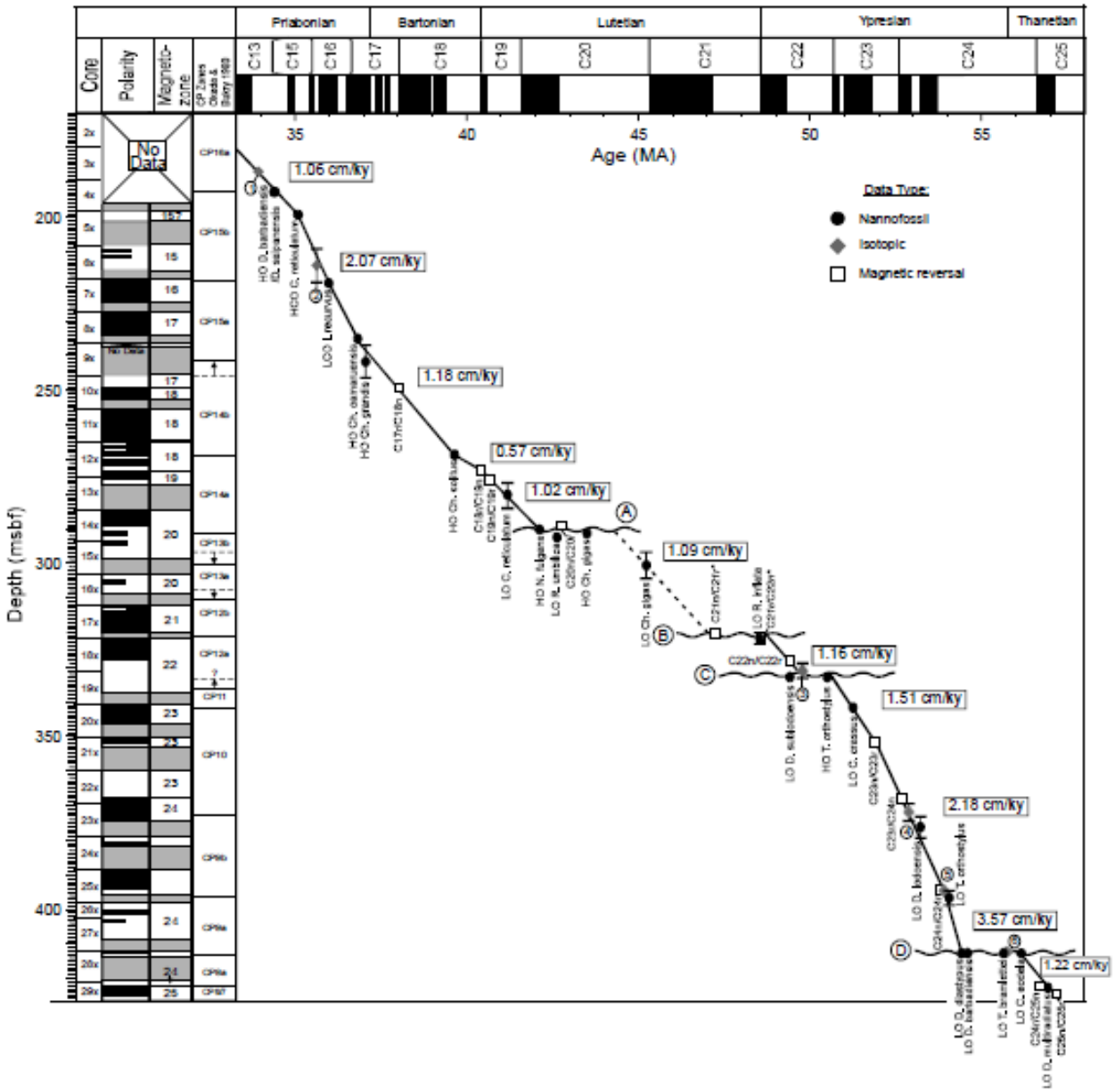

Figure 17 – Revised Age-Depth Model: Age-depth model and derived sediment accumulation rates for ODP Site 762C, correlated to the GPTS of Ogg, Ogg and Gradstein (2008) and Eocene epochs (horizontal axis). Along vertical axis (from left): depth (msbf), core number, magnetic polarity, revised magnetostratigraphy, and nannofossil biostratigraphy. Stratigraphic model derived using calcareous nannofossil, isotopic, and magnetostratigraphic data (Tables 3-5, respectively). Events and depths are shown as sample midpoints. Accumulation rates are calculated between tie-points, assuming constant sedimentation. Where the section is interrupted by a disconformity, sedimentation rates of adjacent sections were used to extrapolate the upper and lower ages and estimate the duration of the hiatus. Three hiatuses (A, C, D) were identified primarily with nannofossil data. Hiatus B was inferred using magnetic polarity and sedimentation rates (See text for further discussion). The large sample gaps around the LO of *Ch. gigas* gives much latitude in interpretation of the sedimentation rate, as indicated by the dashed line (See text for further discussion).

LITHOLOGIC SUMMARY			
Unit	**Core Interval**	**Depth (mbsf)**	**Lithology**
II	3-3-0cm – 12-1-0cm	181.5-265.0	White nannofossil chalk
IIIA	12-1-0cm – 26-10-0cm	265.0-398.0	Light green-grey and white nannofossil chalk with foraminifera
IIIB	26-10-0cm – 29-1-50cm	398.0-554.8	Light green nannofossil chalk

Table 1- Lithologic Summary: Summary of lithologic subunits through the sampled interval at Site 762C, derived from Haq et al. (1990, Table 3, p. 221).

Samp. No.	Core Interval	Depth (mbsf)	Samp. No.	Core Interval	Depth (mbsf)	Samp. No.	Core Interval	Depth (mbsf)	Samp. No.	Core Interval	Depth (mbsf)
1*	3-4-49	184.49	48	10-4-120	251.70	95	16-2-52	303.52	142	22-2-125	362.75
2*	3-4-101	185.01	49*	11-1-50	256.00	96*	16-2-125	304.25	143*	22-3-52	363.52
3*	4-1-46.5	189.47	50	11-1-125	256.75	97*	16-3-52	306.52	144	22-3-125	364.25
4*	4-1-123.5	190.24	51*	11-2-50	257.50	98	16-3-125	307.25	145*	22-4-47.5	364.98
5*	4-2-50	191.00	52	11-2-125	258.25	99*	16-4-45	307.95	146	22-4-125	365.75
6*	4-2-126.5	191.77	53	11-3-51..5	259.02	100*	17-1-51	313.01	147*	22-5-46	366.46
7*	4-3-50	192.50	54*	11-3-125	259.75	101	17-1-145	313.95	148	22-5-125	367.25
8*	4-3-100	193.00	55*	11-4-50	260.50	102*	17-2-52	314.52	149*	22-6-53	368.03
9*	4-4-50	194.00	56	11-4-125	261.25	103	17-2-125	315.25	150	22-6-110	368.60
10	4-4-147	194.97	57*	11-5-50	262.00	104	17-3-52	316.02	151*	23-1-49.5	370.00
11*	5-1-50	199.00	58	11-5-125	262.75	105*	17-3-125	316.75	152*	23-1-125	370.75
12	5-1-125	199.75	59*	11-6-50	263.50	106*	17-4-52	317.52	153*	23-2-49	371.49
13	5-2-53	200.53	60	11-6-140	264.40	107	17-4-116..5	318.17	154	23-2-113	372.13
14*	6-1-48	208.48	61*	12-1-51	265.51	108*	17-5-49.5	319.00	155*	23-3-51	373.01
15	6-1-125	209.25	62	12-1-125	266.25	109	17-5-148	319.98	156*	24-1-54	379.54
16*	6-2-46	209.96	63*	12-2-51	267.01	110*	18-1-50	322.50	157	24-1-142	380.42
17	6-2-125	210.75	64	12-2-125	267.75	111	18-1-124.5	323.25	158*	25-1-50.5	389.01
18*	6-3-50	211.50	65*	12-3-50	268.50	112*	18-2-50	324.00	159	25-1-125	389.75
19	6-3-125	212.25	66	12-3-125	269.25	113	18-2-125	324.75	160*	25-2-47.5	390.48
20*	6-4-50	213.00	67*	12-4-50	270.00	114	18-3-50.5	325.51	161	25-2-115	391.15
21	6-4-125	213.75	68	12-4-125	270.75	115*	18-3-125	326.25	162*	25-3-52	392.02
22*	6-5-40	214.40	69*	12-5-50	271.50	116*	18-4-53	327.03	163	25-3-125	392.75
23*	7-1-50	218.00	70	12-5-125	272.25	117	18-4-125	327.75	164	25-4-54	393.54
24	7-1-125	218.75	71	12-6-50	273.00	118*	18-5-50	328.50	165*	25-4-125	394.25
25	7-2-54	219.54	72*	12-6-147	273.97	119	18-5-125	329.25	166	25-5-43	394.93
26*	7-2-125	220.25	73*	13-1-50	275.00	120*	18-6-52	330.02	167*	26-1-49	398.30
27	7-3-50	221.00	74	13-1-125	275.75	121	18-6-148.5	330.99	168	26-1-125	398.77
28*	7-3-119	221.69	75*	13-2-71	276.71	122	19-1-52	331.52	169*	26-2-49	399.17
29	7-4-50	222.5	76*	14-1-5	284.05	123*	19-1-125	332.75	170	26-2-125	399.69
30*	7-4-146	223.46	77	14-1-72.5	284.73	124*	19-2-52	333.52	171*	26-3-51	400.16
31	8-1-50	227.50	78*	14-2-50	286.00	125	19-2-125	334.25	172	26-3-125	400.62
32*	8-1-125	228.25	79	14-2-125	286.75	126*	19-3-53	335.03	173*	26-4-47	401.06
33*	8-2-53	229.03	80	14-3-52.5	287.53	127	19-3-125	335.75	174	26-4-113.5	401.47
34	8-2-126	229.76	81*	14-3-126	288.26	128*	19-4-52	336.52	175*	26-5-50	402.01
35	8-3-52	230.52	82*	14-4-55	289.05	129*	20-1-50	341.50	176	26-5-148.5	402.61
36*	8-3-125	231.25	83	14-4-125	289.75	130	20-1-125	342.25	177*	27-1-50	403.00
37*	8-4-50	232.00	84*	14-5-50	290.50	131*	20-2-50	343.00	178	27-1-125	403.75
38	8-4-125	232.75	85	14-5-115	291.15	132	20-2-115	343.65	179*	27-2-50	404.50
39*	8-5-50	233.50	86*	14-6-50	292.00	133*	20-3-52	344.52	180	27-2-125	405.25
40*	9-1-46	236.96	87	14-6-147	292.97	134	20-3-125	345.25	181*	27-3-50	406.00
41*	10-1-50	246.50	88*	15-1-48	293.98	135*	20-4-47.5	345.98	182	27-3-125	406.75
42	10-1-125	247.25	89	15-1-125	294.75	136*	21-1-50	351.00	183*	27-4-50	407.5
43*	10-2-49.5	248.00	90	15-2-52	295.52	137	21-1-129	351.79	184	27-4-138	408.38
44	10-2-125	248.75	91*	15-2-124	296.24	138*	21-2-50	352.20	185*	28-1-59	412.59
45*	10-3-50	249.50	92*	15-3-48	296.98	139*	22-1-50	360.50	186*	28-1-125	413.25
46	10-3-115	250.15	93*	16-1-48	303.48	140	22-1-125	361.25	187*	29-1-50	422.00
47*	10-4-50	251.00	94	16-1-125	304.25	141*	22-2-46	361.96			

Table 2 – Nannofossil Sample List: Core intervals and depths (mbsf) for the 187 nannofossil samples used in this study. *Samples used for detailed assemblage study marked with an asterisk

CP Zonation				This study			
Zone/Subzone		Event	Marker Taxa	Sample Interval	Base	Top	Midpoint
16	a	HO	*D. saipanensis; D. barbadiensis*	*4-3-100*/4-3-50	193.00	192.50	192.75
15	b	LO	*I. recurvus*	7-2-125/*7-1-50*	220.25	218.00	219.13
	a	LO	*Ch. grandis*	*10-1-50*/9-1-46	246.50	236.96	241.73
14	b	HO	*C. solitus*	*12-3-125*/12-3-50	269.25	268.50	268.88
	a	LO	*R. umbilica*	14-6-127/*14-6-50*	292.97	292.00	292.49
13	c	HO	*Ch. gigas*	*14-6-50*/14-5-115	292.00	291.15	291.58
	b	LO	*Ch. gigas*	16-1-48/*15-3-48*	303.48	296.98	300.23
	a	LO	*N. fulgens*	17-1-51/*16-4-45*	313.01	307.95	310.48
12	b	LO	*R. inflata*	18-1-50/*17-5-148*	322.50	319.98	321.24
	a	LO	*D. sublodoensis*	19-2-125/*19-2-52*	334.25	333.52	333.89
11		LO	*C. crassus*	20-1-125/*20-1-50*	342.25	341.50	341.88
10		LO	*D. lodoensis*	24-1-54/*23-3-51*	379.54	373.01	376.30
9	b	HO	*T. contortus*	*26-1-49*/25-5-43	398.30	394.93	396.62
	a	LO	*D. diastypus*	28-1-125/*28-1-59*	413.25	412.59	412.92
8	b	LO	*C. eodela; Rhomboaster spp.*	28-1-125/*28-1-59*	413.25	412.59	412.92
	a	LO	*D. multiradiatus*	*29-1-50*	422.00		422.00

NP Zonation				This Study				Siesser & Bralower (1992)			
Zone/Subzone		Event	Marker Taxa	Sample Interval	Base	Top	Midpoint	Sample Interval	Base	Top	Midpoint
21		HO	*D. saipanensis*	*4-3-100*/4-3-50	193.00	192.50	192.75	*5-2-36*/5-1-54	200.36	199.04	199.70
19/20		LO	*I. recurvus*	7-2-125/*7-1-50*	220.25	218.00	219.13	7-4-100/*7-3-100*	223.00	221.50	222.25
18		LO	*Ch. oamaruensis*	9-1-46/*8-5-50*	236.96	233.50	235.23	10-1-105/*9x, CC*	247.05	246.00	246.53
17		HO	*Ch. solitus*	*12-3-125*/12-3-50	269.25	268.50	268.88	*12-6-100*/12-5-100	273.50	272.00	272.75
16		HO	*B. gladius; N. fulgens*	*14-5-115*/14-5-50	291.15	290.50	290.83	**14-1-100*/13x, CC	285.00	284.00	284.50
15	c	HO	*Ch. gigas*	*14-6-50*/14-5-115	292.00	291.15	291.58	*14-6-100*/14-5-100	293.00	291.50	292.25
	b	LO	*Ch. gigas*	16-1-48/*15-3-48*	303.48	296.98	300.23	16-1-99/*15x, CC*	303.99	303.00	303.50
	a	LO	*N. fulgens*	17-1-51/*16-4-45*	313.01	307.95	310.48	16x, CC/*16-3-99*	312.50	306.99	309.75
14	b	LO	*R. inflata*	18-1-50/*17-5-148*	322.50	319.98	321.24	17x, CC/*17-5-99*	322.00	319.49	320.75
	a	LO	*D. sublodoensis*	19-2-125/*19-2-52*	334.25	333.52	333.89	18-6-100/*18-5-100*	330.50	329.00	329.75
13		HO	*T. orthostylus*	*19-2-52*/19-1-125	333.52	332.75	333.14	*19-3-100*/19-2-100	335.50	334.00	334.75
12		LO	*D. lododensis*	24-1-54/*23-3-51*	379.54	373.01	376.28	22x, CC/*23-1-100*	370.50	369.50	370.00
11		HO	*T. contortus*	*26-1-49*/25-5-43	398.30	394.93	396.62	*25-4-100*/25-3-100	394.00	392.50	393.25
10		LO	*T?. bramlettii*	28-1-126/*28-1-59*	413.25	412.59	412.92	27-4-99/*27-3-100*	408.00	406.49	407.25
9		LO	*D. multiradiatus*	*29-1-50*	422.00	NA	422.00	29-1-100/*28x, CC*	422.50	421.50	422.00

Table 3 – Nannofossil Biostratigraphy: Summary of Eocene nannofossil biostratigraphy at Site 762C. Standard CP Zonation of Okada and Bukry (1980) shown above. NP zonation of Martini (1971) with select subzones of Aubry (1991) below, with comparison of the current study (center) and original ODP results of Siesser and Bralower (1992) (right). Bioevents were observed in italicized sample interval. Event midpoints were extrapolated using the sample below (for LOs) or sample above (for HOs).

Table 4 – Additional Nannofossil Bioevents

Event	Species	Sample	Depth
AB	Clausicoccus spp.	3-4-101	185.01
HO	C. reticulatum	4-1-123.5	190.24
LO	H. archus	4-4-50	194.00
HO	D. salpanensis		
HCO	C. reticulatum	5-1-50	199.00
LO	R. oamaruensis	6-4-50	213.00
INC	L. minutus	6-5-40	214.40
LCO	I. recurvus	7-1-50	218.00
HO	H. lophota		
LO	Ch. oamaruensis	8-5-50	233.50
LO	I. recurvus	9-1-46	236.96
LO	H. reticulata		
HO	Ch. titus		
HO	D. strictus		
HO	Ch. grandis	10-1-50	246.50
HO	Cl. vanheckiae		
LO	Ch. eoaltus	10-3-50	249.50
HO	C. dela		
HO	P. inversus		
HO	N. minutus	11-2-50	257.50
HO	S. spiniger		
	C. dela	11-3-125	259.75
LO	D. stavensis	11-5-50	262.00
LCO	R. lockeri	11-6-50	263.50
HO	S. cuniculus		
LCO	D. bisectus	12-1-51	265.51
HO	S. strigosus	12-2-51	267.01
HO	C. prionion	12-3-50	268.50
HO	Ch. solitus	12-3-125	269.25
LCO	R. hillae	12-4-50	270.00
LO	S. pseudoradians	13-1-50	275.00
HCO	Ch. expansus		
LO	D. nodifer	13-2-71	276.71
LO	H. situliformis		
LO	C. reticulatum		
LCO	R. umbilica		
HO	D. wemmelensis	14-1-5	284.05
LO	C. floridanus	14-2-50	286.00
LO	H. compacta	14-3-126	288.26
LO	S. strigosus	14-4-55	289.05
HO	S. furcatolitholdes		
HO	N. fulgens	14-5-115	291.15
HO	Ch. gigas	14-6-50	292.00
LO	B. serraculoides	15-1-48	293.98
LO	S. cuniculus		
LO	Ch. gigas	15-3-48	296.98
LO	S. furcatolitholdes		
HO	D. subiodoensis		
LO	Cr. opacus	15-1-48	303.48
HO	S. perpendicularis		
LO	Ch. titus	15-4-45	307.95
LO	D. salpanensis		
LO	N. fulgens		
LO	S. perpendicularis		
HO	R. inflata	17-1-51	313.01
HO	T. callosus	17-4-52	317.52
HO	T. magnicrassus		
LO	D. wemmelensis	17-5-49.5	319.00
LO	Nannotetrina spp.		
HO	D. kuepperi		
HO	G. gammation		
LO	R. inflata	17-5-148	319.98
LO	Cr. nebulosus	18-1-50	322.50
LO	Cl. vanheckiae		
LO	D. strictus	18-2-50	324.00
HO	D. lodoensis	18-3-125	326.25
LO	C. protoannulus	18-4-53	327.03
LO	C. eopelagicus	18-5-50	328.50
HO	C. crassus		

Event	Species	Sample	Depth
INC	D. scrippsae	18-6-52	330.02
LO	N. minutus		
LO	P. inversus		
LO	S. spiniger		
LO	L. minutus	19-1-125	332.75
AE	Discoaster spp		
HO	Ch. eograndis		
HO	T. pertusus		
HO	E. macellus		
LCO	D. subiodoensis	19-2-52	333.52
HO	T. orthostylus		
HO	S. editus		
HO	D. binodosus		
HO	Ch. californicus		
LO	D. praebifax	19-3-53	335.03
LO	Cl. subdistichus	19-4-52	336.52
LO	D. scrippsae		
HO	L. nascens		
LO	C. crassus		
HO	H. lophota	20-1-50	341.50
HO	D. salisburgensis		
HCO	T. pertusus		
HO	L. reniformis	20-2-50	343.00
AB	Discoaster spp	20-4-47.5	345.98
HO	Chiphragmalithus spp.		
LO	R. dictyoda	21-1-50	351.00
LO	C. prionion	21-2-50	352.20
HO	N. rosenkrantzii	22-5-46	366.46
HO	D. diastypus		
LO	Ch. expansus	22-6-53	368.03
HO	Ch. bidens	23-1-49.5	370.00
LO	C. grandis	23-2-49	371.49
LO	P. larvalis		
LO	N. dubius	23-3-51	373.01
LO	D. kuepperi		
LO	D. lodoensis		
LO	Chiphragmalithus spp.		
LO	G. gammation	24-1-54	379.54
LO	L. reniformis		
HO	C. eodela		
HO	T. eminens	25-1-50.5	389.01
HO	D. multiradiatus	25-2-47.5	390.48
HO	D. lenticularis		
HO	T. serotinus		
LO	D. deflandrei	25-3-52	392.02
LO	T. magnicrassus		
LO	S. radians	25-4-125	394.25
HCO	T. eminens		
LO	T. orthostylus	25-5-43	394.93
HO	T. contortus	26-1-49	398.30
LO	U. jordanii		
LO	S. editus	26-2-49	399.17
HO	Rhomboaster spp.	26-4-47	401.06
LO	C. dela	27-1-50	403.00
LO	Ch. eograndis	27-3-50	406.00
LO	D. elegans		
LO	Cl. fenestratus	28-1-59	412.57
LO	C. eodela		
LO	E. formosa		
HO	Fasciculithus spp.		
LO	D. barbadiensis		
LO	D. diastypus		
LO	L. nascens		
LO	T. bramlettei		
LO	T. contortus		
LO	S. moniformis	28-1-125	413.25
HO	P. bisulcus		
HO	E. robusta	29-1-50	422.00
LO	D. multiradiatus		

Table 4 (Previous Page) – Additional Nannofossil Bioevents: Summary of key Eocene nannofossil bioevents at Site 762C. Samples provided represent the interval and depth in which the event was observed. Midpoints may be extrapolated using sample list in Table 3. LO = lowest occurrence; LCO = lowest common occurrence; HO = highest occurrence; HCO = highest common occurrence; AB= acme begin; AE = acme end; INC = increase; CO = cross-over.

Isotopic Event	Midpoint (msbf)	Age 2008 GPTS, Ogg et al	Age CK95/BKSA95	Reference
Oi-1, Step 1	187.00	33.93	33.75	Pearson et al. 2008
End Late Eocene warming/ "Vonhof" cooling event	213.30	35.50	35.50	Vonhof et al. 2000 Zachos et al. 2001
MECO?	277.00	39.87	40.00	Bohaty et al. 2009 Jovane et al. 2007
End EECO	331.22	49.78	49.00	Bohaty & Zachos 2003
ETM3/"X" event/Event "K"	372.35	52.88		Galeotti et al. 2010
ETM2/H1/ELMO	394.85	53.91	53.44	Lourens et al. 2005
PETM	412.65	55.74	54.98	Cramer et al. 2003

Table 5 – Stable Isotopic Data: Sample midpoints of isotopic excursion events identified at Site 762C from $\delta^{13}C$ and $\delta^{18}O$ data of Thomas Shackleton and Hall (1992). Dates originally given in the CK95 or BKSA95 timescales were also converted to the GPTS of Ogg Ogg and Gradstein (2008). Primary references used to identify and date isotopic events given at far right.

Sample Interval	Depth (mbsf)	Species Richness (S)	Diversity (H)	*Z. bijugatus*		*Fasciculithus* spp.		*Discoaster* spp.		*Chiasmolithus* spp.		*Sphenolithus* spp.		*Toweius* spp.		*Ericsonia* spp.		*Ericsonia formosa*	
				A	B	A	B	A	B	A	B	A	B	A	B	A	B	A	B
27-2-50	404.5	51	2.64	73	14.6	0	0	21	4.2	8	1.6	11	2.2	112	22.4	55	11	19	3.8
27-3-50	406	54	3.04	69	13.8	0	0	39	7.8	18	3.6	12	2.4	133	26.6	61	12.2	23	4.6
27-4-50	407.5	56	2.84	41	8.2	0	0	18	3.6	13	2.6	10	2	113	22.6	76	15.2	21	4.2
28-1-59	412.59	46	2.90	64	12.8	1	0.2	57	11.4	12	2.4	17	3.4	105	21	54	10.8	22	4.4
28-1-125	413.25	29	2.41	38	7.6	170	33.9	25	5	4	0.8	2	0.4	119	23.8	15	3	0	0
29-1-50	422	25	2.33	44	8.8	160	31.9	9	1.8	2	0.4	0	0	140	27.9	20	4	0	0

Table 6 – PETM Nannofossil Trends: Summary of key nannofossil abundance trends through the PETM interval, along with species richness and Shannon diversity. Columns A and B give absolute and relative (%) abundance of taxa, respectively. Maximum ^{13}C excursion occurs at 412.65 msbf, with shaded row highlighting nannofossil sample that most closely approximates this interval (412.59 msbf), with the nannofossil assemblage showing significant increases in species richness and diversity just 0.06 m above the excursion.

Reticulofenestra Group	Warm Taxa	Cool Taxa	Holococcoliths	E-O Transitional (Group 1)
Reticulofenestra spp.	*Discoaster* spp.	*Chiasmolithus* spp.	*Z. bijugatus*	*C. protoannulus*
Dictyococcites spp.: (*D. bisectus, D.stavensis, D. scrippsae*	*Sphenolithus* spp.	*I. recurvus*	*L. minutus*	*R. dictyoda*
	E. formosa	*R. daviesii*		*L. minutus*
				Z. bijugatus

Table 7 – Paleoecological Groupings: Summary of taxa groupings applied in this study. Taxa with questionable or disputed affinity have not been included (See Villa et al. 2008), but abundance patterns are compared to taxa with more confident paleoecological affinities. Eocene-Oligocene transitional group are from Dunkley-Jones et al. (2008, fig. 6). *Pemma papillatum* and *Varolia maceleodii* are not included as they are absent at Site 762C.

Species	FO interval	Depth mbsf	LO interval	Depth mbsf	Zonal marker
Rhabdosphaera inflata	17-5, 49.5-50.5cm	318.995	17-1, 45-46cm	113.01	FO base CP12b/NP14b
Nannotetrina fulgens	16-4, 45-46cm	307.95	14-6, 50-51cm	292.00	FO base CP13a/NP15a LO base NP16
Sphenolithus perpendicularis	16-4, 45-46cm	307.95	16-1, 48-49cm	303.48	FO approximates base of CP13a/NP15a
Chiasmolithus gigas	15-3, 48-49cm	296.48	14-6, 50-51cm	292.00	FO base CP13b/NP15b LO base CP13c/NP15c
Sphenolithus furcatolithoides	15-3, 48-49cm	296.48	14-4, 55-56cm	289.05	FO approximates base of CP13b/NP15b LO near base CP13c
Sphenolithus cuniculus	15-1, 48-49cm	293.98	not encountered		
Reticulofenestra umbilica	13-1, 50-51cm	275.00	not encountered		FO base CP14a

Table 8 – Sphenolithus Range Data: Sample intervals and depths of LOs and HOs of key biostratigraphic markers and species of *Sphenolithus* from Site 762C.

Event	Taxa	Top-Base (msbf)	Midpoint	Age (MA)
HO	*D. saipanensis*	192.50-193.00	192.75	34.35
HO	*D barbadiensis*	192.50-193.00	192.75	34.45
HCO	*C. reticulatum*	199.00-199.75	199.38	35.09
LCO	*I. recurvus*	218.00-220.25	219.13	35.98
HO	*Ch. oamaruensis*	233.50-236.96	235.23	36.83
HO	*Ch. grandis*	236.96-246.50	241.73	36.92
HO	*Ch. solitus*	268.50-269.25	268.88	39.69
LO	*C. reticulatum*	276.71-284.05	280.38	41.10
HO	*N. fulgens*	290.50-291.15	290.83	42.12
LO	*R. umbilica*	292.00-292.97	292.49	42.69
HO	*Ch. gigas*	291.15-292.00	291.58	43.51
LO	*Ch. gigas*	296.98-303.48	300.23	45.18
LO	*R. inflata*	319.98-322.50	321.24	47.95
HO	*T. orthostylus*	332.75-333.52	333.14	50.51
LO	*D. sublodoensis*	333.52-334.25	333.89	49.41
LO*	*C. crassus*	341.50-342.25	341.88	51.26
LO	*D. lodoensis*	373.01-379.54	376.28	53.23
LO	*T. orthostylus*	394.93-398.3	396.62	54.14
LO**	*D. diastypus*	412.59-413.25	412.92	54.42
LO†	*D. barbadiensis*	412.59-413.25	412.92	54.61
LO	*T. bramlettei*	412.59-413.25	412.92	55.65
LO	*C. eodela*	412.59-413.25	412.92	56.21
LO	*D. multiradiatus*		422.00††	56.98

Table 9 – Nannofossil Tie-Points: Depth ranges and midpoints of calcareous nannofossil data integrated into the revised age model. Nannofossil ages represent calibrated dates from BKSA95, converted to the 2008 GPTS of Ogg Ogg and Gradstein, unless otherwise indicated. *Age for LO *C. crassus* derived from Bottaccione, Possango, and Contessa Highway sections (Table 6). **Age for the LO *D. diastypus* from averaging calibrated dates from Site 1262, Site 1215A, and Site 577. †Age for LO D. barbadiensis from averaging calibrated dates from Site 577 and the Bottaccione and Contessa Highway sections (Italy). ††This depth represents the deepest sample examined in Shamrock and Watkins (in press) but also correspond to the midpoint depth of Siesser and Bralower (1992), who samples much deeper in the core.

Chemical Event	Midpoint (msbf)	Age 2008 GPTS, Ogg et al	Age CK95/BKSA95	Chron	Source
Oi-1, Step 1	187.00	33.93	33.75	C13r	Pearson et al. 2008
End Late Eocene warming / "Vonhof" cooling event	213.30	35.5	35.5	C16n.1n	Vonhof et al. 2000 Zachos et al. 2001
End EECO	331.22	49.78	49.00	C22r	Bohaty & Zachos 2003
ETM3/"X" event/Event "K"	372.35	52.88		C24n.1n	Galeotti et al. 2010
ETM2/H1/ELMO	394.85	53.91	53.44	C24r	Lourens et al. 2005
		53.81-54.09	53.35-53.61	C24n	Cramer et al. 2003
PETM	412.65	55.74	54.98	C24r	Cramer et al. 2003

Table 10 – Isotopic Tie-Points: Depth ranges and midpoints of $\delta^{13}C$ and $\delta^{18}O$ isotopic excursion events integrated into the revised age model. Magnetochron correlations from primary references (right). Dates originally given in the CK95 or BKSA95 timescales were converted to the GPTS of Ogg Ogg and Gradstein (2008).

Chron Base	Top-Base (msbf)	Midpoint (msbf)	Age[1] (MA)	Age[2] (MA)
C17r/C18n	248.80-249.41	249.11	38.03	38.43
C18r/C19n	273.11-273.80	273.46	40.44	41.26
C19n/C19r	275.81-276.20	276.01	40.67	41.52
C20n/C20r	288.32-289.00	288.66	42.77	43.79
C21n/C21r*		320.25	47.23	47.91
C21r/C22n*		322.00	48.60	49.03
C22n/C22r	327.60-328.50	328.05	49.43	49.71
C23n/C23r	351.57-352.22	351.90	51.90	51.74
C23r/C24n	367.77-368.31	368.04	52.65	52.36
C24n/C24r	394.40-394.76	394.58	53.81	53.35
C24r/C25n	421.98-422.94	422.46	56.66	55.9
C25n/C25r	424.09-424.80	424.45	57.18	56.39

Table 11 – Magnetostratigraphy Tie-Points: Depth ranges and midpoints for magnetic polarity reversal boundaries integrated into the revised age model. Magnetochron reversal dates of Ogg Ogg and Gradstein (2008)[1] and Cande and Kent (1995)[2].

Table 12 – Nannofossil Event Ages (Following two pages): Summary of derived ages for nannofossil bioevents at Site 762C based on the revised age model, compared to the BSKA95 and several additional, globally distributed sites. Midpoints for Site 762C are extrapolated using sample list in Table 1. Published and extrapolated ages of calcareous nannofossil bioevents are recalibrated to the GPTS of Ogg Ogg and Gradstein (2008). LO = lowest occurrence; LCO = lowest common occurrence; LRO = lowest rare occurrence; HO = highest occurrence; HCO = highest common occurrence; AB = acme begin; AE = acme end; CO = cross-over. Bioevents representing the HCO or LCO for a particular taxa are given in italic. The lowest rare occurrence (LRO), a designation not used in this study but in others, is shown in bold. Events located within a hiatus cannot be accurately dated, are indicated by UNC.

Event	Taxa	Site 762C		BKSA95		SE Pyrenees		Site 1218		Site 1172A	
		Mag	Date	Mag	Date	Mag	Date	Mag	Date	Mag	Date
AB	Clausicoccus spp.		33.91±.21								
HO	D. saipanensis	C13r	34.47±.03	C13r	34.35	C13r		C13r	34.41		
HO	D.barbadiensis	C13r	34.47±.03	C13r	34.45			C13r	34.60		
LO	R. oamaruensis	13r	34.40±.03	16n.1n	35.45						
LCO	I. recurvus	*C16n.2n*	*36.04±.06*								
LO	I. recurvus	C16r	36.37±.12	C16n.2n	35.98	C16n.2n					
HO	C. reticulatum	C13r	34.20±.02	C15r	35.09	C15r					
HCO	C. reticulatum	*C15r*	*35.09*								
HO	N. dubius	C17n.2n	37.39±.40							C16r	36.37
LO	Ch. oamaruensis	C17n.1n	36.83±.20	C17n.1n	36.83	C17n.1n				C18n	38.28
HO	Ch. grandis	C17n.2n	37.39±.41	C17n.1n	36.92	C17n.1n		C17n.2n	37.54		
HO	S. spiniger	*C18n.1n*	*38.65±.06*								
HO	S. radians	C13r	34.41±.04								
LO	S. predistentus	*C18n.2n*	*39.11±.06*								
LO	D. bisecta	C18r	39.96±.13	C17n.3n	37.68			C18n.1n	39.46	C18n	38.50
LCO	D. bisecta	*C18n.2n*	*39.46±.06*								
HO	Ch. expansus	C18r	39.86±.07								
HO	Ch.solitus	C18r	39.71±.03	C18r	39.69			C18r	39.69		
LO	C. reticulatum	C19r	41.10±.36	C19r	41.10					C18r	39.46
LO	R. umblilca	C20n	UNC A	C20n	42.69						
HO	Ch. gigas	C20r	UNC A	C20r	43.51						
HO	N. fulgens	C20n	42.12±.03	C20n	42.12	**Possango**				**NJ Coastal Plain**	
LO	Ch. gigas	C20r	45.18±.30	C20r	45.18						
LO	S. furcatolithoides	C20r	45.18±.02			**Mag**	**Date**			**Mag**	**Date**
LO	D.saipanensis	C21n	46.12±.23								
LO	N. fulgens	C21n	46.12±.23	C21n	46.54	C21n	45.96±.01			C21n	46.27
LO	Nannotetrina spp.	C21n	47.06±.16			C21r	47.33±.01				
LO	R. inflata	C21r	UNC B	C21r	47.95						
HO	C.crassus	C22n	49.10±.06								
HO	D. lodoensis	C22n	48.87±.10			C21r	47.78±.06				
HO	D. kuepperi	C21n	46.83±.11								
AE	Discoaster spp.	C22r	49.93±.20			C22r	50.58±.03				
"AB"	Dict/Reticulo gp.	C22r	49.93±.20			C22r	50.58±.03				
HO	Toweius spp	*C22r*	*49.93±.20*			C23n	51.75±.03				
LO	D. sublodoensis	C22r	50.51±.03	C22n	49.41	C22n	49.13±.02			C21r	48.56
HO	T. orthostylus	C22r	50.71±.10	C22r	50.51	C22r	50.58±.03			C23n	50.73
LO	C. crassus	C23n.2n	51.24±.03			C23n	50.91±.03	**Site 1215A, B**		**Site 577**	
AB	Discoaster spp.	C23n.2n	51.46±.05			C23n	51.75±.03				
HO	D. diastypus	C23n	51.79±.03					**Mag**	**Date**	**Mag**	**Date**
LO	N. dubius	C24n.2r	53.22±.01								
LCO	D. lodoensis	C24n.2r	53.22±.01			C24n.1r	53.06±.06	C23r	52.03±.19		
LO	D. lodoensis	C24n.3n	53.39±.10	C24n.2r	53.23	C24n.3n	53.65±.06				
LCO	Chiphrag. Spp	*C24n.3n*	*53.39±.10*								
HO	C. eodela	C24n.3n	53.39±.10								
LO	G. gammation	C24n.3n	53.49±.01			C24n.3n	53.44±.06			C24n	52.85
HO	D.multiradiatus	C24n.3n	53.61±.13					C24r-24n	54.46±.51	C24n	53.41
HO	T. eminens	C24n.3n	53.69±.13								
LO	D. kuepperii	C24n.3n	53.77±.02							C24r	53.90
HCO	T. eminens	C24r	53.86±.03								
HO	T. contortus	C24r	53.96±.05	C24r	54.10	C24r	54.34±.08	C24r	53.885		
LO	S. radians	C24r	53.95±.06			C24r	54.34±.08	C24r	54.46±.51	C24r	53.90
LO	S. editus	C24r	54.05±.02								
LO	T. orthostylus	C24r	53.96±.07	C24r	54.14	C24r	54.34±.08	C24r	53.915	C24r	53.90
HO	T. bramelttеii	C24r	54.02±.01	C24r	54.42	C24r	54.94±.08	C24r	54.045		
LO	D. diastypus	C24r	54.42±.03			C24r	55.39±.08	C24r	54.31±.07	C24r	54.29; **54.97**
LO	T. contortus	C24r	UNC D	C24r		C24r	55.24±.08	C24r	54.375		
LO	D.barbadiensis	C24r	UNC D							C24r	54.29
HO	Fasciculithus spp	C24r	UNC D			C24r	56.21±.30			C24r	54.64
CO	Fasic/Zygrh CO	C24r	UNC D			C24r	56.57±.01				
LO	T. bramlettei	C24r	UNC D	C24r	55.65	C24r	55.99±.15	C24r	54.765		
LRO	T. bramlettei			**C24r**		**C24r**	**56.645**				
HO	F. tympaniformis	C24r	UNC D	C24r	56.02						
LCO	C. eodela	C24r	56.24±.03	C24r	56.21						
LCO	Z. bijugatus										
LO	Z. bijugatus									C24r	55.28
HO	E. robusta	C24r	56.62±.36					C24r	56.59±.03		
LO	D. multiradiatus	C25n	56.98±.02	C25n	56.98			C25n	56.76±.07	C25n	56.91

Event	Taxa	Site 1090B		Site 1123C		Bottaccione		Contessa Highway		Site 689B	
		Mag	Date	Mag	Date	Mag	Date	Mag	Date	Mag	Date
AB	Clausicoccus spp.			13r	33.80						
HO	D. saipanensis	C13r	34.25	13r	34.12						
HO	D.barbadiensis	C13r	34.36	13r	34.12						
LO	R. oamaruensis	16n.1n	35.44							15r	35.35
LCO	I. recurvus	*C16n.2n*	*35.98*								
LO	I. recurvus	C16r	36.28			C15r?		C15r?		C16n	35.99
HO	C. reticulatum	C13r	34.93							16n	35.99
HCO	C. reticulatum	*C16n.2n*	*36.28*								
HO	N. dubius			**Site 1051A**						17n1n	36.54
LO	Ch. oamaruensis	C18n?	38.12	**Mag**	**Date**					18n1n	36.98
HO	Ch. grandis	C18n?	38.7			C18n	38.74	C18n	39.14		
HO	S. spiniger			C18n	38.14						
HO	S. radians					C18n	38.74	C18n	39.65		
LO	S. predistentus			C18r	39.84						
LO	D. bisecta	C18r?	40.05			C18r	39.97	C18n	39.39	17n1n	37.29
LCO	D. bisecta	*C18n.1n*	*39.76*	*C18r*	*39.73*						
HO	Ch. expansus									18n1n	39.33
HO	Ch.solitus	C18r?	39.91	C18r	39.98						
LO	C. reticulatum	C18r?	40.36	C19r	41.27						
LO	R. umblilca			C20n	42.45	C20n	42.56	C20n	42.64		
HO	Ch. gigas			C20r	43.09						
HO	N. fulgens			C20n	42.61	C20n					
LO	Ch. gigas			C20r	45.11						
LO	S. furcatolithoides			C20r	45.11						
LO	D.saipanensis	*C18r?*	*40.05*	C20r	45.17	C21r	47.78	19r	40.91		
LO	N. fulgens			C20r	45.24	C21n	46.49	C21n	46.91		
LO	Nannotetrina spp.			C21n	45.40						
LO	R. inflata			C21n		C21n	47.17				
HO	C.crassus					C22n	48.84	C22n	48.78		
HO	D. lodoensis					*C22n*	*49.15*	C22n	48.78		
HO	D. kuepperii							C22n	48.78		
AE	Discoaster spp.										
"AB"	Dict/Reticulo gp.										
HO	Toweius spp										
LO	D. sublodoensis					C22r	50.51	C22n	49.37		
HO	T. orthostylus					C23n	52.34	C22r	50.02		
LO	C. crassus	**Site 1262**				C23n	51.10	C23n	51.78		
AB	Discoaster spp.										
HO	D. diastypus	**Mag**	**Date**	C22r	49.85	C23n	51.10	C22n			
LO	N. dubius			C23r	52.54						
LCO	D. lodoensis			C23n	51.76						
LO	D. lodoensis			C24n	53.35	C24n	53.29	C23r			
LCO	Chiphrag. Spp										
HO	C. eodela			C23r	52.54						
LO	G. gammation			C23r	52.55	C24n		C24n	53.58		
HO	D.multiradiatus	*C24r*	*54.145*	C24r	54.21	C24n	53.06	C24r	53.87		
HO	T. eminens			C24n	53.15						
LO	D. kuepperii							C24r	56.14		
HCO	T. eminens										
HO	T. contortus	C24r	54.04±.01	C24r	54.10	C24r	53.99				
LO	S. radians	C24r	54.09±.01	C24r	53.96	C24r	54.84	C24r	56.66		
LO	S. editus	C24r	54.18±.01								
LO	T. orthostylus	C24r	54.23±.01	C24r	54.10	C24r	53.99	C24r	54.72		
HO	T. bramelttеii	C24r	54.27±.01								
LO	D. diastypus	C24r	54.665			C24r	55.26	C24r	56.14		
LO	T. contortus	C24r	54.54±.01	C24r	54.94; *54.61*						
LO	D.barbadiensis					C24r	54.81	C24r	54.72		
HO	Fasiculithus spp	C24r	55.24±.01					C24r	54.72		
CO	Fasic/Zygrh CO	C24r	55.58	C24r	56.61						
LO	T. bramlettei	C24r	55.075	C24r	56.29						
LRO	T. bramlettei	**C24r**	**55.605**								
HO	F. tympaniformis			C24r	56.50	C24r	54.84	C24r	54.72		
LCO	C. eodela	C24r	55.595								
LCO	Z. bijugatus	C24r	55.59								
LO	Z. bijugatus	C24r	56.405	C24r	56.64			C24r	55.24		
HO	E. robusta	C25n	56.66	C24r	56.64						
LO	D. multiradiatus	C25n	56.76			C24r	56.08	C25n	56.96		

UNC.	Depth (msbf)	Upper Date (Ma)	Lower Date (Ma)	Duration (My)	Associated Sequence
A	289.75	42.02	44.22	2.20	Lu3
B	321.13	47.10	48.83	1.74	Lu1
C	332.18	49.79	50.71	0.92	Yp9-Yp10
D	412.78	54.41	56.22	1.81	Yp1-Yp3

Table 13 – Summary of Unconformities: Summary of unconformities identified at Site 762C, including the event depth, upper and lower extrapolated ages, and approximate duration of the stratigraphic hiatus.

Plate 1: Chiastozyga., Calciosolenia., Rhabdosphaera., Zygodisca., Calcidisca.

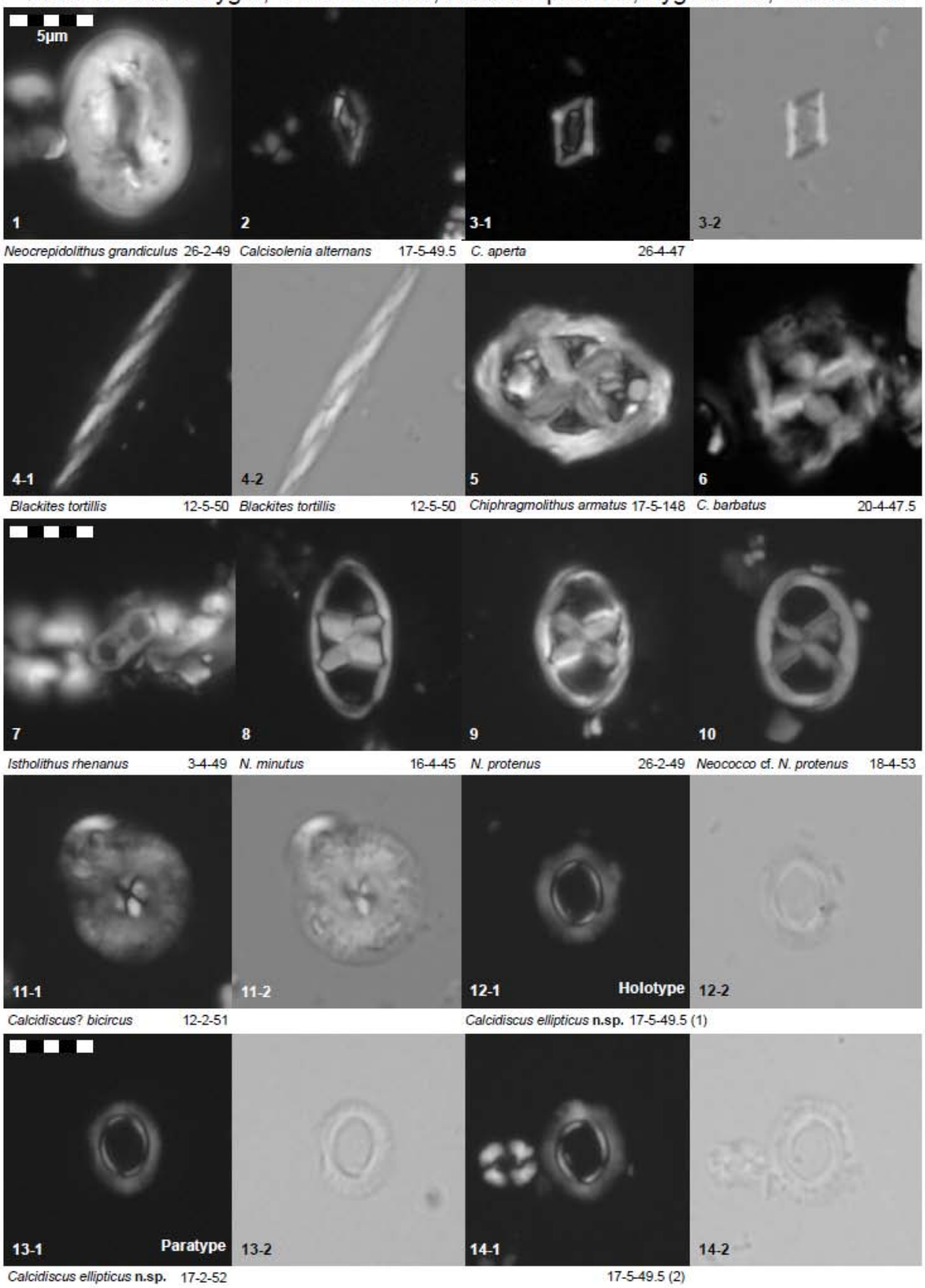

Neocrepidolithus grandiculus 26-2-49 *Calcisolenia alternans* 17-5-49.5 *C. aperta* 26-4-47

Blackites tortillis 12-5-50 *Blackites tortillis* 12-5-50 *Chiphragmolithus armatus* 17-5-148 *C. barbatus* 20-4-47.5

Istholithus rhenanus 3-4-49 *N. minutus* 16-4-45 *N. protenus* 26-2-49 *Neococco* cf. *N. protenus* 18-4-53

Calcidiscus? *bicircus* 12-2-51 *Calcidiscus ellipticus* **n.sp.** 17-5-49.5 (1)

Calcidiscus ellipticus **n.sp.** 17-2-52 17-5-49.5 (2)

Plate 2: Calcidiscaceae

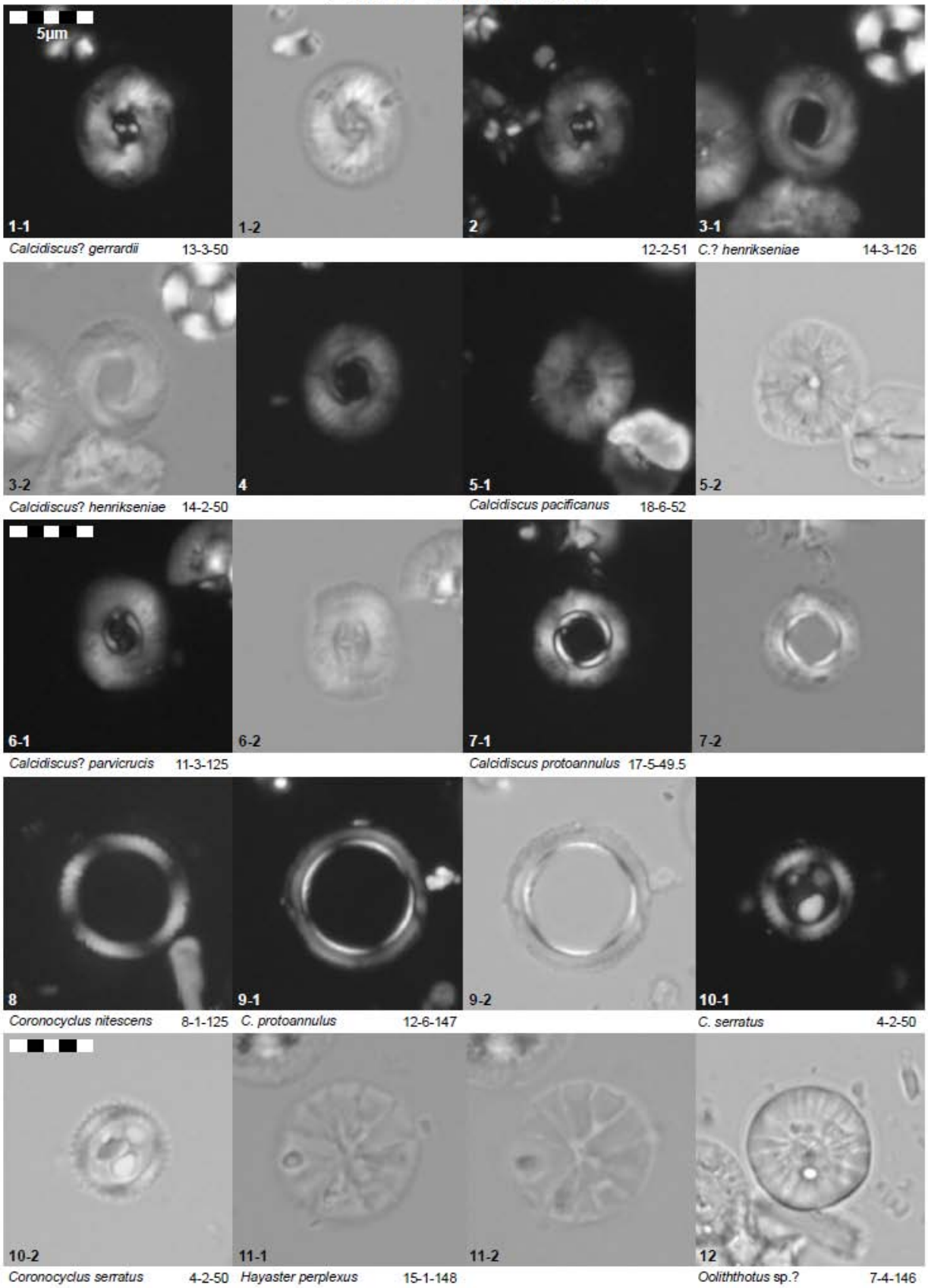

Plate 3: Calcidiscaceae, Coccolithaceae

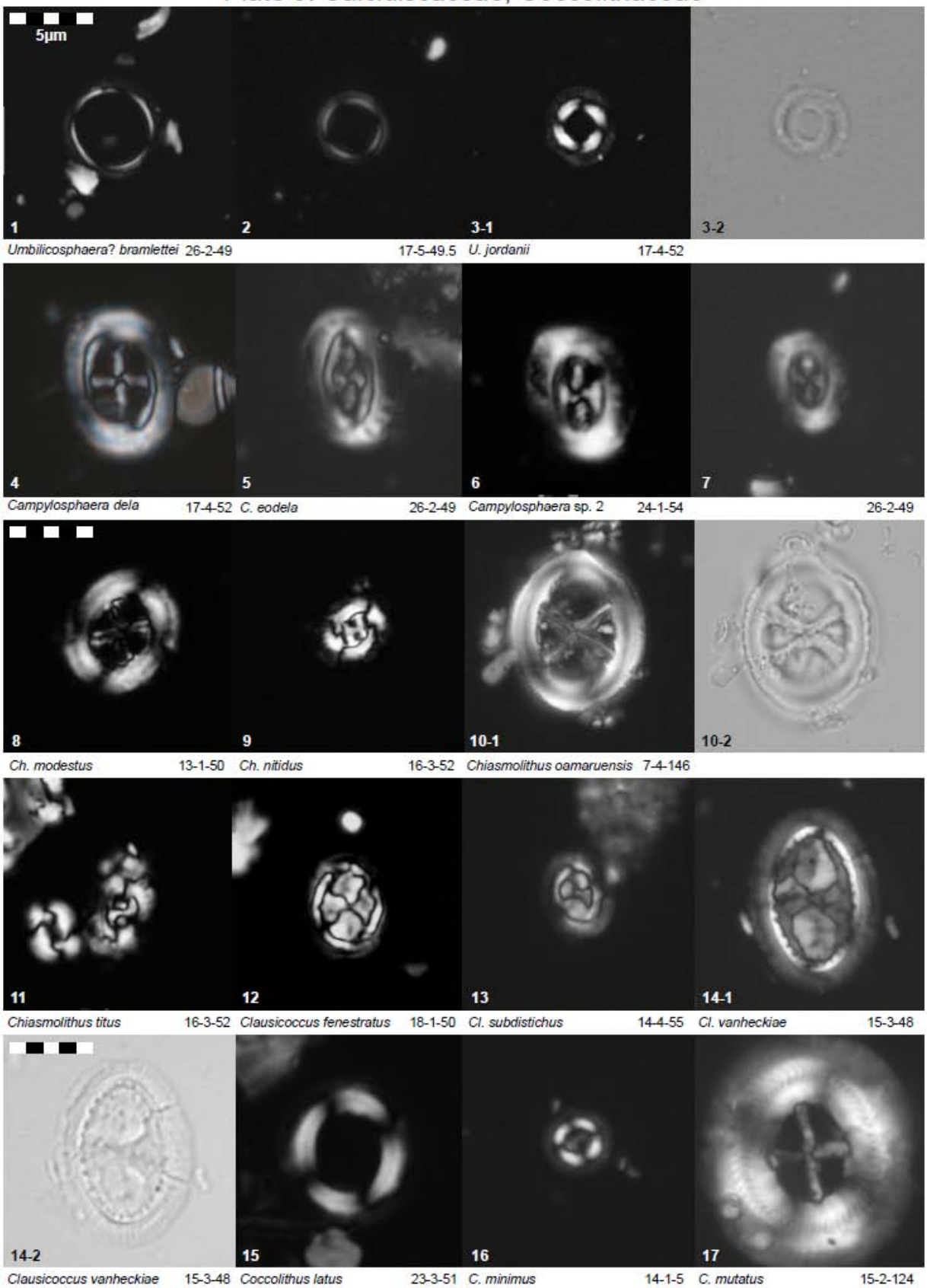

Umbilicosphaera? bramlettei 26-2-49 | 17-5-49.5 *U. jordanii* 17-4-52

Campylosphaera dela 17-4-52 *C. eodela* 26-2-49 *Campylosphaera* sp. 2 24-1-54 | 26-2-49

Ch. modestus 13-1-50 *Ch. nitidus* 16-3-52 *Chiasmolithus oamaruensis* 7-4-146

Chiasmolithus titus 16-3-52 *Clausicoccus fenestratus* 18-1-50 *Cl. subdistichus* 14-4-55 *Cl. vanheckiae* 15-3-48

Clausicoccus vanheckiae 15-3-48 *Coccolithus latus* 23-3-51 *C. minimus* 14-1-5 *C. mutatus* 15-2-124

Plate 4:Coccolithaceae

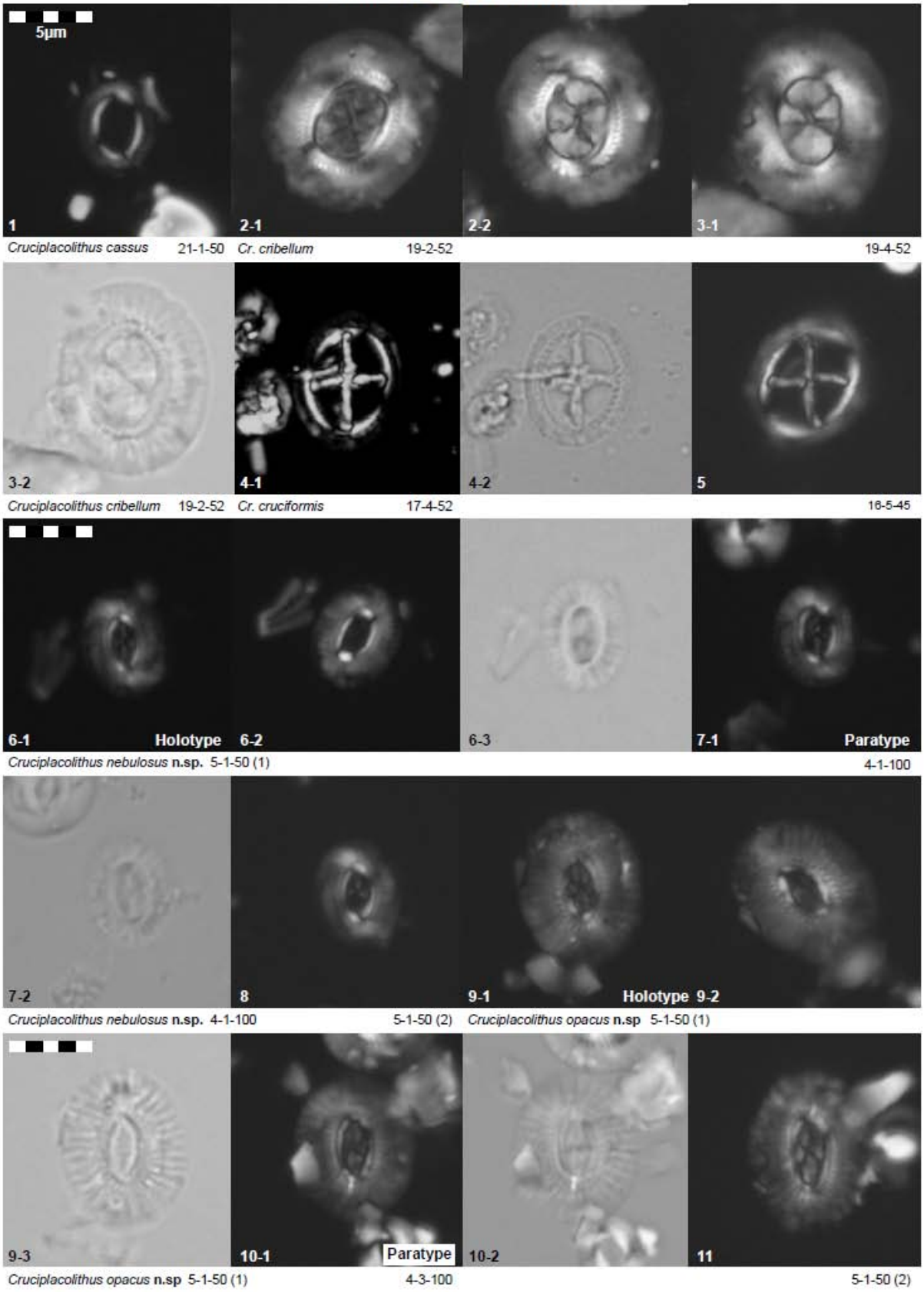

Cruciplacolithus cassus 21-1-50 *Cr. cribellum* 19-2-52 19-4-52

Cruciplacolithus cribellum 19-2-52 *Cr. cruciformis* 17-4-52 16-5-45

Cruciplacolithus nebulosus **n.sp.** 5-1-50 (1) 4-1-100

Cruciplacolithus nebulosus **n.sp.** 4-1-100 5-1-50 (2) *Cruciplacolithus opacus* **n.sp** 5-1-50 (1)

Cruciplacolithus opacus **n.sp** 5-1-50 (1) 4-3-100 5-1-50 (2)

Plate 5: Noelaerhabdaceae, Prinsiaceae

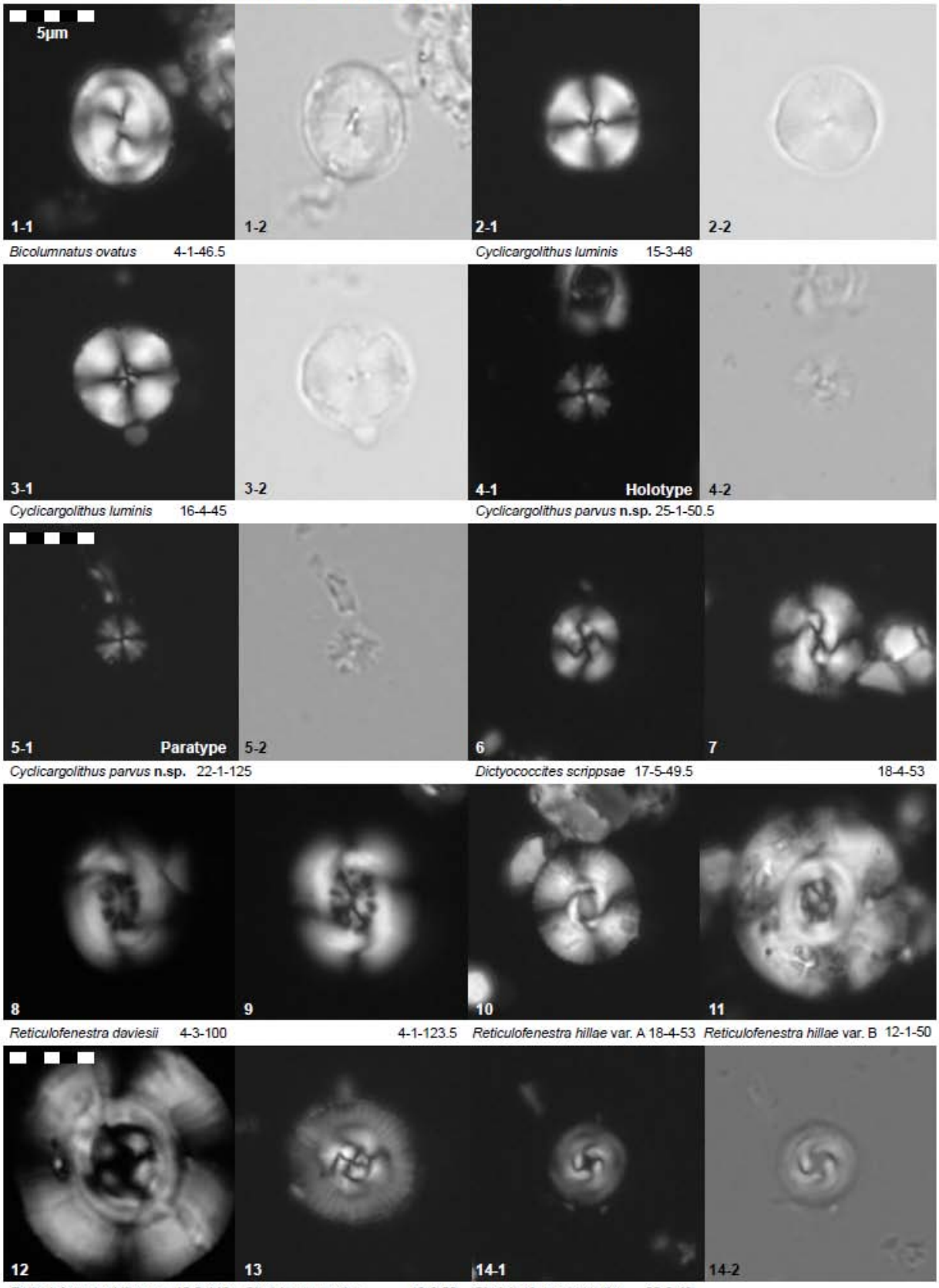

Bicolumnatus ovatus 4-1-46.5

Cyclicargolithus luminis 15-3-48

Cyclicargolithus luminis 16-4-45

Cyclicargolithus parvus **n.sp.** 25-1-50.5

Cyclicargolithus parvus **n.sp.** 22-1-125

Dictyococcites scrippsae 17-5-49.5 18-4-53

Reticulofenestra daviesii 4-3-100 4-1-123.5

Reticulofenestra hillae var. A 18-4-53

Reticulofenestra hillae var. B 12-1-50

Reticulofenestra hillae s.s 15-2-148

Girgisia gammation 18-6-52

Girgisia cf. *g. gammation* 23-2-49

Plate 6: Prinsiaceae, Placolith genera *incertae sedis*

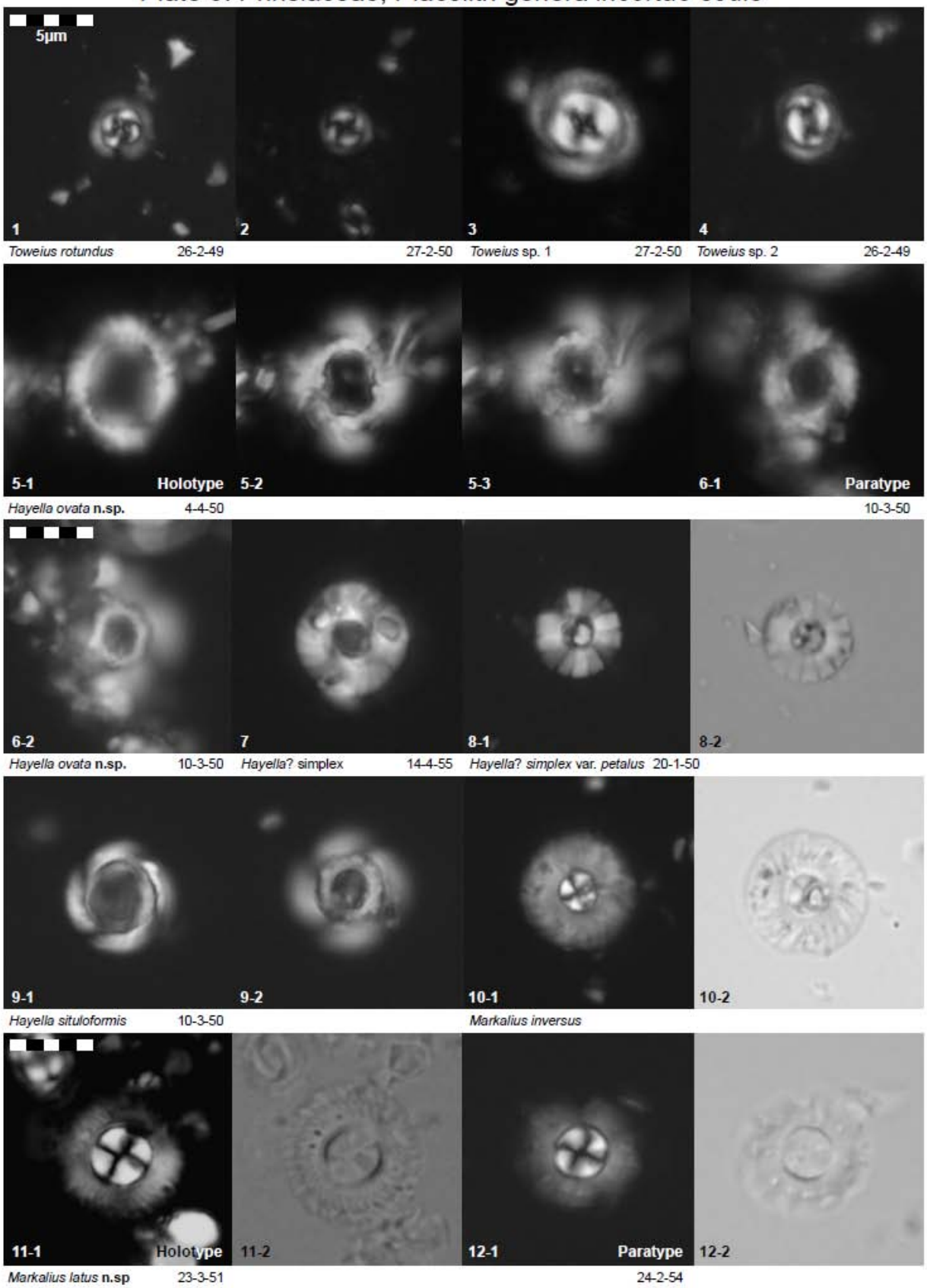

Toweius rotundus 26-2-49 | 27-2-50 *Toweius* sp. 1 27-2-50 | *Toweius* sp. 2 26-2-49

Hayella ovata **n.sp.** 4-4-50 | 10-3-50

Hayella ovata **n.sp.** 10-3-50 | *Hayella*? simplex 14-4-55 | *Hayella*? *simplex* var. *petalus* 20-1-50

Hayella situloformis 10-3-50 | *Markalius inversus*

Markalius latus **n.sp** 23-3-51 | 24-2-54

Plate 7: Placolith genera *incertae sedis*, Calyptrosphaeraceae

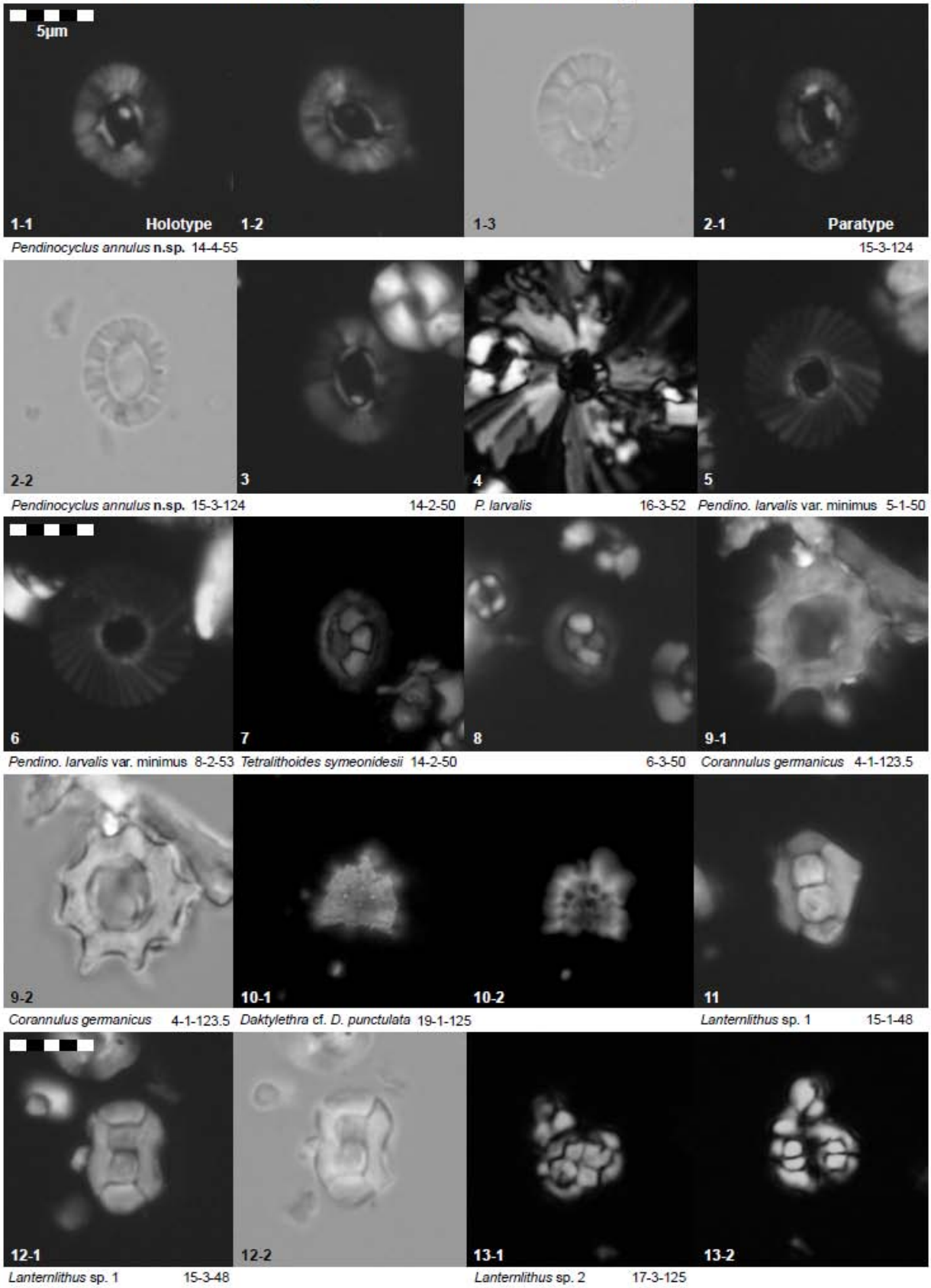

Pendinocyclus annulus **n.sp.** 14-4-55 15-3-124

Pendinocyclus annulus **n.sp.** 15-3-124 14-2-50 *P. larvalis* 16-3-52 *Pendino. larvalis* var. minimus 5-1-50

Pendino. larvalis var. minimus 8-2-53 *Tetralithoides symeonidesii* 14-2-50 6-3-50 *Corannulus germanicus* 4-1-123.5

Corannulus germanicus 4-1-123.5 *Daktylethra* cf. *D. punctulata* 19-1-125 *Lanternlithus* sp. 1 15-1-48

Lanternlithus sp. 1 15-3-48 *Lanternlithus* sp. 2 17-3-125

Plate 8: Calyptrosphaera., Lapideacassa., Discoaster., Sphenolith., Nannoliths *incertae sedis*

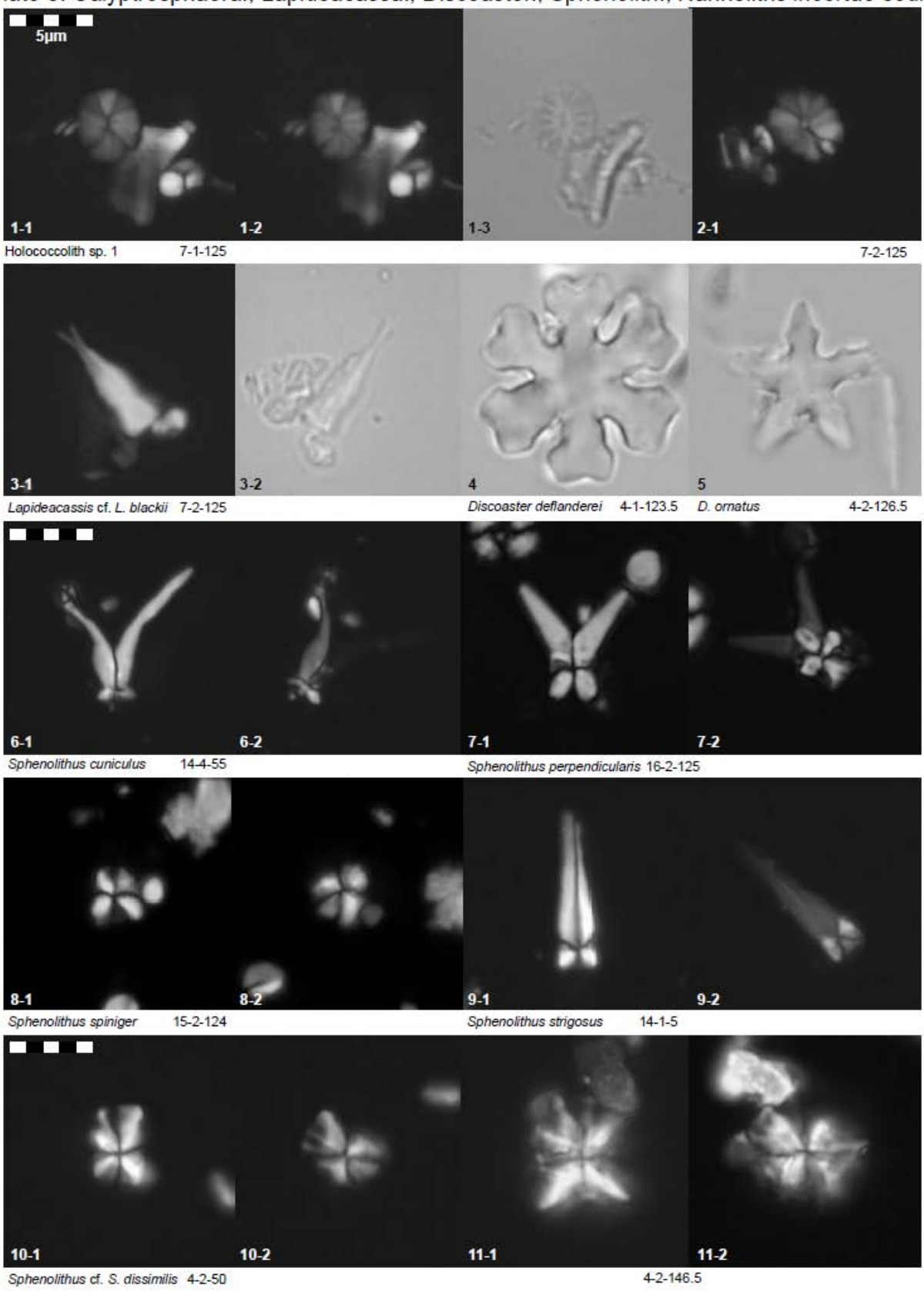

Plate 9: Sphenolithaceae, nannoliths*incertae sedis*, indeterminant nannoliths

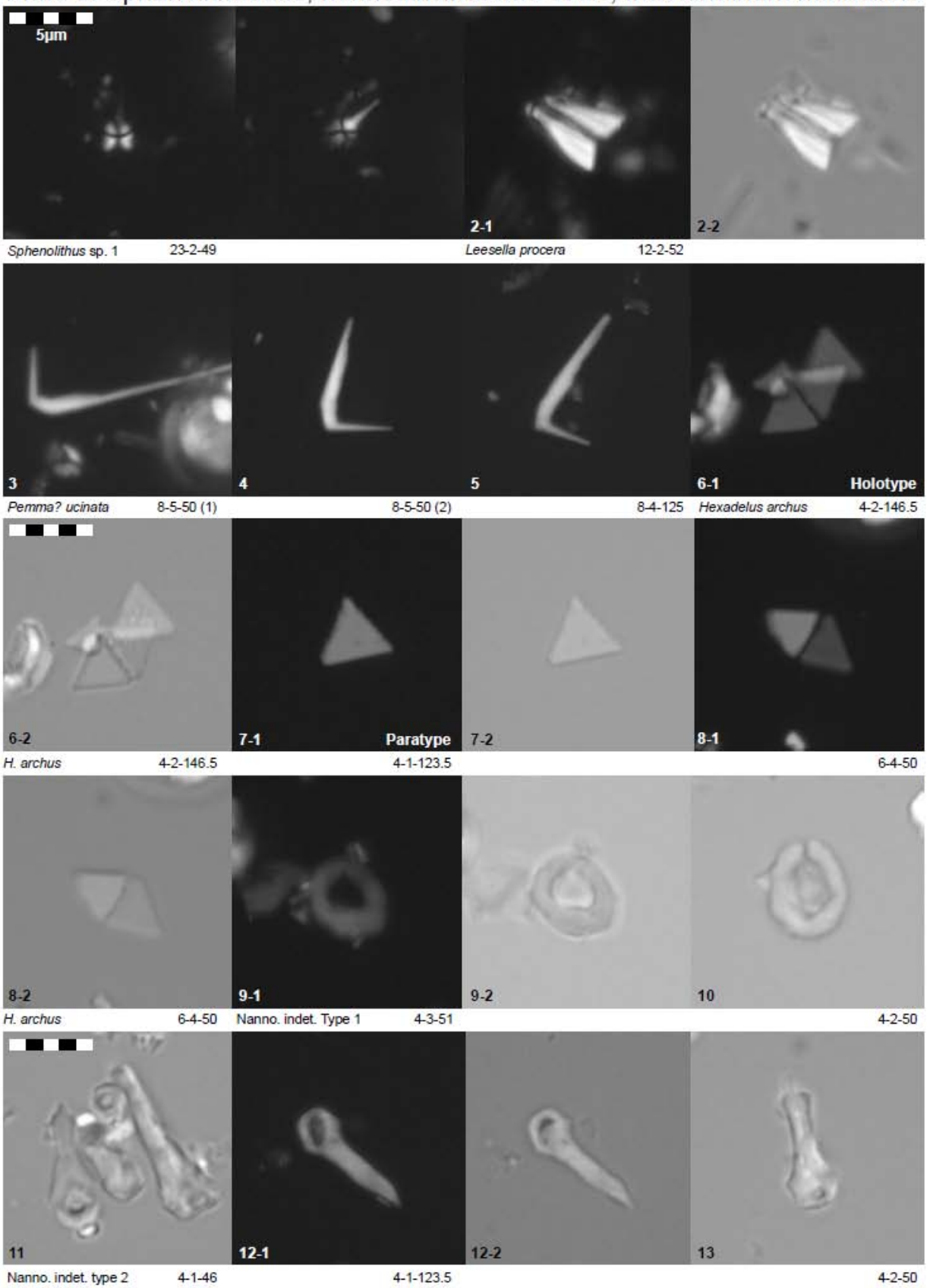

Sphenolithus sp. 1 23-2-49

Leesella procera 12-2-52

Pemma? ucinata 8-5-50 (1)

8-5-50 (2)

8-4-125

Hexadelus archus 4-2-146.5

H. archus 4-2-146.5

4-1-123.5

6-4-50

H. archus 6-4-50

Nanno. indet. Type 1 4-3-51

4-2-50

Nanno. indet. type 2 4-1-46

4-1-123.5

4-2-50

Plate 10: Sphenolithaceae

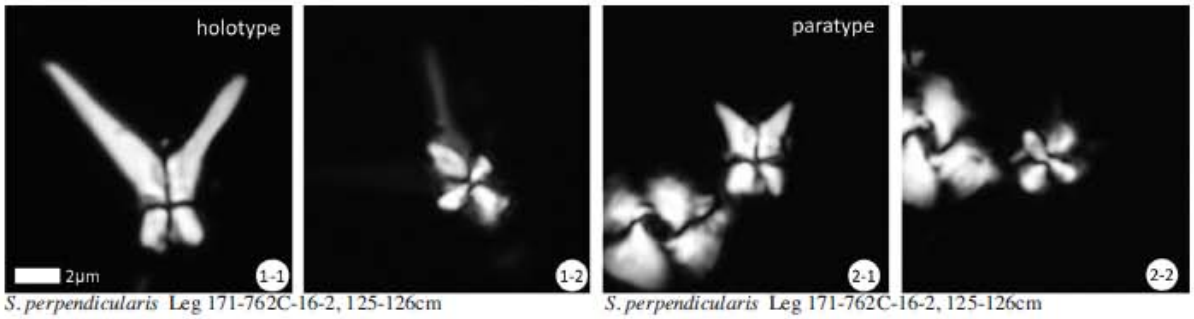

S. perpendicularis Leg 171-762C-16-2, 125-126cm

S. perpendicularis Leg 171-762C-16-2, 125-126cm

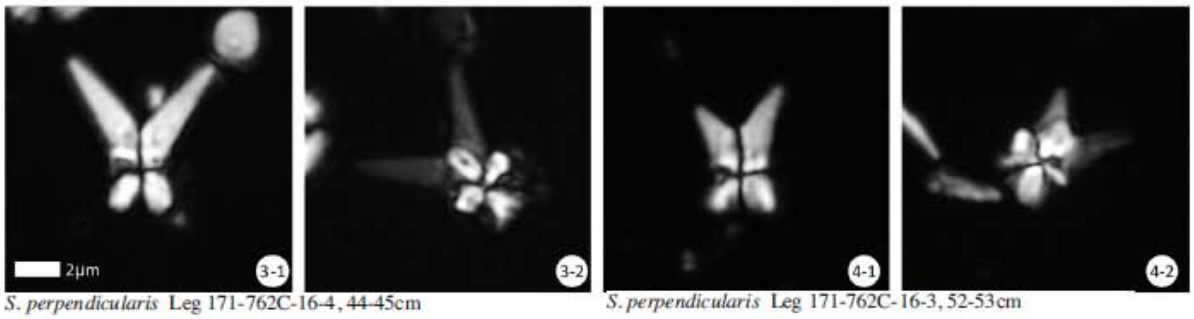

S. perpendicularis Leg 171-762C-16-4, 44-45cm

S. perpendicularis Leg 171-762C-16-3, 52-53cm

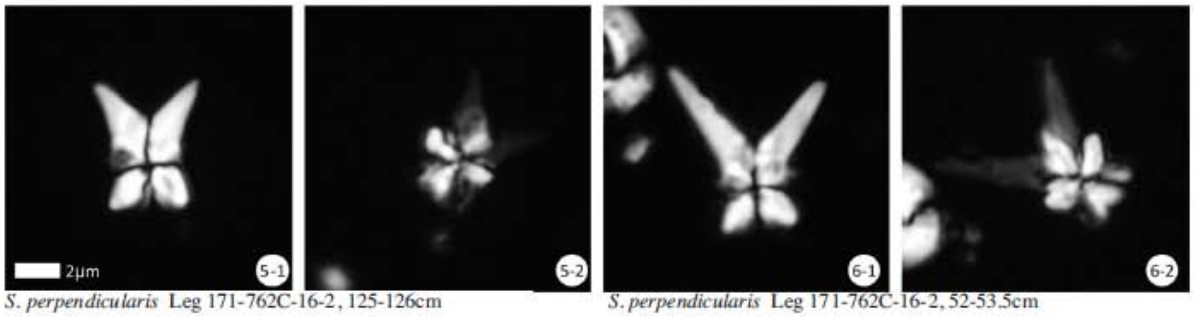

S. perpendicularis Leg 171-762C-16-2, 125-126cm

S. perpendicularis Leg 171-762C-16-2, 52-53.5cm

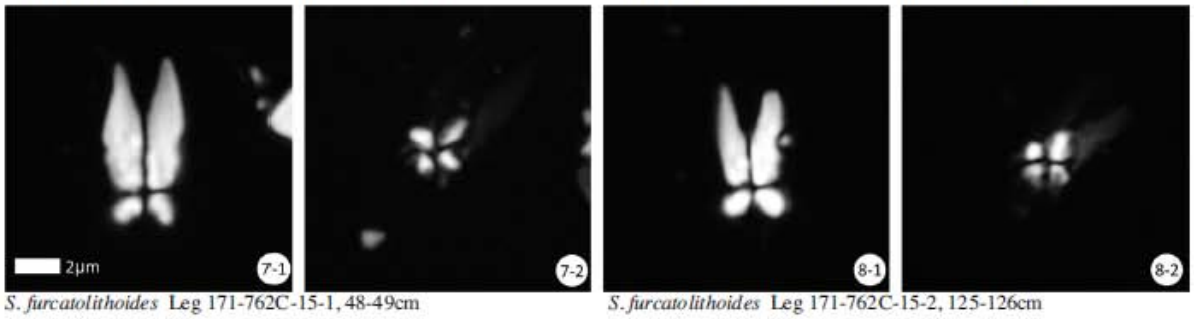

S. furcatolithoides Leg 171-762C-15-1, 48-49cm

S. furcatolithoides Leg 171-762C-15-2, 125-126cm

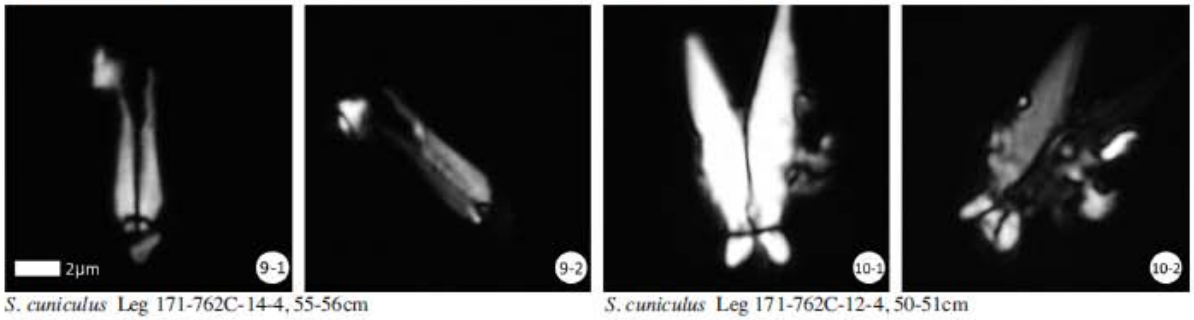

S. cuniculus Leg 171-762C-14-4, 55-56cm

S. cuniculus Leg 171-762C-12-4, 50-51cm

APPENDIX A - CALCAREOUS NANNOFOSSIL SYSTEMATIC PALEONTOLOGY AND TAXONOMIC APPENDIX

Taxonomic and/or stratigraphic notes are gives for all species identified within the section. Notable abundance trends are given for individual species; however, genus and family level abundance trends are treated above. Nannofossil terminology follows guidelines provided in Young et al. (1997).

Recent research on Eocene cores from Tanzania by Bown (2005), Bown and Dunkley-Jones (2006), and Bown, Dunkley-Jones and Young (2007) has generated a significant image atlas, and numerous taxonomic points have been addressed in these works that will not be reiterated here. We restrict our main discussion and imaging to species that were not addressed, recently named species, or where opinions on taxonomy diverge. Many species that are recently named are shown in XPL (Cross-polarized light) only, as they are well illustrated in the original descriptions. Where two images are provided for one specimen, XPL is always shown before PL (Plane-polarized light).

Numerous new species were recently identified by Bown (2005), Bown and Dunkley-Jones (2006) and Bown, Dunkley-Jones and Young (2007). Many of these species were observed in the Exmouth section; however, observed ranges of several species extend above and/or below those provided in the original descriptions. A significant portion of such range extensions are likely due to coring gaps in the Tanzania section (Bown 2005, fig 2; Bown, Dunkley-Jones and Young 2007, fig. 1). To limit redundancy, we do not treat each range issue separately, but refer the reader to these publications for independent comparison.

MUROLITHS

Order **EIFFELLITHALES** Rood, et al., 1971

Family **CHIASTOZYGACEAE** Rood, et al., 1973

Neocrepidolithus grandiculus Bown 2005

Plate 1-1; *Observed range***:** CP9a-13a, NP10-15a

Jakubowskia leoniae Varol 1989

*Observed range***:** CP9a-12a; NP10-14a

Order **SYRACOSPHAERALES** Hay 1977, emend. Young et al., 2003

Family **CALCIOSOLENIACEAE** Kamptner 1927

Calciosolenia alternans Bown and Dunkley-Jones 2006

Plate 1-2; *Observed range***:** CP12a; NP14a

Calciosolenia aperta (Hay & Mohler 1967) Bown 2005

Plate 1-3 *Observed range***:** CP9b, NP11

Family **RHABDOSPHAERACEAE** Haeckel 1894

Most species of *Blackites and Rhabdosphaera* were extremely rare at the locality.

Blackites gracilentus Bown and Dunkley-Jones 2006

*Observed range***:** CP14b; NP17

Blackites morionum (Deflandre in Deflandre and Fert 1954) Varol 1989

*Observed range***:** CP9a; NP10

Blackites perlongus (Deflandre in Grassé 1952) Bramlette and Sullivan 1961

*Observed range***:** CP9b; NP11

Blackites spinosus (Deflandre and Fert 1954) Hay and Towe 1962 **/ *Rhabdosphaera tenuis*** Bramlette and Sullivan 1961

The vast majority of specimens are incomplete, lacking their diagnostic base. As a result, *B. spinosus* has been grouped with *R. tenuis*, though this diminishes the biostratigraphic utility. This group is most abundant in CP10. *Observed range***:** CP9a-16a; NP10-21

Blackites tortillis Bown and Dunkley-Jones 2006

Plate 1-4; The observed LO occurs in mid-CP14a. *Observed range***:** CP14a-15b; NP16-19/20

Rhabdosphaera inflata Bramlette and Sullivan 1961

*Observed range***:** CP12b; NP14b

Rhabdopshaera sola Perch-Nielsen 1971

*Observed range***:** CP9b-10; NP11-12

Rhabdosphaera tenuis Bramlette and Sullivan 1961

See *B. spinosus/R. tenuis*, above.

Rhabdosphaera truncata Bramlette and Sullivan 1961

*Observed range***:** CP9b-12a; NP11-13

Family **SYRACOSPHAERACEAE** Hay 1977

Syracosphaera Lohmann 1902

Specimens of this genus were rare and sporadic throughout the section and have been grouped as *Syracosphaera* spp. for statistical analysis. *Observed range***:** CP9a-16a; NP10-21

Order **ZYGODISCALES** Young and Bown 1997

Family **HELICOSPHAERACEAE** Black 1971

Most species of the genus *Helicosphaera* were rare and sporadic, though the genus as a whole becomes fairly common and consistent in the Upper Eocene. Average relative abundance = ~0.5% from the genus LO through CP15b, but increases at the base of CP16a (μ = 1.6%, Max. = 4.0%)

Helicosphaera bramlettei (Müller 1970) Jafar and Martini 1975

*Observed range***:** CP14a-16a; NP16-21

Helicosphaera compacta Bramlette and Wilcoxon 1967

The LCO occurs in CP14b at this site, with a notable abundance increase in upper CP15b, also shown in Wei and Wise (1990a). *Observed range***:** CP14a?-16a; NP16-21

Helicosphaera dinesenii (Perch-Nielsen 1971) Jafar and Martini 1975

*Observed range***:** CP13a-14a; NP15a-16

Helicosphaera heezenii (Bukry 1971) Jafar and Martini 1975

*Observed range***:** CP13b-14b; NP15b-17

Helicosphaera lophota (Bramlette and Sullivan 1961) Jafar and Martini 1975

LO occurs at the base of CP11, with HO at the base of CP15b. *Observed range***:** CP10-15b; NP12-19/20

Helicosphaera papillata (Bukry and Bramlette 1969) Jafar and Martini 1975

The HO occurs just above base of CP12b. *Observed range***:** CP12a-12b; NP14a-14b

Helicosphaera reticulata Bramlette and Wilcoxon 1967

*Observed range***:** CP15a-16a; NP18-21

Helicosphaera salebrosa Perch-Nielsen 1971

*Observed range***:** CP13b-15b; NP15b-19/20

Helicosphaera seminulum (Bramlette and Sulllivan 1961) Jafar and Martini 1975

*Observed range***:** CP10-15b; NP12-19/20

Helicosphaera wilcoxonii (Gartner 1971) Jafar and Martini 1975

*Observed range***:** CP14b-16a; NP17-21

Family **PONTOSPHAERACEAE** Lemmermann 1908

The genera *Pontosphaera* and *Transversopontis* were observed throughout the section from CP8a-16a. Specimens were generally rare and sporadic at this locality, so were grouped together as *Pontosphaera* spp. for data analysis. Though detailed biostratigraphic analysis was not conducted on individual species within these two genera, species that were identified are listed below.

Pontosphaera formosa (Bukry and Bramlette 1968) Romein 1979

Pontosphaera multipora (Kamptner 1948) Roth 1970, emend. Burns 1973

Pontosphaera pectinata (Bramlette and Sullivan 1961) Sherwood 1974

Pontosphaera plana (Bramlette and Sullivan 1961) Haq 1971

Pontosphaera versa (Bramlette and Sullivan 1961) Sherwood 1974

Pontosphaera rimosa (Bramlette and Sullivan 1961) Roth and Thierstein 1972

Transversopontis duocavus (Bramlette and Sullivan 1961) Locker 1973

Transversopontis exilis (Bramlette and Sullivan 1961) Perch-Nielsen 1971

Transversopontis pulcher (Deflandre in Deflandre and Fert 1954) Perch-Nielsen 1967

Transversopontis pulcheroides (Sullivan 1964) Baldi-Beke 1971

Family **ZYGODISCACEAE** Hay and Mohler 1967

Specimens of *Chiphragmolithus* spp. first occur with the LO of *D. lodoensis*, at the base of CP10. Some specimens could not be differentiated to species level due to overgrowth, and have been identified simply as *Chiphragmolithus* sp.

Chiphragmolithus armatus Perch-Nielsen 1971

Plate 1-5; *Observed range***:** CP10; NP12

Chiphragmalithus barbatus Perch-Nielsen 1967

Plate 1-6; *Observed range***:** CP9b-10; NP11-12

Chiphragmolithus calathus Bramlette and Sullivan 1961

*Observed range***:** CP9b-10; NP11-12

Isthmolithus recurvus Deflandre in Deflandre and Fert 1954

The LCO of *I. recurvus* marks the base of CP15b. The LO of *I. recurvus* and HO of *C. reticulatum* are often reported as contemporaneous markers; however, specimens of *C. reticulatum* are observed well above the LO and LCO of *I. recurvus*. This overlap is also reported in Villa, et al. (2008), Aubry (1992), and Wei and Wise (1990a, 1989a). *Observed range***:** CP15a-16a; NP17-21

Isthmolithus rhenanus Martini 1973

Plate 1-7; *Observed range***:** CP16a; NP21

Lophodolithus mochlophorus Deflandre in Deflandre and Fert 1954

*Observed range***:** CP12a-13b; NP14a-15b

Lophodolithus nascens Bramlette and Sullivan 1961

Peak abundance occurs in CP9b-10. *Observed range***:** CP9a-11; NP10-12

Lophodolithus reniformis Bramlette and Sullivan 1961

The LO was observed very near the CP9b/10 boundary. *Observed range***:** CP9b-10; NP11-12

Lophodolithus rotundus Bukry and Percival 1971

*Observed range***:** CP13a; NP15a

Neochiastozygus concinnus (Martini 1961) Perch-Nielsen 1971

The HO occurs in lower CP9b. *Observed range***:** CP9a-9b; NP10-11

Neochiastozygus distentus (Bramlette and Sullivan, 1961) Perch-Nielsen 1971

*Observed range***:** CP8a-9b; NP9-11

Neochiastozygus junctus (Bramlette and Sullivan 1961) Perch-Nielsen 1971

*Observed range***:** CP9a-10; NP10-12

Neochiastozygus rosenkrantzii (Perch-Nielsen 1971) Varol 1989

This species was observed below the range given by Perch-Nielsen (1985) in both this study and Bown (2005). *Observed range***:** CP9a-10; NP10-12

Neochiastozygus substrictus Bown 2005

*Observed range***:** CP9a-10; NP10-11

Neococcolithes dubius (Deflandre in Deflandre and Fert 1954) Black 1967

The LO is observed just below the base of CP10. Though fairly consistent in its lower range, we observe a significant gap above CP13a, with a sporadic reappearance in CP14b prior to extinction. This species is commonly reported through CP15a (Villa et al. 2008; Wei and Wise 1990a; Perch-Nielsen 1985); however, Wei and Wise (1989b) also show a HO in CP14b, as at 762C. *Observed range***:** CP9b-14b; NP11-17

Neococcolithes minutus (Perch-Nielsen 1967) Perch-Nielsen 1971

Plate 1-8; *Observed range***:** CP12a-14b; NP14a-17

Neococcolithes protenus (Bramlette and Sullivan 1961) Black 1967

Plate 1-9; *Observed range***:** CP9a-10; NP10-12

Neococcolithes* sp. cf. *N. protenus (Bramlette and Sullivan 1961) Black 1967

Plate 1-10; Specimens with strikingly similar morphology to *N. protenus* were observed above its commonly recorded HO of CP10. These specimens did not show the narrowly elliptical outline of *N. minutus,* the 'H'-shaped cross of *N. dubius,* or the vertical relief of *Chiphragmolithus* spp., and are here identified as *Neococcolithes* sp. cf. *N. protenus*. *Observed range***:** CP11-12b; NP13-14b

Zygodiscus adamas Bramlette and Sullivan 1961

*Observed range***:** CP9a-9b; NP10-11

Zygodiscus plectopons Bramlette and Sullivan 1961

This species was observed above the range given by Perch-Nielsen (1985) in both this study and Bown (2005). *Observed range***:** CP9b; NP11

PLACOLITHS

Order **COCCOSPHAERALES** Haeckel 1894, emend. Young and Bown 1997

Family **CALCIDISCACEAE** Young and Bown 1997

Several new species of *Calcidiscus* have recently been identified by Bown (2005), Bown and Dunkley-Jones (2006) and Bown, Dunkley-Jones and Young (2007). All these species have since been identified at Exmouth

Plateau, though with variances in some ranges. Some disagreement is quite likely due to the stratigraphic gap in the Tanzania sections between Cores 2 and 3 (mid-NP11 to lower NP14b) (Bown, Dunkley-Jones and Young 2007, fig. 1). This gap can account particularly for the difference in the LO of *C. bicircus* and the LO of *C. parvicrucis.* Variance in the ranges of other species (*C. henrikseniae*, *C. gerrardii)* may represent true stratigraphic differences between sites or in species concepts. The true range of these species will be further refined as additional data is collected.

Calcidiscus? bicircus Bown 2005

Plate 1-11; Only broadly elliptical forms were identified as *C. bicircus*, as shown in the holotype and paratype (Bown, 2005, pl. 9 figs. 11, 12, 14, and 15). Circular forms (Bown, 2005, pl. 9 fig. 13) were identified as *Markalius inversus. Observed range***:** CP11-14b; NP12-17

Calcidiscus ellipticus **n. sp.**

Holotype: Plate 1-12 *Paratype:* Plate 1-13

Etymology: For the elliptical outline of this species

Diagnosis: Small to medium sized, elliptical placolith with an open central-area and bright inner collar

Description: Small to medium sized, broadly to normally elliptical placolith with non-birefringent shields and bright, narrow collar. The relatively narrow, non-birefringent shields are composed of ~ 35-50 slightly imbricated elements and give a smooth margin. The central-area is moderately wide and vacant, encircled by a narrow, bright inner collar. The collar shows four thin, slightly oblique isogyres, and both the inner and outer perimeters are well-defined by extinction lines in cross-polarized light.

Dimensions: **Length:** 4.8-7.0 μm, μ = 5.8, s.d. = 0.6; **Width:** 3.7-6.0 μm, μ = 4.8, s.d. = 0.6; **Eccentricity:** 1.11-1.38, μ = 1.22, s.d. = 0.1; **CA** (% of size): 40-59%, μ = 49.3%, s.d. = 0.3; N = 30 for all data.

Remarks: This species is tentatively placed into the genus *Calcidiscus* due to its resemblance to *C. protoannulus*, but is readily differentiated from the round *C. protoannulus* by its elliptical outline. The LO of *C. ellipticus* **n. sp.** occurs at the base of CP11 and is most abundant prior to, and for a short time after, the LO of *C. protoannulus* (within CP12a). This stratigraphic relationship, in addition to the morphological similarities, makes *C. ellipticus* **n. sp.** a likely precursor of *C. protoannulus*. *Calcidiscus ellipticus* **n. sp.** was rare but consistent above CP12a.

*Observed range***:** CP11-16a; NP14a-21

Type Section: ODP Leg 122 Site 762C, Exmouth Plateau

Type Level: 17-5-(49.5-50.5 cm), 319.00 mbsf

Calcidiscus*? *gerrardii Bown and Dunkley-Jones 2006

Plate 2-1, 2-2; *Observed range***:** CP14a?-14b; NP16-17

Calcidiscus*? *henrikseniae Bown 2005

Plate 2-3, 2-4; The HO occurs at the base of CP14b. *Observed range***:** CP14a?-14b; NP16-NP17

Calcidiscus*? *pacificanus (Bukry 1971) Varol 1989

Plate 2-5; Peak abundance occurs in CP10-11. *Observed range***:** CP9a-14b; NP10-17

Calcidiscus*? *parvicrucis Bown 2005

Plate 2-6; *Observed range***:** CP9a-10; NP10-12

Calcidiscus protoannulus (Gartner 1971) Loeblich and Tappan 1978

Plate 2-7; Peak abundance occurs in CP14b-15b, also noted in Wei and Wise (1989b). *Observed range***:** CP12b-16a; NP12-21

Coronocyclus nitescens (Kamptner 1963) Bramlette and Wilcoxon 1967

Plate 2-8; The LCO occurs in CP14b. *Observed range***:** CP14a?-16a; NP16-21

Coronocyclus prionion (Deflandre and Fert 1954) Stradner and Edwards 1968

Plate 2-9; This species is considered valid by some authors (e.g. Wise, et al*.,* 2004), while others considered it a synonym of *C. nitescens* (Bown, 2005). Though *C. nitescens* is derived from *C. prionion*, and some intermediate forms can be identified, *C. nitescens* and *C. prionion* do show unique characteristics and should be differentiated. *Coronocyclus nitescens* is characterized by serrate or toothed margin with little to no differentiation between the inner and outer cycles, while *C. prionion* is distinctly bicyclic with a bright, gyred, inner cycle and non-birefringent outer shield. If it is shown that these two species are indeed synonyms then the earlier named *C. prionion* (Deflandre and Fert, 1954) would take precedence over *C. nitescens* (Kamptner, 1963).

Coronocyclus prionion is also notably similar to *Umbilicosphaera*? *bramlettei* and is differentiated here by size. Descriptions by Bown (2005) and Bown, Dunkley-Jones and Young (2007) describe *U.*? *bramlettei* as 3.5-7.5µm. This designation has been followed, and specimens >7.5 µm have been identified as *C. prionion*. Max abundance (2-3%) occurs early in its range (CP10-12a), becoming rare above CP12a. *Observed range***:** CP10-14b; NP12-17.

Coronocyclus serratus Hay, et al. 1966

Plate 2-10; Though *C. serratus* may be a preservational variant of *C. nitescens,* the observed range is notably consistent with other published data. In addition, ranges of these species are significantly different, suggesting a valid species. *Observed range***:** CP15b-16a; NP19/20-21

Hayaster perplexus (Bramlette and Riedel 1954) Bukry, 1973

Plate 2-11; Perch-Nielsen (1985) identifies the FO of *H. perplexus* in the Oligocene; however, both this study and Bown, Dunkley-Jones and Young (2007) show evidence for a considerably earlier first appearance, though extremely rare. *Observed range***:** CP13b; NP15b

***Oolithotus* sp.?**

Plate 2-12; Several specimens of uncertain origin have been tentatively assigned to the genus *Oolithotus,* due to the slightly asymmetrical central depression, characteristic of the type species *O. fragilis (*Lohmann, 1912) Martini and Müller 1972. *Observed range***:** CP15a-15b; NP18-19/20

Umbilicosphaera? bramlettei (Hay and Towe 1962) Bown, Dunkley-Jones and Young 2007

Plate 3-1, 3-2; This species shows peak abundance in CP9b-10, becoming rare in CP12a, and sporadic from CP14a. This species has been limited to specimens < 7.5 µm. *Observed range***:** CP9b-14a; NP11-16

Umbilicosphaera jordanii Bown 2005

Plate 3-3; *Observed range***:** CP9a-16a; NP10-21

Family **COCCOLITHACEAE** Poche 1913, emend. Young and Bown 1997

Bramletteius serraculoides Gartner 1969

The LO is observed near the top of CP13b, with LCO within CP14a, also noted in Wei and Wise (1990a). Peak abundance occurs in CP15a-b (µ = 2.0, Max. = 5.4%). *Observed range***:** CP13b-16a; NP15b-21

Campylosphaera dela (Bramlette and Sullivan 1961) Hay and Mohler 1967

Plate 3-4; Though the HO of *C. dela* is reported by Perch-Nielsen (1985) as CP14a, Bown (2005), Bralower and Mutterlose (1995), and this study identified *C. dela* in CP14b/NP17. Peak abundance occurs through CP10-11 (µ = 2.1%), with maximum abundance (3.6%) near the ETM3/"X"-event, also shown in Agnini, et al. (2007a). *Observed range***:** CP9a-14b; NP10-17

Campylosphaera eodela Bukry and Percival 1971

Plate 3-5; This species can be differentiated from *C. dela* by its robust cross inside a more narrow and elliptical CA, in contrast to *C. dela,* which bears a more delicate cross within a larger CA that is 'sub-

rectangular' in outline. Intermediate forms may be difficult to differentiate, as *C. eodela* and *C. dela* co-occur for a time at Exmouth Plateau, though most specimens are readily identified. *Observed range***:** CP9a-9b; NP10-11

Campylosphaera eroskayi (Varol 1989) Bown 2005

*Observed range***:** CP9a-9b; NP10-11

***Campylosphaera* sp.2** Bown 2005

Plate 3-6, 3-7; This form shows consistent morphology throughout its observed range and should be given a unique species name; however, this should be done in conjunction with a more thorough quantitative study of *C. dela* and *C. eodela. Observed range***:** CP9a-10; NP10-12

Chiasmolithus eoaltus Persico and Villa 2008

The LO occurs near the top of CP14b, before the LO of *Ch. oamaruensis,* as shown in the original description. Persico and Villa show a stratigraphic gap between the HO of *Ch. eoaltus* in CP15a and the LO of *Ch. altus* in CP16; however, *Ch. eoaltus* was observed throughout this interval at Site 762C. *Observed range***:** CP14b-16a; NP17-21

Chiasmolithus bidens (Bramlette and Sullivan 1961) Hay and Mohler 1967

HO observed just above the CP10 boundary. *Observed range***:** CP8a-10; NP9-12

Chiasmolithus californicus (Sullivan 1964) Hay and Mohler 1967

HO observed at the base of CP12a. *Observed range***:** CP 8a-12a; NP9-14a

Chiasmolithus consuetus (Bramlette and Sullivan) Hay and Mohler, 1967

This species was consistent through CP12b, but rare and/or sporadic above CP14a. The HCO is observed in CP14b, with HO at the top of CP15b. *Observed range***:** CP8a-15b; NP18

Chiasmolithus eograndis Perch-Nielsen 1971

*Observed range***:** CP9a-11; NP10-13

Chiasmolithus expansus (Bramlette and Sullivan 1961) Gartner 1970

The HCO occurs within CP14a with HO at the base of CP14b. *Observed range***:** CP10-14b; NP12-17

Chiasmolithus gigas (Bramlette and Sullivan 1961) Radomski 1968

*Observed range***:** CP13b; NP15b

Chiasmolithus grandis (Bramlette and Riedel 1954) Radomski 1968

As noted in Marino and Flores (2002), this species is very rare at the top of its range, though the HO used to mark the base of CP15a is consistent with published data. *Observed range***:** CP10-14b; NP12-17

Chiasmolithus minimus Perch-Nielsen 1971

*Observed range***:** CP14a; NP16

Chiasmolithus modestus Perch-Nielsen 1971

Plate 3-8; *Observed range***:** CP14a; NP16

Chiasmolithus nitidus Perch-Nielsen 1971

Plate 3-9; *Observed range***:** CP13a-14b; NP15a-17

Chiasmolithus oamaruensis (Deflandre 1954) Hay, et al. 1966

Plate 3-10; This species is rare and sporadic at Site 762C. *Observed range***:** CP15a-16a; NP18-21

Chiasmolithus solitus (Bramlette and Sullivan 1961) Locker 1968

The HO marks the base of CP14b/NP17, but this species is very rare at this locality. *Observed range***:** CP8a-14a; NP9-16

Chiasmolithus titus Gartner 1970

Plate 3-11; Peak abundance occurs in CP14a (Max. = 2.6%), becoming rare and sporadic above CP14b. *Observed range***:** CP13a-15b; NP15a-19/20

Clausicoccus fenestratus (Deflandre and Fert 1954) Prins 1979

Plate 3-12; Several issues have been encountered concerning the relationships, both taxonomic and stratigraphic, between *C. fenestratus* and *Cruciplacolithus cribellum.* Though Perch-Nielsen (1985) shows the HO of *C. cribellum* within CP9b and the LO of *C. fenestratus* in CP12, similar forms were observed throughout this intermediate interval. The morphological character of these species is quite similar, and the absence of a stratigraphic gap raises questions about the true relationship between them. Bown (2005) has suggested that *C. cribellum* is, in fact, a synonym of *C. fenestratus.* That recommendation has been followed here only for specimens <10μm in length: *Clausicoccus fenestratus* was originally described as a notably small species (4.3 x 3.1 μm), whereas *C. cribellum* was first described with greater size variation (6-14 μm). Later work by Romein (1979, fig. 29) shows a distinct offset between the appearance of small and large forms of *C. cribellum*, in the *Discoaster multiradiatus* zone (CP8) and *Tribrachiatus orthostylus* zone (CP10), respectively. Such large specimens (>10 μm) also appear consistently in CP10 at Exmouth Plateau. Though no specific size division was noted, the authors in this study have informally divided small and large version of "*C. cribellum"* at 10 μm. As a result, those specimens <10 μm are considered synonymous with *C. fenestratus*, while those >10 μm are identified as *C. cribellum* until a more detailed study can be conducted. *Observed range***:** CP9a-16a; NP10-21

Clausicoccus subdistichus (Roth and Hay, in Hay et al. 1967) Prins 1979

Plate 3-13; Peak abundance occurs at the top of the section, from ~1.0% in CP15b and lower CP16a to ~4.0% in the upper two samples, and likely indicates the base of the *Clausicoccus* acme. *Observed range***:** CP11-16a; NP12-21

Clausicoccus vanheckiae (Perch-Nielsen 1986) DeKaenel and Villa 1996

Plate 3-14; This species is observed above and below the range given in Perch-Nielsen (1985). The LO occurs very near the CP12a/b boundary, with HO at the top of CP14b. *Observed range***:** CP12a-14b; NP14a-17

Coccolithus cachaoi Bown 2005

*Observed range***:** CP12a-14b; NP14a-17

Coccolithus crassus Bramlette and Sullivan 1961

The HO occurs just above the CP11/12a boundary, with a significant acme (Max. = 8.6%) and

rapid decline over its short range. *Observed range***:** CP11-12a; NP12-14a

Coccolithus crucis Bown 2005

*Observed range***:** CP13b-14b; NP15b-17

Coccolithus eopelagicus (Bramlette and Riedel 1954) Bramlette and Sullivan 1961

*Observed range***:** CP12a-16a; NP14a-21

Coccolithus foraminis Bown 2005

The HO of *C. foraminis* occurs significantly above that given in the original description (NP10; CP9a), though rare above CP9b. *Observed range***:** CP9a-12a; NP10-14a

Coccolithus latus Bown 2005

Plate 3-15; *Observed range***:** CP9a-10; NP10-12

Coccolithus minimus Bown 2005

Plate 3-16; Most abundant in CP9a - lower CP10, *C. minimus* is rare but consistent through CP14a. *Observed range***:** CP9b-14a; NP10-16/17

Coccolithus mutatus (Perch-Nielsen 1971) Bown, 2005

Plate 3-17; *Observed range***:** CP13a-14b; NP15a-17

Coccolithus pelagicus (Wallich 1877) Schiller 1930

*Observed range***:** CP8a-16a; NP9-21

Coccolithus staurion Bramlette and Sullivan 1961

*Observed range***:** CP14a?-14a; NP16

Cruciplacolithus arenosa Perch-Nielsen 1971

*Observed range***:** CP10-13b; NP12-15b

Cruciplacolithus cassus Bown 2005

Plate 4-1; *Observed range***:** CP9a-12a; NP10-14a

Cruciplacolithus cribellum (Bramlette and Sullivan 1961) Romein 1979

Plate 4-2, 4-3; Only specimens ≥10 µm were identified as *C. cribellum,* due to the morphological issues discussed in *Clausicoccus fenestratus* (above). Often reported through CP9, work by Sullivan (1965) shows consistent co-occurrence with *D. sublodoensis* in CP12a. This large form was present, though rare, through CP14b at 762C, and Bralower and Mutterlose (1995) provide a similar range (CP10-CP13b). This robust form may have been previously grouped with the large *Clausicoccus vanheckiae*, but is easily distinguished by its wide shield and broadly elliptical outline. *Clausicoccus vanheckiae* is normally to narrowly elliptical (1.24-1.51, µ = 1.34, N =20) and the CA accounts for a significantly greater proportion of the coccolith (% CA: $\mu_{C.\ cribellum} = 45.9\%$; $\mu_{C.\ vanheckiae} = 61.6\%$; $p_{same} = 1.01E^{-64}$), so that the shield is significantly more narrow. Dimensions are as observed at Site 762C (N = 20): **Length**: 10.0-13.7 µm, µ = 11.8 µm, s.d. = 1.3; **Width**: 7.9-12.6 µm, µ = 9.9 µm, s.d. = 1.3; **Eccentricity**: 1.09-1.27, µ = 1.19, s.d. = 0.1; **CA Ratio (% total size)**: 38.6-55.5%; µ = 47.1%, s.d. = 3.6. *Observed range***:** CP9b-14b; NP11-17

Cruciplacolithus cruciformis (Hay and Towe 1962) Roth 1970

Plate 4-4, 4-5; This species was consistent from CP9a through the HCO in CP12a. Several short pulses were observed above this level in CP12a, CP13a, and CP14a. This late appearance is also seen by Bown (2005) in CP13a-14b (NP15a-17). Single specimens are also observed in several samples from CP15a and CP15b. It is difficult discern if these specimens are reworked, as they are well-preserved, with delicate structures intact. The angle of the cross-bars relative to the axes varied throughout the section, and additional research would establish if these phenotypic variations occur in any systematic fashion.

*Observed range***:** CP9a-15b?; NP10-19/20?

Cruciplacolithus latipons Romein 1979

*Observed range***:** CP8a; NP9

***Cruciplacolithus nebulosus* n. sp.**

Holotype: 5-1-(50-51 cm) *Paratype*: 4-1-(100-101 cm)

Cruciplacolithus cf. *C. primus* Bown, 2005, pl. 5: 20, 22-23

Etymology: (L.) hazy, obscure, cloudy, for the characteristic appearance of the shield.

Diagnosis: Small to medium, elliptical placolith with a thin axial-cross spanning the CA.

Description: Small to medium, broadly to normally elliptical placolith with an open CA spanned by an axial cross. The distal shield is comprised of 30-45 weakly birefringent elements that are radially oriented, though interference figures and extinction lines show weak obliquity. Though the elements are discrete in plane light, the shield has a distinctly 'fuzzy' appearance under cross polarizers, for which the species is named. The CA is surrounded by a highly birefringent collar crossed by thin, gyred, off-axis extinction lines. When rotated, the extinction lines within the inner cycle converge toward the longitudinal axis, highlighting a bright element at either end. The open CA comprises 35-50% (μ = 42%) of the long axis and 25-40% (μ = 32%) of the transverse axis of the ellipse. The CA is spanned by a thin, delicate, axial cross which may be slightly asymmetrical. This central cross is birefringent when aligned to the polarizers but extinct at 45°.

Dimensions: **Length:** 4.4-6.9 μm, μ = 6.0, s.d. = 0.7; **Width:** 3.4-5.5 μm, μ = 4.7 μm, s.d. = 0.6; **CA Length:** 2.0-3.0 μm, μ = 2.5 μm, s.d. = 0.2; **CA Width:** 1.2-1.8 μm, μ = 1.5, s.d. = 0.2; **Eccentricity:** 1.23-1.39, μ = 1.29, s.d. = 0.05**;** N = 30 for all data

*Remarks***:** *Cruciplacolithus nebulosus* **n sp.** is extremely rare from the LO near the CP12b boundary, but shows a minor increase in abundance toward the end of its observed range, in upper CP15b. The central cross is extremely delicate and may be absent even in relatively well-preserved material, but can be indicated by the four, birefringent points of attachment that remain along the collar. *Cruciplacolithus nebulosus* **n. sp.** can be readily differentiated from other species of *Cruciplacolithus* by size and stratigraphic range, as well as the distinct, 'fuzzy' appearance of the shield. *Cruciplacolithus nebulosus*

can be differentiated from *Bramletteius serraculoides,* which also bears a delicate axial cross, by the notably wider shield of the former.

*Observed range***:** CP12a-16a; NP14a-21

Type Locality: ODP Leg 122 Site 762C, Exmouth Plateau

*Type Level***:** 5-1-(50-51 cm), 199.00 mbsf

***Cruciplacolithus opacus* n. sp.**

Holotype: 5-1-(50-51 cm) *Paratype*: 4-3-(100-101 cm)

Etymology: (L.) shady, dark, opaque, for the predominantly non-birefringent character of the entire coccolith

Diagnosis: Medium to large, elliptical placolith with a non-birefringent central cross

Description: Medium to large placolith that is broadly to narrowly elliptical, though most specimens show normal eccentricity (μ = 1.28, s.d. = 0.07). The broad shields are composed of 30-40, non-birefringent, radial elements. Weak sutures across the shield bend near the inner margin, giving a weakly birefringent, beaded appearance, particularly at 45° to the polarizers. The CA is narrowly elliptical (μ = 2.06) and encircled by a thin, birefringent inner cycle, crossed by four, curved extinction lines. The center of the coccolith is spanned by a small, non-birefringent, axial cross that appears to fill the small central opening, with sharp, low-angle, diagonal extinction lines at 0°.

*Dimensions***: Length:** 6.7-10.3 μm, μ = 8.9 μm, s.d. = 1.0; **Width:** 4.8-8.5 μm, μ = 6.9 μm, s.d. = 0.9; **Eccentricity:** 1.19-1.58, μ = 1.28, s.d. = 0.07; **CA Length:** 2.3-4.5 μm, μ = 3.6 μm, s.d. = 0.6; **CA Width:** 1.1-2.9 μm, μ = 1.8 μm, s.d. = 0.4; **CA Eccentricity:** 1.51-2.87, μ = 2.06, s.d. = 0.35; N = 30 for all data

*Remarks***:** This species is quite rare from its FO just below the CP13b boundary, but becomes more consistent within CP15b. *Cruciplacolithus opacus* **n. sp.** can be differentiated form *C. latipons* and *C. cribellum*, which also have axial crosses that appears to fill the CA, by its narrow CA and dark, non-birefringent appearance.

*Observed range***:** CP13a-16a; NP15a-21

*Type Locality***:** ODP Leg 122 Site 762C, Exmouth Plateau

*Type Level***:** 5-1-(50-51 cm), 199.00 mbsf

Cruciplacolithus* sp. cf. *C. primus Perch-Nielsen 1977

Though the HO is typically shown within the Paleocene, several specimens of *C. primus* are

observed in the lowermost Eocene. Though consistently present through this interval, these specimens still may be reworked. *Observed range***:** CP9a-9b; NP10-11

***Cruciplacolithus tarqu*inius** Hay et al.1967

This species is exceedingly rare in this section. *Observed range***:** CP13b; NP15b

Ericsonia cava (Hay and Mohler 1967)

This species is most abundant in the early Eocene, but becomes increasingly rare through its range. *Observed range***:** CP8a-16a; NP9-21

Ericsonia robusta (Bramlette and Sullivan 1961) Perch-Nielsen 1977

*Observed range***:** CP8a; NP9

Ericsonia formosa (Kamptner 1963) Haq 1971

Abundance of this species fluctuates throughout its observed range (Min = 0.4%; Max = 6.6%; μ. = 3.2%). *Observed range***:** CP9a-16a; NP10-21

Order **ISOCHRYSIDALES** Pascher 1910

Family **NOELAERHABDACEAE** Jerković 1970, emend. Young and Bown 1997

Bicolumnatus ovatus Wei and Wise 1990

Plate 5-1; Some authors consider this species to be a preservational variant of *D. bisectus* (Young and Bown, 1997), while others [Monechi, Buccianti and Gardin (2000); DeKeanel and Villa (1996)] consider it a unique species. The LCO of *B. ovatus* does not occur until the uppermost portion of CP14b, significantly above the LCO of *D. bisectus.* In addition, the relative abundance of this species does not mimic the changes seen in *D. bisectus*, suggesting *B. ovatus* is a unique species. *Observed range***:** CP14b-16a; NP17-21

Cribrocentrum reticulatum (Gartner and Smith 1967) Perch-Nielsen 1971

This species is a significant proportion of the assemblage from LO into CP15a (5-10%). Sporadic but well-preserved specimens were observed through early CP16a. It is difficult to determine if such specimens are reworked or represent a true HO, as Bralower and Mutterlose (1995) also identify this species within CP16. *Observed range***:** CP14a-16a; NP16-21

Cribrocentrum* sp. cf. *C reticulatum (Gartner and Smith 1967) Perch-Nielsen 1971

Frequent specimens are observed similar to *C. reticulatum* in size, shape, and rim structure, but lacking the diagnostic central grill. Trends in abundance mimic those of *C. reticulatum* and stratigraphic ranges are nearly identical, therefore, this form is considered a preservational variant. *Observed range***:** CP14a?-15b; NP16-19/20

Cyclicargolithus floridanus (Hay et al. 1967) Bukry 1971

This species shows an abundance increase within CP14a and an abundance acme (5-10%) within CP15a. *Observed range***:** CP14a?-16a; NP16-21

Cyclicargolithus luminis (Sullivan 1965) Bukry 1971

Plate 5-2, 5-3; Sporadic specimens were identified in the middle Eocene. See also Sullivan (1965, plate 3, #9a-b), Perch-Nielsen (1985, fig. 59: 26-27) and Bybell (1975, pl 5: #6). *Observed range***:** CP11-13b; NP12-15b

***Cyclicargolithus parvus* n. sp.**

Cyclicargolithus luminis Bown (2005); pl. 2: 1-2

Holotype: Plate 5-4 *Paratype:* Plate 5-5

Etymology: (L.) For the small size (μ = 4.2 μm) of this form

Diagnosis: Small, circular placolith with a quadrate interference figure.

*Description***:** Small circular placolith with a small central opening and a bicyclic shield. The central opening is square to sub-circular in shape and is surrounded by a bright inner cycle. The shields are composed of 25-40 thin, slightly imbricated elements with clear sutures at the periphery that become less distinct inward. The larger proximal shield is 40-60% larger than the distal shield, and both are weakly birefringent. The quadrate interference figure is thin and sharp as it curves across the bright inner cycle and broadens outward across the shields.

Dimensions: **Proximal shield:** 3.2-5.0 μm, μ = 4.2 μm, s.d. = 0.5; **Distal shield:** 1.6-2.8 μm, μ = 2.2 μm, s.d. = 0.3; N = 30 for all data

Remarks: Cyclicargolithus parvus differs from *C. lumin*is in both stratigraphic range and morphology: *C. parvus* is restricted to CP8a-CP10, while *C. luminis* is generally reported from the middle to late Eocene, though it was observed low in this section (CP11). *Cyclicargolithus luminis* was originally described as 6-8 μm in diameter and measured specimens all fall within this range (6.15-7.89 μm), while *C. parvus* **n. sp.** is ≤ 5.0 μm. Sutures between shield elements are very distinct in *C. parvus* but are not readily visible in *C. luminis*. In addition, *C. parvus* shows low order grey interference colors while *C. luminis* shows higher order birefringence, primarily pale yellow with a faint orange ring. *Cyclicargolithus parvus* was consistently present through its observed range and is most abundant within CP9b (μ = 2-3%).

Type Locality: ODP Leg 122 Site 762C, Exmouth Plateau

Type Level: 25-1-(50.5-51.5 cm), 389.01mbsf

*Observed range***:** CP8a-10; NP9-12

Dictyococcites bisectus (Hay, et al. 1966), Bukry and Percival 1971

As noted by Villa et al. (2008), this species rapidly becomes a significant proportion of the assemblage, with values > 10% early in its range, but shows a relative decline (~3-4%) by the top of the Eocene. *Dictyococcites bisectus* shows two notable abundance peaks, also shown in Wei and Wise (1990a), in CP14b (μ = 8%) and CP15b (μ = 10%), with a maximum abundance of 14.6%. *Observed range***:** CP14b-16a; NP17-21

Dictyococcites filewiczii Wise and Wiegand in Wise 1983

*Observed range***:** CP15a-16a; NP18-21

Dictyococcites scrippsae Bukry and Percival 1971

Plate 5-6, 5-7; This species shows a notable acme from CP12a-14a (max 15%), decreases steadily through CP14, becoming rare within CP15b. Though considered a synonym of *D. stavensis* by Bown (2005), these species are distinct in several ways: Stratigraphically, *D. scrippsae* appears before both *D. bisectus* and *D. stavensis*. Morphologically, the vast majority of *D. scrippsae* specimens were significantly smaller (≤7.5μm) than the holotype (~ 9.5 μm), while *D. stavensis* must be >10μm. *Dictyococcites scrippsae* shows continuous, sharp extinction figures within the CA that bend sharply before broadening across the shield, while the CA of *D. stavensis* shows a prominent plug with notable relief, showing bright, 2nd order interference colors. *Observed range***:** CP11-16a; NP13-21

Dictyococcites stavensis (Levin and Joerger 1967) Varol 1989

Morphologically similar to *D. bisectus* but >10μm in length. The LO occurs slightly above *D. bisectus*, and these two species show similar patterns of abundance. *Observed range***:** CP14b-16a; NP17-21

Reticulofenestra daviesii (Haq 1968) Perch-Nielsen 1971 (d)

Plate 5-8, 5-9; This species is included in this genus rather than *Dictyococcites,* since the CA is not filled by a solid plug of radially oriented elements. *Observed range***:** CP14a?-16a; NP15b-21

Reticulofenestra dictyoda (Deflandre in Deflandre and Fert 1954) Stradner in Stradner and Edwards 1968

The FO of *R. dictyoda* occurs within CP10, earlier than commonly reported, also noted in Bown (2005) and Bralower and Mutterlose (1995). Both small (3-5μm) and large (6-14μm) forms appear in the same sample interval, and patterns of abundance suggest that these size variants are likely the same species. This species shows a significant increase in abundance in CP12a and comprises≥15% of the assemblage through CP14a. A second increase is observed near the top of CP15 to >20% relative abundance in CP16a. *Observed range***:** CP10-16a; NP12-21

Reticulofenestra hillae Bukry and Percival 1971

Smaller specimens with similar morphology to *Reticulofenestra hillae* were identified and informally grouped relative to size into *R. hillae A* (5-10μm), *R. hillae B* (>10-14μ), and *R. hillae C* (s.s.) (>14μm). Unlike *R. dictyoda,* these size groups show a distinct sequence of appearance, and could benefit significantly from a systematic, statistical revision.

Reticulofenestra hillae* var. *A

Plate 5-10; Though extremely rare, specimens 5-10µm are first seen in upper CP10, increasing significantly in CP12a up to 15-20% of the total assemblage in CP13b-14a. Though slightly less abundant above these subzones, this form remains dominant through the top of the section (>10%) and is significantly more abundant than larger forms. *Observed range***:** CP10-16a; NP12-21

Reticulofenestra hillae* var. *B

Plate 5-11; This size range is significantly less abundant than those 5-10µm in size, generally < 2%. *Observed range***:** CP12a-16a; NP14a-21

***Reticulofenestra hillae* s.s**.

Plate 5-12; Extremely rare specimens were seen in CP14a with the LCO observed just below the CP14b boundary. *Observed range***:** CP12b-16a; NP15b-21

Reticulofenestra lockeri Müller 1970

One specimen was observed in CP14a, with LCO in CP14b, and a notable abundance increase within CP15a. *Observed range***:** CP14a-16a; NP16-21

Reticulofenestra minuta Roth 1970

Though present from the middle Eocene, specimens of *Reticulofenestra* ≤ 3µm in length show a notable increase in abundance within CP15 (Max.: =5.2%; µ = 2.8%) *Observed range***:** CP12a-16a; NP14a-21

Reticulofenestra oamaruensis (Deflandre in Deflandre and Fert 1954) Stradner in Haq 1968

The LO is observed above the LO of *I. recurvus* but below the LO of *C. reticulatum. Observed range***:** CP15b-16a; NP19/20-21

Reticulofenestra samodurovii (Hay et al. 1966) Roth 1970

*Observed range***:** CP14a-15b; NP16-18

Reticulofenestra umbilica (Levin 1965) Martini and Ritzkowski 1968

Rare and sporadic early in its range, this species becomes relatively common and consistent above ~280 mbsf. *Observed range***:** CP14a-16a; NP16-21

Reticulofenestra wadeae Bown 2005

This species was observed both below and above the range provided in the original description (NP15b-c; CP13b-c). *Observed range***:** CP12b-15a; NP14b-18

Family **PRINSIACEAE** Hay and Mohler 1967 emend. Young and Bown 1997

Girgisia gammation (Bramlette and Sullivan 1961) Varol 1989

Plate 5-13; The LO is observed just below the LO of *D. lodoensis* at Site 762C, and approximates this biomarker (Agnini et al. 2007a, 2006; Bralower and Mutterlose 1995). The HO of *G. gammation* is observed well below the commonly reported CP14a, though a HO in CP12b is also noted in Bralower and

Mutterlose (1995). This species is most abundant from upper CP10-CP11 (Max. = 5.0%; μ = 3.5%), also shown in Agnini et al. (2007a). *Observed range***:** CP9b-12b; NP11-14b

Girgisia* cf. *G. gammation

Plate 5-14; The LO of a *Girgisia* spp. is noted as *Girgisia* cf. *G. gammation*, as it exhibits diagnostic characteristics of this species, but bears a square-shaped opening in the CA. This variation is concurrent with *G. gammation* through much of its range, and may be a preservational variant. *Girgisia* sp. cf. *G. gammation* is distinguished here from *G. gammation* s.s. as it differs from the explicit note of Perch-Nielsen stating that *G. gammation* bears "no central opening" (1985, p 505). In addition, *Girgisia* cf. *G. gammation* appears smaller than *G. gammation* s.s., but we would like to evaluate these characteristics from additional sections with better preservation. This form shows peak abundance in CP10-11, with HCO at the base of CP12a, and may be an indication of reduced preservation. *Observed range***:** CP9b-12a; NP11-13

Prinsius bisulcus (Stradner 1963) Hay and Mohler 1967

*Observed range***:** CP8a; NP9

Toweius callosus Perch-Nielsen 1971

The observed LO in CP8a is well below that commonly reported (CP10). This species shows a considerable acme in CP9a-10 (Min.: 7.4%; Max.: 11.8%; μ: 9.3%) followed by a rapid decline within CP10. Wei and Wise (1990a; 1989b) show similar trends, with LO in lower CP8a and acme in CP9a. In addition, images of this species in Bown (2005) are derived from cores spanning CP8a-9b. These three accounts give robust evidence for a significantly earlier LO than has been commonly reported. *Observed range***:** CP8a-12b; NP9-14b

Toweius eminens (Bramlette and Sullivan 1961) Perch-Nielsen 1971

The HCO of this species occurs at the base of CP9b, with HO within this subzone. *Toweius eminens* is extremely abundant in CP8a (Max.: > 17%); however, this interval may be affected by the PETM and indicates a skewed assemblage toward more dissolution resistant species. Though notably robust at the base of the section, the overall size of *T. eminens* appears to decrease through its observed range. This large morphotype may be associated with the Paleocene-Eocene boundary interval, and would benefit from a more detailed investigation. *Observed range***:** CP8a-9b; NP9-11

Toweius*? *magnicrassus (Bukry 1971) Romein 1979

*Observed range***:** CP9b-12b; NP11-14b

Toweius occultatus (Locker 1967) Perch Nielsen 1971

*Observed range***:** CP9b-11; NP11-12

Toweius pertusus (Sullivan 1965) Romein 1979

This species is most abundant in CP9a-b, with μ= ~6.6% through CP9a. The HCO of *T. pertusus* occurs near the top of CP10, but continues sporadically above this range to the base of CP12a. *Observed*

*range***:** CP8a-12a; NP9-14a

Toweius rotundus Perch-Nielsen in Perch-Nielsen et al. 1978

Plate 6-1, 6-2; The LO is observed in upper CP9a with peak abundance in CP9b - lower CP10. Though Bown (2005) documented this species in CP9 (NP11), Bown and Pearson (2009) show *T. rotundus* as an extinction taxa across the PETM. This is in contrast to our observations and the original description by Perch-Nielsen, which gives an early Eocene type level (CP9b/NP11) and shows a consistent to common abundance through this interval. It is possible that this species showed a significant contraction in its range and/or abundance during the PETM, but recovered sometime after the excursion. *Observed range***:** CP9a-10; NP10-12

Toweius serotinus Bybell and Self-Trail 1995

This species is notably abundant during CP8a-9a (μ: ~3.0%; max.: 4.4%). *Observed range***:** CP8a-9b; NP9-10

Toweius tovae Perch-Nielsen 1971

*Observed range***:** CP8a; NP9

***Toweius* sp. 1** Bown 2005

Plate 6-3; *Observed range***:** CP9a-10; NP10-12

***Toweius* sp. 2** Bown 2005

Plate 6-4; *Observed range***:** CP9a-10; NP10-12

Placolith Genera *incertae sedis*

Ellipsolithus distichus (Bramlette and Sullivan 1961) Sullivan 1964

*Observed range***:** CP8a-10; NP9-12

Ellipsolithus lajollaensis Bukry and Percival 1971

*Observed range***:** CP12b-13b; NP14a-15b

Ellipsolithus macellus (Bramlette and Sullivan 1961) Sullivan 1964

This species varies considerably in size, with several specimens <7μm, notably smaller than the size range provided in the original description (9-15 μm). The LO is observed at the base of CP9a, and HO near the top of CP12a. *Observed range***:** CP9a-12a; NP10-14a

Hayella*? *gauliformis Troelsen and Quadros, 1971

This species is rare and sporadic throughout its range. *Observed range***:** CP9b-14a?; NP11-16

***Hayella ovata* n. sp.**

Hayella situliformis, Bown 2005, pl. 10, fig. 9

Holotype: Plate 6-5 *Paratype*: Plate 6-6

Etymology: For the elliptical outline of both shield and collar

Diagnosis: Elliptical placolith with a birefringent shield and high, constricted collar.

Description: Medium to large, broadly to normally elliptical placolith with a wide, open central-area. The birefringent shield is constructed of 25-40 elements that show a quadrate interference figure ~45° to the

axes of the ellipse. Elements of the proximal shield appear sinistrally oblique when the distal side (collar) is oriented upward. The form shows high relief, tapering upward like a truncated cone, with the constricted end bearing a distinctly elliptical beaded collar.

Dimensions: **Length:** 6.9-9.1 μm; μ = 8.1 μm, s.d. = 0.7; **Width:** 5.6-7.8 μm, μ = 6.6 μm, s.d. = 0.7; **Collar Length**: 2.3-3.4 μm, μ = 3.0 μm, s.d. = 0.4; **Collar Width:** 1.7-2.9 μm, μ = 2.0 μm, s.d. = 0.3; **Collar Eccentricity:** 1.12-1.95, μ = 1.5 μm, s.d. = 0.23; N =17 for all data

Remarks: This species is similar to *H. situliformis* with respect to shield type and high conical taper, but shows a distinctly elliptical outline of both shield and collar. This form was rare at this locality, so biometric data is available for only 17 specimens.

*Observed range***:** CP14b-16b; NP16-21

Type Locality: ODP Leg 122 Site 762C, Exmouth Plateau

Type Level: 4-4-(50-51 cm), 194.00 mbsf

Hayella? simplex Bown and Dunkley-Jones 2006

Plate 6-7; This species is most abundant in CP10-11, becoming rare from CP12a, with HCO at the base of CP15a. The LO was observed well below the ranges provided in Bown and Dunkley-Jones (2006) or Bown, Dunkley-Jones and Young (2007, fig. 1). *Observed range***:** CP10-15b; NP12-19/20

Hayella? simplex* var. *petalus Bown and Dunkley-Jones 2006

Plate 6-8

Etymology: For the petal like shape of shield elements

Diagnosis: Medium-sized, circular placolith with petal-like shield elements and open central-area.

Description: Medium-sized, circular placolith comprised of a vacant central-area surrounded by a thin, birefringent collar and 13-18 radially oriented, petal-like shield elements. The shield is also birefringent and bears a quadrate extinction figure. Specimens show some vertical relief and weak taper upward.

Dimensions: **Shield diameter:** 5.6-7.8 μm, μ = 6.5 μm, s.d. = 0.5.; **CA:** 1.7-2.9 μm; μ = 2.2 μm, s.d. = 0.3; **Ratio CA Ratio** (% of size): 26.6-39.8 %, μ = 33.7%, s.d. = 3.3. **Shield elements**: 13-18, μ = 15.6, s.d. = 1.4.

Remarks: This form is currently identified as a preservational variant of *H.*? *simplex*. These two forms do not differ significantly with respect to the size of the shield or CA, and both show similar degrees of vertical relief and taper. The only morphological variable in which these two forms show statistically significant variation is with respect to the number of shield elements ($\mu_{H.\ simplex} = 30.5$; $\mu_{H.\ simplex\ petalus} = 15.6$; $p_{same} = 1.3E^{-31}$). The full stratigraphic range of *H.*? *simplex* var. *petalus* is contained within a notable abundance peak of *H. simplex* , during an interval of reduced preservation relative to the entire section. This form is likely the result of either loss of the distal shield of *H.*? *simplex* or coarsening of shield elements via dissolution and re-precipitation. It may be shown that this form is indeed independent of *H.*? *simplex,* but will require identification in a section with better preservation. *Hayella* is still considered a provisional genus for this species. Though both of these forms show some constriction when focusing upwards, they lack the vertical relief and strong conical taper that characterizes the type species *H.*

situliformis.

*Observed range***:** CP10-12a; NP12-14a

Hayella situliformis Gartner 1969

Plate 6-9; The LCO was observed within CP15a. *Observed range***:** CP14a-16a; NP16-21

Markalius inversus (Deflandre in Deflandre and Fert 1954) Bramlette and Martini 1964

Plate 6-10; Specimens where the central-area is ≤ 33% the total diameter of the coccolith have been identified as *M. inversus* in accordance with the original description. Measurements of the holotype of Deflandre (Deflandre and Fert, 1954, pl. 9, fig. 4-5) give a CA of ~33%. In addition, measurements provided in the original description of *M. astroporus* (Stradner 1963, considered a synonym by Bramlette and Martini, 1964) indicate a maximum CA diameter of ~30%. Both the original micrograph and sketch in this publication show a CA that is ≤ 33 % of the CA. These accounts suggest that the earliest species concepts of *M. inversus* pertain to specimens with a relatively constricted CA, as opposed to those forms with a more expanded CA, discussed below. CA: 22.4-33.2 %, μ = 27.8 %, s.d. = 2.5, N = 28. *Observed range***:** CP9a-16a?; NP10-21

Markalius latus **n.sp.**

Holotype: Plate 6-11 *Paratype*: Plate 6-12

Bramlette and Martini 1964, plate 2, #7-8

Etymology: (L.) broad or wide, for the expanded central-area that occupies approximately > 33% of the coccolith diameter.

Diagnosis: Medium to large, circular placolith with broad, birefringent CA

Description: Medium to large, bicyclic, circular placolith with a wide CA occupying > 33 % of the coccolith diameter. The upper shield is narrower than the lower shield, and each is composed of 30-50 oblique elements that are weakly birefringent. The broad CA is depressed and filled with blocky element that are highly birefringent and show a thin, quadrate extinction figure that is slightly off-axis.

Dimensions: **Shield diameter:** 5.5-9.1 μm; μ = 7.2 μm, s.d. = 1.13; **CA diameter:** 2.3-3.8 μm, μ = 3.1 μm, s.d. = 0.44; **CA/Shield ratio:** 36.9-48.7 %; μ = 43.8 %; s.d. = 2.9; N = 23 for all data

Remarks: The relative size of the CA was measured in 50 specimens of *Markalius*. This data shows a distinctly non-normal distribution (Figure 8a), with specimens clustering into two dominant populations (Fig 8b), those with a relatively constricted CA (< 33%) and those with a more expanded CA (> 33%). When separated, both groups approach normal distribution (Figure 8c, d), and comparison of these two populations indicate that they are morphologically distinct ($\mu_{M.\ Inversus\ s.s.}$ = 27.8%, $\mu_{M.\ Inversus\ var.\ latus}$ = 43.9%, $p_{same} = 3.24\ E^{-26}$).

Type Locality: ODP Leg 122 Site762C, Exmouth Plateau

Type Level: 23-3-(51-52 cm), 373.01 msbf

*Observed range***:** CP9ba-12b

Pedinocyclus annulus **n. sp.**

Holotype: Plate 7-1 *Paratype:* Plate 7-2

Etymology: (L.) from ring, for the open CA

Diagnosis: Medium to large elliptical placolith with a bright inner cycle and open CA

Description: Medium to large, broadly to normally elliptical placolith with a wide, weakly birefringent shield, showing a range of first-order grays. The shield is composed of 35-50 slightly imbricated elements that are radially oriented along most of the shield, but show slight curvature near the longitudinal axis of the ellipse. The open CA occupies ~40% of the longitudinal axis and is surrounded by a thin, birefringent inner cycle. The gyred extinction lines within the inner cycle are off-axis at 0° but approach the long axis when rotated to 45°.

Dimensions: **Length:** 6.7-10.3 µm, µ = 8.1 µm, s.d. = 0.9.; **Width:** 5.3-8.1 µm, µ = 6.7 µm, s.d. = 0.8; **Eccentricity:** 1.11-1.30, µ = 1.20, s.d. = 0.05; **CA Length:** 2.6-5.4 µm, µ = 3.3 µm, s.d. = 0.6; **CA Length Ratio** (% of size): 33.0-52.5%, µ = 40.3%, s.d. = 4.9; **CA Width:** 1.7-3.1 µm, µ = 2.3 µm, s.d. = 0.3; **CA Width Ratio** (% of size): 27.3-41.7%, µ = 33.9%, s.d. = 4.2; N = 30 for all data

Remarks: The LO is observed near the base of CP13a, and is very rare and sporadic throughout its range. This species is tentatively placed into the genus *Ped*i*nocyclus* due to similarities with *P. larvalis* with respect to shape, orientation, and birefringence of the shield elements. *Ped*i*nocyclus annulus* **n. sp.** can be differentiated from *Calcidiscus ellipticus* **n. sp**. by the wider shield of the former, and from *C.? henrikseniae* which shows strong, gyred extinction from the CA outward across the shield.

Type Locality: ODP Leg 122 Site 762C, Exmouth Plateau

Type Level: 14-4-(55-56 cm), 289.05 mbsf

*Observed range***:** CP12b-CP16a; NP14b-21

Pedinocyclus larvalis (Bukry and Bramlette 1969) Loeblich and Tappan 1973

Plate 7-4; The oldest specimens of *P. larvalis* were identified only as fragments; however, the distinct shield structure and low order birefringence allows confidence in identification. The first whole specimens are observed in CP11, accompanied by a modest increase in abundance. *Observed range***:** CP10-16a; NP12-21

Pedinocyclus larvalis* var.? *minimus (Bukry and Bramlette 1969) Loeblich and Tappan 1973

Plate 7-5, 7-6; Whole specimens of *P. larvalis* were generally > 10 µm as indicated in the original description; however, beginning in CP13 very rare specimens < 10µm are observed, with several as small as 7.0 µm, becoming more common upward. Due to the rarity of this genus in this section, it is difficult to determine if this form is either a morphological variant or an independent species that can be reliably differentiated from *P. larvalis* s.s. This taxonomic issue may be resolved with sufficient statistical data via study from multiple sections. Observed measurements are provided, though note that this is not a statistically significant population: **Shield Diameter:** 7.0-9.5 µm, µ = 8.4 µm, s.d = 0.8; **CA Diameter:** 1.3-2.8 µm, µ = 2.3 µm, s.d. = 0.4; N = 10 for all data. *Observed range***:** CP13a?-16a?; NP15a?-21?

Tetralithoides symeonidesii Theodoridis 1984

Plate 7-7, 7-8; As indicated in Bown (2005), this species is not typically known prior to the Miocene. Observations of Bown (2005) from CP13b-c (NP15b-c), coupled with identification in this

section indicate this species does occur in the Eocene, though extremely rarely. *Observed range***:** CP12a-15b; NP14a-19/20

HOLOCOCCOLITHS

Family **CALYPTROSPHAERACEAE** Boudreaux and Hay 1969

Corannulus germanicus Stradner 1962

Plate 7-9; This species is extremely rare at 762C. *Observed range***:** CP15b-16a; NP19/20-21

Corannulus horridulus Bown 2005

*Observed range***:** CP9a; NP10

Daktylethra* cf. *D. punctulata Gartner and Bukry 1969

Plate 7-10; Only one specimen of this species was observed. *Observed range***:** CP12a; NP14a

Lanternithus arcanus Bown 2005

*Observed range***:** CP12b-13b; NP14b-15b

Lanternithus simplex Bown 2005

*Observed range***:** CP9a-12b; NP10-14b

Lanternithus minutus Stradner1962

The LO is observed at the base of CP12a, below the CP12b LO of Bown (2005) and Wise, et al. (2004). A significant increase in abundance is observed through CP15b (Max: 8.6%). A notable proportion of specimens were somewhat overgrown, obscuring the central opening. *Observed range***:** CP12a-16a; NP14a-21

Several unique specimens of *Lanternithus* were observed through the section, with two example provided below.

***Lanternithus* sp. 1**

Plate 7-11, 7-12; This form bears two robust blocks of calcite that fill the CA. *Observed range***:** CP13b; NP15b

***Lanternithus* sp. 2**

Plate 7-13; This form bears four blocks of calcite that are aligned to the axes, filling the CA with an axial cross. *Observed range***:** CP12b; NP14b

Peritrachelina joidesa Bukry and Bramlette, 1968

*Observed range***:** CP16a; NP21

Youngilithus oblongatus Bown 2005

This very rare species is observed below the range given in the original description (NP15b-c). *Observed range***:** CP13a-13b; NP15a-15b

Zygrhablithus bijugatus (Deflandre Deflandre and Fert 1954) Deflandre 1959

Noted in numerous publications and above, this species shows a significant rise in abundance above the HO of *Fasciculithus spp.,* slightly above the PETM (>12-20%). Though fairly abundant below and within the PETM interval (~5-8%), most observed specimens were reduced in length and notably dissolved. *Observed range***:** CP8a-16a; NP9-21

Holococcolith sp. 1

Plate 8-1, 8-2; Small, elliptical holococcolith composed of 10-12 radially oriented elements that are weakly to moderately birefringent and show a quadrate extinction figure. *Observed range***:** CP15b; NP19/20

NANNOLITHS

Family **BRAARUDOSPHAERACEAE** Deflandre (1947)

This family was extremely rare at 762C, with no observed *Micrantholithus spp.* and only an occasional *Braarudosphaera* or rare *Pemma* fragment.

Braarudosphaera bigelowii (Gran and Braarud, 1935) Deflandre, 1947

This species is rare and sporadic throughout the section, though most consistent in CP10. *Observed range***:** CP9a-15b; NP10-21

Pemma papillatum Martini, 1959

Only extremely rare, disarticulated plates of this species were observed. *Observed range***:** CP15b; NP19/20

Family **LAPIDEACASSACEAE** Bown and Young 1997

Lapideacassis* cf. *L. blackii Perch-Nielsen in Perch Nielsen and Franz, 1977

A short but notable abundance peak was observed at the top of CP15a. *Observed range***:** CP15a-15b; NP18

Order **DISCOASTERALES** Hay, 1977

Family **DISCOASTERACEAE** Tan, 1927

Relative abundance varied considerably among species within this genus. Please see (location of data) for more detailed abundance data.

Discoaster acutus Bown 2005

*Observed range***:** CP9a-9b; NP10-11

Discoaster cf. ***D. backmanii*** Agnini et al. 2008

Similar to *D. backmanii*, but observed above the range provided in the original description. This may extend the true range of this species or may be a unique form. *Observed range:* CP10-12b; NP12-14b

Discoaster barbadiensis Tan 1927, emend. Bramlette and Riedel 1954

This species shows two abundance peaks, first in upper CP11-12b, and again within CP14b. This species and *D. saipanensis* become very rare near the end of their range, which has caused difficulty in placement of the CP15b/16a boundary, typically marked by the concurrent HO of these species. The boundary is placed at the HCO of both species, though both occur sporadically in CP16a. Though some specimens in CP16a are poorly preserved and likely reworked, others are quite well preserved. *Observed range***:** CP9a-15b; NP10-19/20

Discoaster bifax Bukry, 1971

This species was very rare in this assemblage so that range and abundance could not be adequately tracked. *Observed range***:** CP14

Discoaster binodosus Martini, 1958

The HO is observed at the base of CP12a. *Observed range***:** CP9a-12a; NP10-14a

Discoaster cruciformis Martini 1958

*Observed range***:** CP10-12a; NP12-14a

Discoaster decoratus Dang Dik Nga and Shumenko 1975

*Observed range***:** CP16a; NP21

Discoaster deflandrei Bramlette and Riedel 1954

Plate 8-4; *Observed range***:** CP9b-16a; NP11-21

Discoaster diastypus Bramlette and Sullivan 1961

*Observed range***:** CP9a-10; NP10-12

Discoaster distinctus Martini 1958

*Observed range***:** CP10; NP12

Discoaster elegans Bramlette and Sullivan 1961

*Observed range***:** CP9a-9b; NP10-11

Discoaster falcatus Bramlette and Sullivan 1961

*Observed range***:** CP9a; NP10

Discoaster gemmeus Stradner 1959

*Observed range***:** CP13a-14b; NP15a-17

Discoaster gemmifer Stradner 1961

The LO occurs just below the CP10 boundary. *Observed range***:** CP9b-12b; NP11-14b

Discoaster germanicus Martini 1958

The HO of *D. germanicus* is considerably lower than commonly reported (near the CP14a-b boundary). *Observed range***:** CP10-12a; NP12-14a

Discoaster kuepperi Stradner 1959

Numerous specimens are observed early in CP10 that are smaller in size (4.5-6.0μm) than previously described (7-15μm). *Discoaster kuepperi* shows a notable acme (Max. = 6.6%; μ. = 5.9%) from upper CP10-lower CP12, which coincides with the *Discoaster* spp. acme observed at 762C. *Observed range***:** CP10-12b; NP12-14b

Discoaster lenticularis Bramlette and Sullivan 1961

*Observed range***:** CP8a-9b; NP9-10

Discoaster lodoensis Bramlette and Riedel 1954

Though rare early in its range, *D. lodoensis* shows a notable acme in upper CP10 - basal CP12a (Max. =7.2%; μ = 5.7%) followed by rapid decrease prior to extinction. *Observed range***:** CP10-12a; NP12-14a

Discoaster mediosus Bramlette and Sullivan 1961

*Observed range***:** CP9a; NP10

Discoaster minimus Sullivan 1964

*Observed range***:** CP10; NP12

Discoaster mohleri Bukry and Percival 1971

*Observed range***:** CP8a; NP9

Discoaster multiradiatus Bramlette and Riedel 1954

Abundance and range data of this species is similar to Agnini, et al. (2007a), with peak abundance through the PETM. *Observed range***:** CP8a-9b; NP9-11

Discoaster nobilis Martini 1961

*Observed range***:** CP8a; NP9

Discoaster nodifer (Bramlette and Riedel 1954) Bukry 1973

*Observed range***:** CP14a-16a; NP16-21

Discoaster nonaradiatus Klumpp 1953

*Observed range***:** CP11-12a; NP12-14a

Discoaster ornatus (Bramlette and Wilcoxon 1967) Bown 2005

Plate 8-5; Specimens of *D. ornatus* were identified when diagnostic nodes were present, but were grouped with *D. tanii* when overgrowth prohibited such differentiation. *Observed range***:** CP14b-16a; NP17-21

Discoaster pacificus Haq 1969

*Observed range***:** CP9b-11; NP11-12

Discoaster perpolitus Martini 1961

*Observed range***:** CP9a; NP10

Discoaster praebifax Wei and Wise 1989

The authors agree with Wei and Wise (1989a) in that *D. bifax* may be an unreliable marker for the base of CP14a, as *D. praebifax* transitions into *D. bifax*, creating issues with intermediate forms and synchroniety. This species is most abundant from LO through CP12a. *Observed range***:** CP11-13b: NP13-15b

Discoaster robustus Haq 1970

*Observed range***:** CP9b-11; NP10-13

Discoaster saipanensis Bramlette and Riedel 1954

Though rare in its lower range, this species shows a significant abundance increase in CP14b, becoming rare again within CP15b. See *D. barbadiensis* above. *Observed range***:** CP13a-15b; NP15a-19/20

Discoaster salisburgensis Stradner 1961

The HO is observed at the base of CP11. *Observed range***:** CP9a-11; NP10-12

Discoaster septemradiatus (Klumpp 1953) Martini 1958

*Observed range***:** CP10-12a; NP12-14a

Discoaster strictus Stradner 1961

The LO was observed earlier than commonly reported (CP12b), in the upper portion of CP12a. The HCO corresponds to Perch-Nielsen (1985, CP14b), but it is seen sporadically above this range at Site 762C. *Observed range***:** CP12a-15a; NP14a-17

Discoaster sublodoensis Bramlette and Sullivan 1961

This species is consistently present in the range provided below, though a pulse of specimens seemingly identical to *D. sublodoensis* are observed in upper CP10 and CP11. These specimens (8.1-21.6 µm, µ = 13.4, s.d. = 3.0) do not differ in size or morphology from specimens observed higher in the section (7.8-19.8 µm, µ = 14.6 µm, s.d. = 3.3). Specimens of *D. sublodoensis* are also observed by Agnini et al. (2006) and Wei and Wise (1990a) in CP10 and CP11, prior to the LCO and base of CP12a. It is possible that *D. sublodoensis* shows an early LO at Site 762C. *Observed range***: CP**12a-13b; NP14a-15b

Discoaster tanii Bramlette and Riedel 1954

The LO occurs in upper CP14a. *Observed range***:** CP14a-16a; NP17-21

Discoaster cf. ***D. tanii*** Bramlette and Riedel 1954

Very rare but fairly consistent specimens of *Discoaster* cf. *D. tanii* were observed well below the

commonly reported LO of CP14b/NP17. Specimens show typical characteristics of *D. tanii,* and biometric analysis shows early specimens marginally smaller; however, they do not vary significantly enough from specimens higher in the section to be differentiated ($\mu_{D.\ tanii}$ = 10.9 µm, $\mu_{D.\ cf.\ D.\ tanii}$ = 9.5 µm, $p_{same} = 3.2E^{-2}$). It should be noted that the maximum size of *D. tanii* (17.6 µm) is much greater than those identified as *D.* cf. *D. tanii* (13.8 µm). Specimens are identified as *D.* cf. *D. tanii* until the base of CP14b, though these specimens may represent an early occurrence of *D. tanii* at this locality. *Observed range***:** 12a-14a; NP14a-16

Discoaster wemmelensis Achuthan and Stradner 1969

*Observed range***:** CP12a-14a?; NP14b–16

Family **FASCICULITHACEAE** Hay and Mohler 1967

Fasciculithus alanii Perch-Nielsen 1971

*Observed range***:** CP8a; NP9

Fasciculithus clinatus Bukry 1971

*Observed range***:** CP8a; NP9

Fasciculithus hayii Haq 1971

*Observed range***:** CP8a; NP9

Fasciculithus lillianae Perch-Nielsen 1971

*Observed range***:** CP8a; NP9

Fasciculithus tonii Perch-Nielsen 1971

*Observed range***:** CP8a; NP9

Fasciculithus tympaniformis Hay and Mohler 1967

*Observed range***:** CP8a; NP9

***Fasciculithus* spp.** base

*Observed range***:** CP8a-9a; NP9-10

Family **HELIOLITHACEAE** Hay and Mohler 1967

Bomolithus elegans Roth 1973

*Observed range***:** CP8a; NP9

Heliolithus kleinpellii Sullivan 1964

*Observed range***:** CP8a; NP9

Family **RHOMBOASTERACEAE** Bown 2005

All observed genera within Rhomboasteraceae were rare at Exmouth Plateau.

***Nannotetrina* sp.** Achuthan and Stradner, 1969

Some specimens of this genus could not be identified to species level due to preservation or

specimen orientation and have been identified simply as *Nannotetrina* sp. *Observed range***:** CP13a-14b; NP15a-16

Nannotetrina cristata (Martini 1958) Perch-Nielsen 1971

*Observed range***:** CP13a-14a?; NP15a-16

Nannotetrina fulgens (Stradner in Martini and Stradner 1960) Achuthan and Stradner 1969

This species was grouped with *N. quadrata,* as overgrowth inhibited differentiation. *Observed range***:** CP13a-14a?; NP15a-15b

Nannotetrina nitida (Martini, 1961) Aubry 1983

*Observed range***:** CP12b; NP14b

Nannotetrina quadrata (Bramlette and Sullivan 1961) Bukry 1973

*Observed range***:** See *N. fulgens*

Rhomboaster cuspis Bramlette and Sullivan 1961

*Observed range***:** CP9a; NP10

Tribrachiatus* (*Rhomboaster*) *bramlettei (Brönnimann and Stradner 1960) Bybell and Self-Trail 1995

*Observed range***:** CP9a; NP10

Tribrachiatus contortus (Stradner 1958) Bukry 1972

*Observed range***:** CP9a; NP10

Tribrachiatus digitalis Aubry 1996

The range of *T. digitalis* occurs within the lower range of *T. contortus* at Site 762C. This is in agreement of findings of Raffi, Backman and Pälike (2005) and Agnini et al. (2007a), creating a crossover of the NP10a-d subzones of Aubry (1995). Results from these three studies include sites from the Indian, equatorial Pacific and North Atlantic Oceans, and likely indicate a global signal. *Observed range***:** CP9a; NP10

Tribrachiatus orthostylus (Bramlette and Riedel 1954) Shamrai 1963

This species was consistently present to the HO at the base of CP12a, the LCO of *D. sublodoensis. Observed range***:** CP9b-12a; NP11-13

Family **SPHENOLITHACEAE** Deflandre 1952

Sphenolithus acervus Bown 2005

Specimens of *S. acervus* (>8.0 µm) are rare in the early Eocene. Similar large forms are also seen in the middle Eocene, as noted in Bown (2005). *Observed range***:** CP9a and CP13b-c; NP10 and NP15b-16.

Sphenolithus anarrhopus Bukry and Bramlette 1969

*Observed range***:** CP8a-9b; NP9-11

Sphenolithus celsus Haq 1971

*Observed range***:** CP16a; NP21

Sphenolithus conspicuus Martini 1976

The LO is just below the CP10 boundary, with HO at the base of CP11. *Observed range***:** CP9b-11; NP11-12

Sphenolithus cuniculus Bown 2005

Plate 8-6*;* This species shows an abundance increase near the CP14a/b boundary (max. = 3%). *Observed range***:** CP13b-14b; NP15b-17

Sphenolithus editus Perch-Nielsen in Perch Nielsen *et al*. 1978

The LO occurs just below the CP9a/b boundary, with HO at the base of CP12a. *Observed range***:** CP9a-12a; NP10-13

Sphenolithus elongatus Perch-Nielsen 1980

This species is extremely rare and sporadic at this locality. *Observed range***:** CP13b; NP15b

Sphenolithus furcatolithoides Locker 1967

This species is most common in CP13b. *Observed range***:** CP13b-14a?; NP15b-16

Sphenolithus intercalaris Martini 1976

*Observed range***:** CP14a-15a; NP16-17

Sphenolithus moriformis (Brönnimann and Stradner 1960) Bramlette and Wilcoxon 1967

Peak abundance (4.4%; 276.71 m) is observed during an abundance increase (μ: 3.1%) that may be associated with the MECO (276 m). *Observed range***:** CP8a-16a; NP9-21

Sphenolithus obtusus Bukry 1971

The LCO (CP14b) agrees with Perch-Nielsen (1985); however, very rare specimens are observed in two samples within CP14a. *Observed range***:** CP14a-14b; NP16-17

Sphenolithus orphanknollensis Perch-Nielsen 1971

This species was rare through its range. *Observed range***:** CP11-14a?; NP13-16

Sphenolithus perpendicularis Shamrock 2010

Plate 8-7; *Observed range***:** CP13a; NP15a

Sphenolithus predistentus Bramlette and Wilcoxon 1967

Though consistently present in CP14b and 15b, no specimens were observed in CP15a. This curious absence was also noted by Wei and Wise (1990a; 1989b), who show a gap from CP14b-15b. *Observed range***:** CP14b-16a; NP16-21

Sphenolithus primus Perch-Nielsen 1971

*Observed range***:** CP9a-9b; NP10-11

Sphenolithus pseudoradians Bramlette and Wilcoxon 1967

*Observed range***:** CP14a-16a; NP16-21

Sphenolithus radians Deflandre in Grasse 1952

This species is fairly abundant and consistent from the LO, but rare above CP10 and sporadic above CP13b. *Observed range***:** CP9b-16a; NP11-21

Sphenolithus runus Bown and Dunkley-Jones 2006

*Observed range***:** CP14a?-14b; NP16-NP17

Sphenolithus spiniger Bukry 1971

Plate 8-8; This species is consistently observed above the commonly reported range of CP13/NP15. *Observed range***:** CP12a-14b; NP14a-17

Sphenolithus stellatus Gartner 1971

This species is very rare and sporadic. *Observed range***:** CP12b-13b; NP14b-15b

Sphenolithus strigosus Bown and Dunkley-Jones 2006

Plate 8-9; This species is seen consistently through lower CP14b. *Observed range***:** CP14a?-14b; NP16-17

Sphenolithus villae Bown 2005

Only one specimen of this species was observed. *Observed range***:** CP10

Sphenolithus* cf. *S. dissimilis Bukry and Percival 1971

Plate 8-10, 8-11; Specimens similar to *S. dissimilis*, bearing a tripartite apical spine, are observed in the middle and upper Eocene at Site 762C. Specimens with four apical terminations are also observed. Similar specimens are also reported from Bown (2005, pl. 45:21-25), but are identified as *S. conicus*. *Observed range***:** CP14b-16a; NP17-21

***Sphenolithus* sp. 1**

Plate 9-1; Several, notably small (3-5 μ) specimens of *Sphenolithus* were identified in the Ypresian at Site 762C. These forms show a bright proximal and lateral cycle when aligned to the polarizers (0°), and a small apical spine birefringent at 45° to the polarizers. Observed range: CP9a-CP11; NP10-12

Nannoliths *incertae sedis*

Biantholithus flosculus Bown 2005

The HO is occurs near the CP9b boundary. *Observed range***:** CP8a-9a; NP9-10

Leesella procera Bown and Dunkley-Jones 2006

Plate 9-2; *Observed range***:** CP14b; NP17

Pemma*? *uncinata Bown and Dunkley-Jones 2006

Plate 9-3, 9-4, 9-5; Numerous specimens are observed that resemble this form, but lack the thin connective structures shown in the type specimens. This form was tentatively assigned to the genus *Pemma* by Bown and Dunkley-Jones (2005) as it closely resembles disarticulated pentaliths, Though that assignment is followed here, the form is still considered in*certae sedis,* as all specimens were observed as individual segments. Measurement of the interior and exterior angles are highly variable, both in our specimens and those provided in the original description (**Holotype** (pl. 9, fig. 17): Interior angle: 62.8°, Exterior angle: 57.8°; **Paratype** (pl. 9, fig. 13): Interior angle: 103.76°, Exterior angle: 89.3°; **All specimens** (N = 50): Interior angle: 68.0-104.9, μ = 87.5, s.d. = 7.0; Exterior angle: 57.5-82.7, μ = 71.7°,

s.d. = 4.8). Despite the high angular variability, the mean external angle approximates that need to form a pentalith, and may suggest this is the correct affiliation for this strange form. Specimens should continue to be tentatively assigned to the genus *Pemma* until more is understood. *Observed range***:** CP14b-15a; NP17-18

Pseudotriquetrorhabdulus inversus (Bukry and Bramlette 1969) Wise in Wise and Constans 1976

This species occurs consistently below its commonly reported range of CP12b. *Observed range***:** CP12a-14b; NP14a-17

INDETERMINATE NANNOLITHS

There is a notable increase in indeterminant nannoliths in the uppermost Eocene, particularly within CP15b-16a, many of which are extremely thin and non-birefringent. This increase may be due to increased preservation or may be environmentally driven by Late Eocene cooling.

Genus *Hexadelus* new genus

Etymology: (Gr.) From *hexa*, referring to the six-fold arrangement of plates, and *adelus* (unseen, unknown, secret), for the delicate and enigmatic nature of the specimens.

Description: Hexagonal form composed of six flat, triangular plates. Each plate has three sides of equal length with three 60° angles, forming an equilateral triangle. This genus is extremely delicate, occurring primarily as disarticulated plates, though several partially articulated specimens suggests the relative relationships between these individual segments. Although similar plates belong to members of the pentalith family Braarudosphaeraceae, the consistent angular measurements indicate that these plates belong to a separate group: The interior angle of a pentalith must average ~72° (69.9°-75.1°, $\mu = 72.3°$, s.d. = 1.28, N = 90), while plates that are 60° require six segments in order to complete the cycle (Figure 9). Univariate t-tests show distinct separation between plate geometry of pentaliths and the type specimen *Hexadelus archus* **n. sp**.: At the 95% confidence level pentalith angle = 72.0-72.5°, while *Hexadelus archus* = 60.4-61.2°; $p_{(same\ \mu)} = 9.93\ E^{-100}$ (Figure 10).

Type species: *Hexadelus archus* **n. sp.**

***Hexadelus archus* n. sp.**

Holotype: Plate 9-6 *Paratype*: Plate 9-7

Etymology: (Gr.) from *arche*, meaning beginning, first, or chief

Description: Small to medium hexagonal form composed of six, flat plates, each a near equilateral triangle. The plates are very thin and show relatively low birefringence. The form is extremely fragile, and is

observed primarily as disarticulated plates. Articulated specimens show weak alternating birefringence between plates.

Measurements: **Length** (of individual plates): 1.9-4.0 µm, µ = 3.1, s.d. = 0.6, N = 30; **Diameter** (whole specimen, as shown in Figure 9): 3.3-7.0 µm, µ = 5.3 µm, s.d. = 1.0, N = 30; **Plate angle**: 55.6-64.5°, µ = 60.8°. s.d. = 2.0, N = 90

Remarks: Extremely fragile, this species will likely be found only in well preserved samples. This species can be differentiated from the disarticulated plates of pentaliths such as *Braarudosphaera* spp. and *Micrantholithus* spp. by the more narrow angles of the plates. Pentaliths must have at least one angle that is ~72°, while plates from this species show all three angles at ~60° (Figure 9). *Hexadelus archus* **n. sp.** shows a HO just below the CP16a boundary.

Observed Range: CP15b-16a; NP19/20-21

Type Locality: ODP Leg 122 Site 762C, Exmouth Plateau

Type Level: 4-2-(146.5-147.5 cm), 191.77 mbsf

Hexadelus triquetra Bown and Dunkley-Jones 2006

Pemma? triquetra Bown and Dunkley-Jones 2006, pl. 9, fig. 1-4, 6-8

This species was tentatively placed into the genus *Pemma*, as it is quite similar to the disarticulated plates of known pentaliths. Measurements of specimens from the original description, as well as that identified at Site 762C, indicate that this species also shows interior angles of ~60°, indicating that plates would also create a hexagonal form if articulated by their edges. Only one specimen from these original images (pl 9: 5) illustrates interior angles (52.4°, 52.0°, 86.0°) or side lengths (6.5 µm, 5.6 µm, 5.4 µm) that do not fit the necessary geometric relationships, and may in fact be a different species. Measurements are given for the holotype and paratype, as well as additional specimens provided in Bown and Dunkley-Jones (2006, pl. 9: 4-5): **Holotype**(pl 9: 6-8): *Angle*: θ1 = 62.7°, θ2 = 62.5°, θ3 = 57.6°; *Length*: L1 = 4.9 µm, L2 = 5.2 µm, L3 = 5.3 µm; **Paratype** (pl 9: 1-3): *Angle*: θ1 = 62.6°, θ2 = 58.4°, θ3 = 61.8°; *Length*: L1 = 5.8 µm, L2 = 5.9 µm, L3 = 5.8 µm; **All specimens**: *Angle*: 57.6-63.5°, µ = 60.8, s.d. = 1.8, N = 30; *Length*: 4.57-6.0 µm, µ = 5.3 µm, s.d. 0.5, N = 10; *Diameter*: 7.9-10.4, µ = 9.2, s.d. = 0.9, N = 10. *Observed Range:* CP15a-15b; NP18-19/20

Indeterminate nannolith- Type 1 Bown and Dunkley-Jones 2006

Plate 9-8, 9-9; There is a notable increase in abundance at the base of CP16a (max. = 2.6%). Two variations are observed: complete rings as shown in Bown and Dunkley-Jones (2006, pl. 9: 21-25) and those that appear as a recumbent horseshoe, where the tips remain unattached. These variations were not separated in this study due to the generally enigmatic nature of this form. *Observed range***:** CP15b-16a; NP19/20-21

Indeterminate nannolith - Type 2

Plate 9-10, 9-11, 9-12; An unidentifiable nannolith was identified just below the CP16a boundary and was consistently observed through the remaining section examined. There is some indication that these nannoliths may be highly dissolved or weakly calcified remnants of *Zygrhablithus bijugatus*, where the form is broken along the central suture, so that half of the base and stem remain. *Observed range***:** CP15b-16a; NP19/20-21

APPENDIX B - PLANKTONIC FORAMINIFERA TAXONOMIC APPENDIX

Genus/Species	**Reference**
Morozovella aragonensis	Nuttall 1930
Morozovella formosa	Bolli 1957
Turborotalia pomeroli	Toumarkine & Bolli 1970

REFERENCES

Due to the large number of taxonomic references, particularly within the appendix, the authors refer the reader to Perch-Nielsen (1985), which contains all taxonomic references prior to that reference's publication date. Taxonomic references not included in Perch-Nielsen (1985) are given below.

A -AGNINI, C., FORNACIARI, E., RAFFI, I., RIO, D., RÖHL, U. and WESTERHOLD, T., 2007. High-resolution nannofossil biochronology of middle Paleocene to early Eocene at ODP Site 1262: Implications for calcareous nannoplankton evolution. *Marine Micropaleontolgoy*, 64:215-248.

B - AGNINI, C., FORNACIARI, E., RIO, D., TATEO, F., BACKMAN, J. and GIUSBERTI, L., 2007. Responses of calcareous nannofossil assemblages, mineralogy and geochemistry to the environmental perturbations across the Paleocene/Eocene boundary in the Venetian Pre-Alps. *Marine Micropaleontology*, 63:19-38.

AGNINI, C., MUTTONI, G., KENT, D.V. and RIO, D., 2006. Eocene biostratigraphy and magnetic stratigraphy from Possango, Italy: the calcareous nannofossil response to climate variability. *Earth and Planetary Science Letters*, 241:815-830AUBRY, M. -P., 1995. Toward an upper Paleocene-lower Eocene high resolution stratigraphy based on calcareous nannofossil stratigraphy. *Israel Journal of Earth Sciences*, 44:239-253.

--- 1992. Late Paleogene calcareous nannoplankton evolution: a tale of climatic deterioration. In: Prothero, D. R. and Berggren, W.A. (Eds). *Eocene-Oligocene Climatic and Biotic Evolution,* 272-309. Princeton: Princeton University Press.

--- 1991. Sequence stratigraphy: Eustacy or tectonic imprint? *Journal of Geophysical Research*, 96: 6641-6679.

ALI, J. R. and HAILWOOD, E. A., 1995. Magnetostratigraphy of upper Paleocene through lower middle Eocene strata of Northwest Europe. In: In: Berggren, W. A., Kent, D., V., Aubry, M. -P. and Hardenbol, J. (Eds), *Geochronology, Time Scales and Global Stratigraphic Correlations.* Society for Sedimentary Geology (SEPM) Special Publication, 54: 275-280.

AUBRY, M. -P., 1995. From chronology to stratigraphy: interpreting the lower and middle Eocene stratigraphic records in the Atlantic Ocean. In: Berggren, W. A., Kent, D., V., Aubry, M. -P. and Hardenbol, J. (Eds), *Geochronology, Time Scales and Global Stratigraphic Correlations.* Society for Sedimentary Geology (SEPM) Special Publication, 54: 213-274.

AUBRY, M. -P., 1991. Sequence stratigraphy: Eustacy or tectonic imprint? *Journal of Geophysical Research*, 96: 6641-6679.

BERGGREN, W. A. and PEARSON, P. N., 2005. A revised tropical to subtropical Paleogene planktonic foraminiferal zonation. *Journal of Foraminiferal Research*, 35-4: 279-298.

A - BERGGREN, W. A., KENT, D., V., AUBRY, M. -P. and HARDENBOL, J. (Eds), *Geochronology, Time Scales and Global Stratigraphic Correlations.* Society for Sedimentary Geology (SEPM) Special Publication, 54: 386 pp.

B - BERGGREN, W. A., KENT, D. V., SWISHER, C. C. III and AUBRY, M. –P., 1995. A revised Cenozoic geochronology and chronostratigraphy. In: Berggren, W. A., et al. (Eds), *Geochronology, Time Scales and Global Stratigraphic Correlation*, SEPM Special Publication 54: 129-212.

BERGGREN, W. A. and MILLER, K. G., 1988. Paleogene tropical planktonic foraminiferal biostratigraphy and magnetostratigraphy. *Micropaleontology,* 34: 362-380.

BLEIL, U., 1985. The magnetostratigraphy of northwest Pacific sediments, Deep Sea Drilling Project Leg 86. In: Heath, G. R., Burckle, L. H., et al. (Eds), *Init. Repts. DSDP*, 86: Washington (U.S. Govt. Printing Office), 441-458. doi:10.2973/dsdp.proc.86.117.1985

BOHATY, S. M., ZACHOS, J. C., FLORINDO, F. and DELANEY, M. L., 2009. Coupled greenhouse warming and deep-sea acidification in the Middle Eocene. *Paleoceanography*, 24:PA2207. doi: 10.1029/2008PA001676

BOHATY, S. M. and ZACHOS, J. C., 2003. Significant Southern Ocean warming event in the late middle Eocene. *Geology*, 31:1017-1020.

BOWLES, J., 2006. Data report: revised magnetostratigraphy and magnetic mineralogy of sediments from Walvis Ridge, Leg 208. In: Kroon, D., Zachos, J.C., and Richter, C. (Eds.), *Proc. ODP, Sci. Results,* 208: College Station, TX (Ocean Drilling Program), 1–24. doi:10.2973/odp.proc.sr.208.206.2006

BOWN, P. R., 2005. Paleogene calcareous nannofossils from the Kilwa and Lindi areas of coastal Tanzania (Tanzania Drilling Project 2003-4). *Journal of Nannoplankton Research*, 27(1): 21-95.

BOWN, P. R. and PEARSON, P., 2009. Calcareous plankton evolution and the Paleocene/Eocene Thermal Maximum event: new evidence from Tanzania. *Marine Micropaleontolgoy*, 71: 60-70

BOWN, P.R., DUNKLEY-JONES, T. and YOUNG, J.R., 2007. *Umbilicosphaera jordanii* Bown, 2005 from the Paleogene of Tanzania: confirmation of generic assignment and Paleocene origination for the Family Calcidiscaceae. *Journal of Nannoplankton Research*, 29(1):25-30.

BOWN, P. R. and DUNKLEY-JONES, T., 2006. New Paleogene calcareous nannofossils taxa from coastal Tanzania: Tanzania Drilling Project Sites 11 to 14. *Journal of Nannoplankton Research*, 28(1):17-34.

BOWN, P. R. and Young, J. R., 1998. Techniques. In: Bown, P. E. (Ed). *Calcareous Nannofossil Biostratigraphy*. Kluwer Academic, London: 16-28.

BRALOWER, T. J., 2002. Evidence of surface water oligotrophy during the Paleocene-Eocene thermal maximum: Nannofossil assemblage data from Ocean Drilling Program Site 690, Maud Rise, Weddell Sea. *Paleoceanography,* 17(2): 1–12. doi: 10.1029/2001PA000662

BRALOWER, T. J. and MUTTERLOSE, J., 1995. Calcareous nannofossil biostratigraphy of Site 865, Allison Guyot, Central Pacific Ocean: a tropical Paleogene reference section. In: Winterer, E.L., et al. (Eds), *Proceedings of the Ocean Drilling Program, Scientific Results,* 143: 31-74. College Station, TX (Ocean Drilling Program).

BUFFLER, R. T., *et al*. 1984. *Deep Sea Drilling Program, Initial Reports* **77**: Washington (U.S. Govt. Printing Office), 738pp.

BYBELL, L. M. and SELF-TRAIL, J. M., 1995. Evolutionary, biostratigraphic, and taxonomic study of calcareous nannofossils from the continuous Paleocene-Eocene boundary section in New Jersey. *US Geological Survey Professional Paper,* 1554:36pp.

BYBELL, L. and GARTNER, S., 1972. Provincialism among mid-Eocene calcareous nannofossils. *Micropaleontology*, 18(3):319-336.

CANDE, S. C. and KENT, D. V., 1995. Revised calibration of the geomagnetic polarity time scale for the Late Cretaceous and Cenozoic. *Journal of Geophysical Research*, 100 (B4): 6093-6096. doi: 10.1029/94JB03098

CASCELLA, A. and DINARÉS-TURELL, J., 2009. Integrated calcareous nannofossil biostratigraphy and

magnetostratigraphy from the uppermost marine Eocene deposits of the southeastern Pyrenean foreland basin: evidences for marine Priabonian deposition. *Geologica Acta*, 7(1-2):281-296

CHANG, Y. -M., 1967. Accuracy of fossil percentage estimation. *Journal of Paleontology*, 41:500-502.

CHANNEL, J. E. T., GALEOTTI, S., MARTIN, E. E., BILLUPS, K., SCHER, H. D. and STONER, J.S., 2003. Eocene to Miocene magnetostratigraphy, biostratigraphy, and chemostratigraphy at ODP Site 1090. *Geological Society of America Bulletin*, 115(5): 607-623.

CRAMER, B. S., TOGGWEILER, J. R., WRIGHT, J, D., KATZ, M. E. and MILLER, K. G., 2009. Ocean overturning since the Late Cretaceous: Inferences from a new benthic foraminiferal isotope compilation. *Paleoceanography*, 24: PA4216, 14 pp. doi: 10.1029/2008PA001683

CRAMER, B. S., WRIGHT, J. D., KENT, D. V. and AUBRY, M. -P., 2003. Orbital climate forcing of $\delta^{13}C$ excursions in the late Paleocene-early Eocene (chrons C24n –C25n). *Paleoceanography*, 18(4):1097. doi: 10.1029/2003PA000909

DEFLANDRE, G., 1952. Classe des Coccolithophoridés *(Coccolithophoridae Lohmann, 1902)*. *Traite de Zoologie,* Masson: 439-470.

DEKAENEL, E. and VILLA, G., 1996. Oligocene-Miocene calcareous nannofossil biostratigraphy and paleoecology from the Iberia Abyssal Plain. In: Whitmarsh, R. B., et al. (Eds), *Proceedings of the Ocean Drilling Program, Scientific Results,* 149: 79-145. College Station, TX (Ocean Drilling Program).

DENNISON, J. M. and HAY, W. W., 1967. Estimating the needed sampling area for subaquatic ecologic studies. *Journal of Paleontology*, 41(3):706-708.

DUNKLEY-JONES, T., BOWN, P. R., PEARSON, P. N., WADE, B. S., COXALL, H. K. and LEAR, C. H., 2008. Major shifts in calcareous phytoplankton assemblages through the Eocene-Oligocene transition of Tanzania and their implications for low-latitude primary production. *Paleoceanography*, 23:PA4204. doi: 10.1029/2008PA001640

FLORINDO, F. and ROBERTS, A. P. 2005. Eocene-Oligocene magnetobiochronology of ODP Sites 689 and 690, Maud Rise, Weddell Sea, Antarctica. *Geological Society of America Bulletin*, 117: 46-66. doi:10.1130/B25541.1

GAELOTTI, S., KRISHNAN, S., PAGANI, M., LANCI, L., GAUDIO, A., ZACHOS, J. C., MONECHI, S., MORELLI, G., LOURENS, L., 2010. Orbital chronology of Early Eocene hyperthermals from the Contessa Road section, central Italy. *Earth and Planetary Science Letters*, 290: 192-200.

GALBRUN, B., 1992. Magnetostratigraphy of Upper Cretaceous and lower Tertiary sediments, Sites 761 and 762, Exmouth Plateau, northwest Australia. In: von Rad, U., Haq, B.U., et al., *Proc. ODP, Sci. Results,* 122: College Station, TX (Ocean Drilling Program), 699–716. doi:10.2973/odp.proc.sr.122.149.1992

A - GIBBS, S. J., BRALOWER, T. J., BOWN, P. R., ZACHOS, J. C. and BYBELL, L. M., 2006. Shelf and open ocean calcareous phytoplankton assemblages across the Paleocene-Eocene thermal Maximum: Implications for global productivity gradients. *Geology*, 34(4):233-236.

B - GIBBS, S. J., BOWN, P. R., SESSA, J. A., BRALOWER, T. J. and WILSON, P. A., 2006. Nannoplankton extinction and origination across the Paleocene-Eocene Thermal Maximum. *Science*, 314:1770-1773.

GOLOVCHENKO, X., BORELLA, P. E. and O'CONNELL, S, 1992. Sedimentary cycles on the Exmouth Plateau. In: von Rad, U., et al. (Eds), *Proceedings of the Ocean Drilling Program, Scientific Results,* 122: 279-291. College Station, TX (Ocean Drilling Program). doi:10.2973/odp.proc.sr.122.141.1992

GRADSTEIN, F. M., 1992. Legs 122 and 123, northwestern Australian margin – a stratigraphic and paleogeographic summary. In: Gradstein, F. M., et al. (Eds), *Proceedings of the Ocean Drilling Program, Scientific Results,* 123: 801-816. College Station, TX (Ocean Drilling Program). doi:10.2973/odp.proc.sr.123.110.1992

GRADSTEIN, F., OGG, J. and SMITH, A., 2004. *A Geologic Time Scale 2004*. Cambridge: Cambridge University Press, 589pp.

HAMMER, Ø., HARPER, D. A. T. and RYAN, P. D. 2001. PAST: Paleontological Statistics Software Package for Education and Data Analysis. *Palaeontologia Electronica* 4(1): 9pp. http://palaeo-electronica.org/2001_1/past/issue1_01.htm, 5-27-2009.

HAQ, B. U., BOYD, R. L., EXON, N. F., and VON Rad, U., 1992. Evolution of the central Exmouth Plateau: a post-drilling perspective. *In* von Rad, U., Haq, B.U., et al., *Proc. ODP, Sci. Results,* 122: College Station, TX (Ocean Drilling Program), 801-818. doi: 10.2973/odp.proc.sr.122.182.1992

HAQ, B.U., 1970. The structure of Eocene Coccoliths and Discoasters from a Tertiary deep-sea core in the Central Pacific. *Stockholm University Contributions to Geology*, 21(1):1-19.

HAQ, B. U., BOYD, R. L., EXON, N. F., and VON Rad, U., 1992. Evolution of the central Exmouth Plateau: a post-drilling perspective. *In* von Rad, U., Haq, B.U., et al., *Proc. ODP, Sci. Results,* 122: College Station, TX (Ocean Drilling Program), 801-818. doi: 10.2973/odp.proc.sr.122.182.1992

HAQ, B. U., RAD, U. VON, O'CONNELL, S., et al., 1990. *Proceedings of the Ocean Drilling Program, Initial Reports,* 122: College Station, TX (Ocean Drilling Program). doi:10.2973/odp.proc.ir.122.1990

HAQ, B. U., and LOHMANN, G. P., 1976. Early Cenozoic calcareous nannoplankton biogeography of the Atlantic Ocean. *Marine Micropaleontology* **1**: 119–194. doi: 10.1016/0377-8398(76)90008-6.

HARDENBOL, J., THIERRY, J., FARLEY, M. B., JACQUIN, T., DE GRICIANSKY, P. –C., 1998. *Mesozoic and Cenozoic sequence stratigraphy of European basins.* Society for Sedimentary Geology (SEPM), Special Publication 60: 786pp.

JIANG, S. and WISE, S. W., JR, 2009. Distinguishing the influence of diagenesis on the paleoecological reconstruction of nannoplankton across the Paleocene/Eocene Thermal Maximum: An example from the Kerguelen Plateau, southern Indian Ocean. *Marine Micropaleontolgoy*, 72:49-59.

JOVANE, L., FLORINDO, F., COCCIONI, R., DINARES-TURELL, J., MARSILI, A., MONECHI, S., ROBERTS, A. P. and SPROVIERI, M., 2007. The middle Eocene climatic optimum event in the Contessa Highway section, Umbrian Apennines, Italy. *Geological Society of America Bulletin*, 119:413-427. doi: 10.1130/1325917.1

KAHN, A. and AUBRY, M. -P., 2004. Provincialism associated with the Paleocene/Eocene thermal maximum: temporal constraint. *Marine Micropaleontology*, 52:117-131.

LANG, T.H. and WATKINS, D.K. 1984. Cenozoic calcareous nannofossils from Deep Sea Drilling Project Leg 77: biostratigraphy and delineated hiatuses. *Initial Reports of the Deep Sea Drilling Program*, **77**: 629-648.s

LEES, J. A., 2002. Calcareous nannofossil biogeography illustrates paleoclimate change in the Late Cretaceous Indian Ocean. *Cretaceous Research*, 23(5): 537-634. doi: 10.1006/cres.2003.1021

LOURENS, L. J., SLUIJS, A., KROON, D., ZACHOS, J. C., THOMAS, E., ROHL, U., BOWLES, J. and RAFFI, I., 2005. Astronomical pacing of late Paleocene to early Eocene global warming events. *Nature*, 435:1083-1087. doi: 10.1038/nature03814

LOWRIE, W., ALVAREZ, W., NAPOLEONE, G., PERCH-NIELSEN, K., PREMOLI SILVA, I. and TOUMARKINE, M., 1982. Paleogene magnetic stratigraphy in Umbrian pelagic carbonate rocks: the Contessa sections, Gubbio. *Geological Society of America Bulletin*, 93: 414-432. doi: 10.1130/0016-7606(1982)93<414:PMSIUP>2.0CO;2

LYLE, M. W., WILSON, P. A., JANECEK, T. R., et al., 2002. Leg 199 summary. *Proc. of the ODP, Init. Reports*.,199, College Station, TX (Ocean Drilling Program), pp 1-87.

A MARINO, M. and FLORES, J. –A., 2002. Data report: calcareous nannofossil data from the Eocene to Oligocene, Leg 177, Hole 1090B. In: Gersonde, R., Hodell, D.A., and Blum, P. (Eds), *Proc. of the ODP, Sci. Results*, 177: 9pp. doi: 10.2973/odp.proc.sr.177.115.2002

B MARINO, M. and FLORES, J. A., 2002. Middle Eocene to early Oligocene calcareous nannofossil stratigraphy at Leg 177 Site 1090. *Marine Micropaleontology*, 45:383-398.

MARTINI, E., 1971. Standard Tertiary and Quaternary calcareous Nannoplankton zonation. In*:* Farinacci, A. (Ed), *Proceedings of the Second Planktonic Conference, Roma, 1970*, 2:739-785. Rome: Edizioni Tecnoscienza.

MASCLE, J. *et al*. 1996. *Proceedings of the Ocean Drilling Program, Initial Reports,* **159**: College Station, TX (Ocean Drilling Program).

MCGONIGAL, K. and DI STEFANO, A., 2002. Calcareous nannofossil biostratigraphy of the Eocene-Oligocene transition, ODP Sites 1123 and 1124. In: Richter, C. (Ed), *Proc. ODP, Sci. Results*, 181: 22 pp. doi:10.2973/odp.proc.sr.181.207.2002

MILLER, K. G., KENT, D. V., BROWER, A. N., BYBELL, L. M., FEIGENSON, M. D., OLSSON, R. K., and POORE, R. Z., 1990. Eocene-Oligocene changes on the New Jersey coastal plain linked to the deep-sea record. *Geological Society of America Bulletin*, 102: 331-339. doi:10.1130/0016-7606(1990)102<0331:EOSLCO>2.3.CO;2

MITA, I., 2001. Data Report: Early to late Eocene calcareous nannofossil assemblages of Sites 1051 and 1052, Blake Nose, northwestern Atlantic Ocean. In: Kroon, D., et al. (Eds), *Proceedings of the Ocean Drilling Program, Scientific Results,* 171B, 1-28. doi: 10.2973/odp.proc.sr.171B.122.2001

MONECHI, S, 1985. Campanian to Pleistocene calcareous nannofossil stratigraphy from the northwest Pacific Ocean, Deep Sea Drilling Project Leg 86. In: Heath, G. R., Burckle, L. H., et al., *Init. Repts. DSDP*, 86: 301-336. doi: 10.2973/dsdp.proc.86.110.1985

MONECHI, S. and ANGORI, E., 2006. Data report: calcareous nannofossil biostratigraphy of the Paleocene/Eocene boundary, Ocean Drilling Program Leg 208 Hole 1266C. In: Kroon, D., et al. (Eds), *Proceedings of the Ocean Drilling Program, Scientific Results,* 208: 1-9. College Station, TX (Ocean Drilling Program). doi:10.2973/odp.proc.sr.208.2006

MONECHI, S., ANGORI, E. and SALIS, K. VON, 2000. Calcareous nannofossil turnover around the Paleocene/Eocene transition at Alamedilla (southern Spain). *Bulletin de la Societe Geologique de France*, 171:477-489.

MONECHI, S., BUCCIANTI, A. and GARDIN, S., 2000. Biotic signals from nannoflora across the iridium anomaly in the upper Eocene of the Massignano section: evidence from statistical analysis. *Marine Micropaleontology*, 39:219-237.

MONECHI, S. and THIERSTEIN, H. R., 1985. Late Cretaceous-Eocene nannofossil and magnetostratigraphic correlations near Gubbio, Italy. *Marine Micropaleontology*, 9: 419-440. 58pp. doi:10.2973/odp.proc.sr.171B.104.2001

NAPOLEONE, G., PREMOLI SILVA, I., HELLER, F., CHELI, P., COREZZI, S., and FISCHER, S. G., 1983. Eocene magnetic stratigraphy at Gubbio, Italy, and its implications for Paleogene geochronology. *Geological Society of America Bulletin*, 94: 181-191.

NEAL, J. E. and HARDENBOL, J., 1998. Introduction to the Paleogene. In: de Graciansky, P. –C., Hardenbol, J., Jaquin, T. and Vail, P. R., *Mesozoic and Cenozoic Sequence Stratigraphy of European Basins*. Society for Sedimentary Geology (SEPM) Special Publication 60: 87-90.

NICOLO, M. J., DICKENS, G. R., HOLLIS, C. J. and ZACHOS, J. C., 2007. Multiple early Eocene hyperthermals: Their sedimentary expression on the New Zealand continental margin and in the deep sea. *Geology,* 35(8):699-702.

OGG, J. G, OGG, G. and GRADSTEIN, F. M., 2008. *The Concise Geologic Time Scale.* Cambridge University Press, 177 pp.

OGG, J. G. and BARDOT, L., 2001. Aptian through Eocene magnetostratigraphic correlation of the Blake Nose Transect (Leg 171B), Florida continental margin. In: Kroon, D., Norris, R. D., and Klaus, A. (Eds), *Proc, of the ODP, Sci, Results*, 171B: 58pp. doi:10.2973/odp.proc.sr.171b.104.2001

OKADA, H. and BUKRY, D., 1980. Supplementary modification and introduction of code numbers to the low-latitude coccolith biostratigraphic zonation (Bukry, 1973, 1975). *Marine Micropaleontology*, 5: 321-325.

PÄLIKE, H., NORRIS, R. D., HERRLE, J. O., WILSON, P. A., COXALL, H. K., LEAR, C. H., SHACKLETON, N. J., TRIPATI, A. K. and WADE, B. S., 2006. The heartbeat of the Oligocene climate system. *Science,* 314 (5807): 1894-1898. doi:10.1126/science.1133822

PASCHER, A., 1910. Chrysomonaden aus dem Hirschberger Grossteiche. *Monographien und Abhandlungen zur Internationalen Revue der gesamten hydrobiology und Hydrographie*, 1:66pp.

PEARSON, P. N., MCMILLAN, I. K., WADE, B. S., DUNKLEY-JONES, T., COXALL, H. K., BOWN, P. R., and LEAR, C. H., 2008. Extinction and environmental change across the Eocene-Oligocene boundary in Tanzania. *Geology*, 36: 179-182.

PERCH-NIELSEN, K., 1985. Cenozoic calcareous nannofossils. In: Bolli, H.M., Saunders, J.B. and Perch-Neilsen, K., Eds, *Plankton Stratigraphy*, 427-554. Cambridge: Cambridge University Press.

- 1986. New Mesozoic and Paleogene calcareous nannofossils. *Eclogae Geologicae Helvetiae*, 79-3:835-847.

PERSICO, D. and VILLA, G., 2008. A new Eocene *Chiasmolithus* species: hypothetical reconstruction of its phyletic lineage. *Journal of Nannoplankton Research*, 30(1): 23-33.

PHLEGER, F. B., 1960. *Ecology and distribution of recent Foraminifera*. Baltimore: John Hopkins Press. Pp. viii + 297, II plates and 83 text-figures.

Rad, U.Von, *et al*. 1992. Rift-to-drift history of the Wombat Plateau, northwestern Australia: Triassic to Tertiary Leg 122 results. *Proceedings of the Ocean Drilling Program, Scientific Results*, **122**: 765-800.

RAD, U. VON, HAQ, B. U., et al., Eds., 1992. *Proceedings of the Ocean Drilling Program, Scientific Results,* 122. College Station, TX: Ocean Drilling Program. doi:10.2973/odp.proc.sr.122.1992

RAFFI, I. and BERNARDI, B. DE, 2008. Response of calcareous nannofossils to the Paleocene-Eocene Thermal Maximum: Observations on composition, preservation and calcification in sediments from ODP Site 1263 (Walvis Ridge – SW Atlantic). *Marine Micropaleontology*, 69:119-138.

RAFFI, I., BACKMAN, J., FORNACIARI, E**., PÄLIKE, H**., RIO, D., LOURENS, L., HILGEN, F., 2006. A Review of calcareous nannofossil astrobiochronology encompassing the past 25 million years. *Quaternary Science Reviews,* **25**(23-24): 3113-3137. doi:10.1016/j.quascirev.2006.07.007

RAFFI, I., BACKMAN, J. and PÄLIKE, H., 2005. Changes in calcareous nannofossil assemblages across the Paleocene/Eocene transition from the paleo-equitorial Pacific Ocean. *Palaeogeography, Palaeoclimatology, Palaeoecology*, 226:93-126.

REVETS, S. A., 2004. On confidence intervals from micropalaeontological counts. *Journal of Micropaleontolgoy*, 23:61-65.

RÖHL, U, WESTERHOLD, T., MONECHI, S., THOMAS, E., ZACHOS, J. C. and DONNER, B., 2005. The third and final Early Eocene thermal maximum: characteristics, timing, and mechanisms of the "X" event. Geological Society of America, Salt Lake City, Abstract Program, Vol 37(7): p 264.

ROTH, P. H. and BERGER, W. H., 1975. Distribution and dissolution of coccoliths in the south and central Pacific. *Cushman Foundation for Foraminiferal Research, Special Publication*, 13:87-113.

SALAMY, K. A. and ZACHOS, J. C., 1999. Latest Eocene-Early Oligocene climate change and Southern Ocean fertility: inferences from sediments accumulation and stable isotope data. *Palaeogeography, Palaeoclimatology, Palaeoecology*, 145:61-77.

SHAFIK, S., WATKINS, D.K., and SHIN, I.C. 1998. Calcareous nannofossil Paleogene biostratigraphy, Côte D'Ivoire-Ghana Marginal Ridge, eastern Equatorial Atlantic. *Proceedings of the Ocean Drilling Program, Scientific Results*, **159**: 413-431.

SHAMROCK, J. L., 2010. A new calcareous nannofossil species of the genus *Sphenolithus* from the Middle Eocene (Lutetian) and its biostratigraphic significance. *Journal of Nannoplankton Research,* 31(1): 5-10

SHIPBOARD SCIENTIFIC PARTY, 1990. Site 762. *In* Haq, B.U., von Rad, U., O'Connell, S. et al., *Proc. ODP, Init. Repts.,* 122: College Station, TX (Ocean Drilling Program), 213–288. doi:10.2973/odp.proc.ir.122.108.1990

SHIPBOARD SCIENTIFIC PARTY, 2000. Site 1123: North Chatham Drift--a 20-Ma Record of the Pacific Deep Western Boundary Current. In: Carter, R.M., McCave, I.N., Richter, C., Carter, L., et al., *Proc. ODP, Init. Reports*, 181, 1–184. doi:10.2973/odp.proc.ir.181.107.2000

SIESSER, W. G., 1998. Calcareous nannofossil genus *Syracosphaera*: structure, taxonomy, biostratigraphy, and phylogeny. *Micropaleontology*, 44:351-384.

SIESSER, W. G. and BRALOWER, T. J., 1992. Cenozoic calcareous nannofossil biostratigraphy of the Exmouth Plateau, eastern Indian Ocean. In: von Rad, U., et al. (Eds), *Proceedings of the Ocean Drilling Program, Scientific Results,* 122: 601-631. College Station, TX (Ocean Drilling Program). doi:10.2973/odp.proc.sr.122.162.1992

SLUIJS, A., BRINKHUIS, H.,CROUCH, E. M., JOHN, C. M., HANDLEY, L., MUNSTERMAN, D., BOHATY, S. M., ZACHOS, J. C., REICHART, G. J., SCHOUTEN, S., PANCOST, R. D., DAMSTE, J. S. S., WELTERS, N. L. D., LOTTER and A. F., DICKENS, G. R., 2008. Eustatic variations during the Paleocene-Eocene greenhouse world. *Paleoceanography*, 23-4: PA4216. doi: 10.1029/2008PA001615

STICKLEY, C.E., BRINKHUIS, H., MCGONIGAL, K.L., CHAPRONIERE, G.C.H., FULLER, M., KELLY, D.C., NÜRNBERG, D., PFUHL, H.A., SCHELLENBERG, S.A., SCHOENFELD, J., SUZUKI, N., TOUCHARD, Y., WEI, W., WILLIAMS, G.L., LARA, J., and STANT, S.A., 2004. Late Cretaceous–Quaternary biomagnetostratigraphy of ODP Sites 1168, 1170, 1171, and 1172, Tasmanian Gateway. In: Exon, N.F., Kennett, J.P., and Malone, M.J. (Eds), *Proc. ODP, Sci. Results*, 189, 1–57. doi:10.2973/odp.proc.sr.189.111.2004

SULLIVAN, F. R., 1965. Lower Tertiary Nannoplankton from the California Coast Ranges II. Eocene. *University of California Publications in Geological Science*, 53:1-74.

THEODORIDIS, S., 1984. Calcareous nannofossil biostratigraphy of the Miocene and revision of Heliolithus and Discoasters. *Utrecht Micropaleontological Bulletin,* 32:1-271.

THOMAS, E., SHACKLETON, N. J. and HALL, M. A., 1992. Data Report: carbon isotope stratigraphy of Paleogene bulk sediments, Hole 762C (Exmouth Plateau, eastern Indian Ocean). In: von Rad, U., et al. (Eds), *Proceedings of the Ocean Drilling Program, Scientific Results,* 122: 897-901. College Station, TX (Ocean Drilling Program). doi:10.2973/odp.proc.sr.122.195.1992

TREMOLADA, F. and BRALOWER, T. J., 2004. Nannofossil assemblage fluctuations during the Paleocene-Eocene Thermal Maximum at Sites 213 (Indian Ocean) and 401 (North Atlantic Ocean): paleoceanographic implications. *Marine Micropaleontology*, 52:107-116.

TRIPATI, A. K., DELANEY, M. L., ZACHOS, J. C., ANDERSON, L. D., KELLY, D. C. and ELDERFIELD, H., 2003. Tropical sea-surface temperature reconstruction for the early Paleogene using Mg/Ca ratios of planktic foraminifera. *Paleoceanography*, 18:1101, doi: 10.1029/2003PA000937

VAROL, O., 1989. Eocene calcareous nannofossils from Sile, (Northwest Turkey). *Revista Española de Micropaleontología*, 21(2):273-320.

VILLA, G., FIORONI, C., PEA, L., BOHATY, S. and PERSICO, D., 2008. Middle Eocene-late Oligocene climate variability: calcareous nannofossil repsonse at Kerguelen Plateau, Site 748. *Marine Micropaleontology*, 69(2):173-192.

VONHOF, H. B., SMITH, J., BRINKHUIS, H., MONTANARI, A. and NEDERBERG**,** A. J., 2000. Global cooling accelerated by early late Eocene impacts? *Geology***, 28(**8**)**: 687-690.

WATKINS, D.K. and BERGEN, J.A. 2003. Late Albian adaptive radiation of the calcareous nannofossil genus *Eiffellithus*. Micropaleontology, **49**: 231-252.

WEI, W., MCGONIGAL, K. L., and ZHONG, S., 2003. Data report: Paleogene calcareous nannofossil biostratigraphy of ODP Leg 189 (Australia-Antarctica Gateway). In: Exon, N.F., Kennett, J.P., and Malone, M.J. (Eds), *Proc. ODP, Sci. Results*, 189, 1–14. doi:10.2973/odp.proc.sr.189.103.2003

A - WEI, W. and WISE, S.W., Jr., 1990(a). Middle Eocene to Pleistocene calcareous nannofossils recovered by Ocean Drilling Program Leg 113 in the Weddell Sea. In: P.F. Breker, et al. (Eds), *Proceedings of the Ocean Drilling Program*, *Scientific Results*, 113: 639-666. College Station, TX (Ocean Drilling Program). doi:10.2973/odp.proc.sr.113.125.1990

B - 1990(b). Biogeographic gradients of middle Eocene-Oligocene calcareous nannoplankton in the South Atlantic Ocean. *Palaeoceanography, Palaeoclimatology, Palaeoecology*, 79:26-61.

A - WEI, W. and WISE, S. W., JR, 1989(a). Discoaster praebifax n. sp.: a possible ancestor of Discoaster bifax Bukry (coccolithophoridae). *Journal of Paleontology*, 63:10-14.

B - 1989(b). Paleogene calcareous nannofossil magnetobiochronology: results from South Atlantic DSDP Site 516. *Marine Micropaleontology*, 14:119-152.

WILKENS, R. H., CARLO, E. H. DE and TRIBBLE, J. S., 1992. Data Report: X-ray bulk mineralogy of Exmouth and Wombat Plateau sediments, northwest Australian margin. In: von Rad, U., et al. (Eds), *Proceedings of the Ocean Drilling Program, Scientific Results,* 122: 887-896. College Station, TX (Ocean Drilling Program). doi:10.2973/odp.proc.sr.122.191.1992

WISE, S. W., Jr., 1983. Mesozoic and Cenozoic calcareous nannofossils recovered by Deep Sea Drilling Project Leg 71 in the Falkland Plateau region, Southwest Atlantic Ocean. In: Lugwig, W. J., et al. (Eds), *Initial Reports of the Deep Sea Drilling Program,* 71: 481-550.Washington (U.S. Govt. Printing Office).

WISE, S. W., JR, BYBELL, L. M, COVINGTON, J. M., DEKAENEL, E., LANDER, B. C., MAIORANO, P., MCGONIGAL, K. L., MILLIMAN, D. D., MUZA, J. P., POSPICHAL, J. J., SELF-TRAIL, J., SALIS, K. VON, VILLA, G. and WEI, W., 2004. *Cenozoic Nannoware database version 2004.1.3*. International Nannoplankton Association CD ROM No.1

YOUNG, J. R., GEISEN, M., CROS, L., KLEIJNE, A., SPRENGEL, C., PROBERT, I. and OSTERGAARD, J., 2003. *A guide to extant coccolithophore taxonomy. Journal of Nannoplankton Research, Special Issue* 1: 125pp.

YOUNG, J. R., BERGEN, J. A., BOWN, P. R., BURNETT, J. A., FIORENTIONO, A., JORDEN, R. W.,

KLEIJNE, A., NIEL, B. E. VON, ROMEIN, A. J. TON and SALIS, K. VON, 1997. Guidelines for coccolith and calcareous nannofossil terminology. *Paleontology*, 40(4):875-912.

YOUNG, J. R. and BOWN, P. R., 1997. Proposals for a revisited classification system for calcareous nannoplankton. *Journal of Nannoplankton Research*, 19(1):15-47.

ZACHOS, J. C., PAGANI, M., SLOAN, L., THOMAS, E. and BILLUPS, K., 2001. Trends, rhythms, and aberrations in global climate 65 Ma to present. *Science*, 292:686-693.